ALMA MATER STUDIORUM - UNIVERSITÀ DI BOLOGNA

FACOLTÀ DI CHIMICA INDUSTRIALE

Dipartimento di Chimica Industriale e dei Materiali

Master of Science in Advanced Spectroscopy in Chemistry

Classe LM/71 - Scienze e Tecnologie della Chimica Industriale

Anaerobic oxidation of ethanol over spinel mixed oxides: the first step in the steam-iron process for H₂ production

EXPERIMENTAL THESIS

Presented by: Supervisor:

Juliana Velásquez Ochoa   ***Prof.* Fabrizio Cavani**

Co-supervisor:

MSc. Cristian Trevisanut

First Session

Academic Year 2011-2012

TABLE OF CONTENTS

SUMMARY

The future hydrogen demand is expected to increase, both in existing industries (including upgrading of fossil fuels or ammonia production) and in new technologies, like fuel cells. Nowadays, hydrogen is obtained predominantly by steam reforming of methane, but it is well known that hydrocarbon based routes result in environmental problems and besides the market is dependent on the availability of this finite resource which is suffering of rapid depletion. Therefore, alternative processes using renewable sources like wind, solar energy and biomass, are now being considered for the production of hydrogen. One of those alternative methods is the so-called "steam-iron process" which consists in the reduction of a metal-oxide by hydrogen-containing feedstock, like ethanol for instance, and then the reduced material is reoxidized with water to produce "clean" hydrogen (water splitting). This kind of thermochemical cycles have been studied before but currently some important facts like the development of more active catalysts, the flexibility of the feedstock (including renewable bio-alcohols) and the fact that the purification of hydrogen could be avoided, have significantly increased the interest for this research topic.

With the aim of increasing the understanding of the reactions that govern the steam-iron route to produce hydrogen, it is necessary to go into the molecular level. Spectroscopic methods are an important tool to extract information that could help in the development of more efficient materials and processes. In this research, ethanol was chosen as a reducing fuel and the main goal was to study its interaction with different catalysts having similar structure (spinels), to make a correlation with the composition and the mechanism of the anaerobic oxidation of the ethanol which is the first step of the steam-iron cycle. To accomplish this, diffuse reflectance spectroscopy (DRIFTS) was used to study the surface composition of the catalysts during the adsorption of ethanol and its transformation during the temperature program. Furthermore, mass spectrometry was used to monitor the desorbed products. The set of studied materials include Cu, Co and Ni ferrites which were also characterized by means of X-ray diffraction, surface area measurements, Raman spectroscopy, and temperature programmed reduction.

1. INTRODUCTION

1.1 Hydrogen

1.1.1 Properties

Among common fuels, hydrogen has the highest specific energy and is the only one with zero CO_2 emission (see Table 1). this makes it a good alternative especially when compared to fossil fuels that are more contaminant and whose reserves are decreasing drastically with time. The challenge about moving into a hydrogen-based economy is the cost of the present production methods, the storage and transportation of it [1]. However, due to the importance of this kind of technology (especially hydrogen for fuel cells), the scientific community is working to overcome those issues. The present research work, for instance, is concerned with the development of a more efficient and clean hydrogen production process.

Table 1. Energetic characteristic for common fuels

Fuel	Specific Energy KJ/g	Density KHW/gal	Chemical Formula	Lbs CO_2/gal
Propane	50.4	26.8	C_3H_8	13
Ethanol	29.7	24.7	C_2H_5OH	13
Gasoline	46.5	36.6	C_7H_{16}	20
Diesel	45.8	40.6	$C_{12}H_{26}$	22
Biodiesel	39.6	35.0	$C_{18}H_{32}O_2$	19
Methane	55.8	27.0	CH_4	3
Oil	47.9	40.5	$C_{14}H_{30}$	20
Wood	14.9	11.3	--	9
Coal	30.2	22.9	--	19
Hydrogen	141.9	10.1	H_2	0

1.1.2 Production

Hydrogen does not exist alone in nature; it must be extracted from a hydrogen-containing feedstock. This can be done in different ways depending on the sources and technologies available as illustrated in Figure 1.1—1. There, it is also presented the different final uses of this gas [2]. Nowadays steam reforming of methane and electrolysis are the two main commercial processes. Nevertheless, hydrogen production from alternative pathways (as from biomass) is a strategic area of development since the demand of this gas is expected to increase rapidly in the future. The following paragraphs present the description and main facts of the two mentioned main processes. On the other hand, session 1.2 presents the description of the unconventional route studied in this research project (steam-iron process).
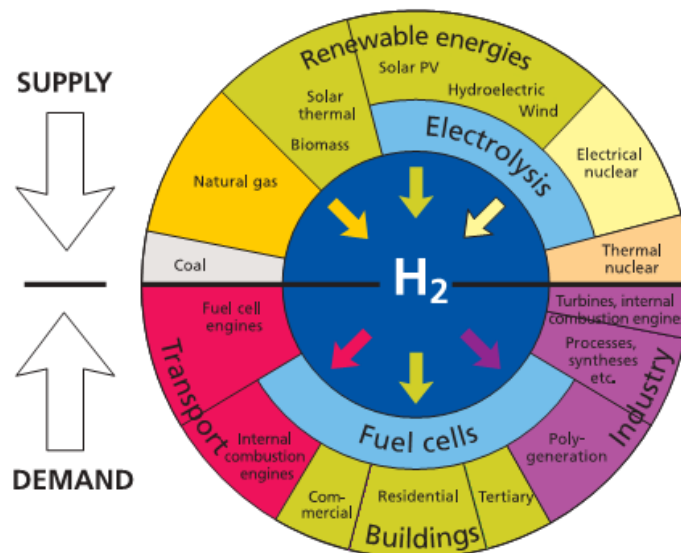

Figure 1.1—1. Summary of the hydrogen economy. Upper part: production – Lower part: uses.

Steam methane reforming (SMR)

In this process the methane source (usually natural gas) is put in contact with high temperature steam (700°C - 1000°C) at high pressure (3-25 bar). The products obtained in this step include hydrogen, carbon monoxide and carbon dioxide. Afterwards there is a second reaction called "water-gas shift" in which the resulting carbon monoxide is reacted with more steam to produce carbon dioxide and hydrogen.

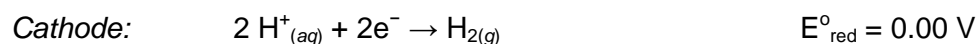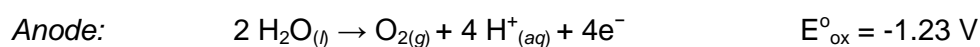The final step is a purification of the hydrogen produced in a reaction known as "pressure swing absorption (PSA)" that condenses and removes all the carbon dioxide and impurities leaving only the hydrogen gas. The reactions representing this process are as following:

Steam-Methane reforming: $CH_4 + H_2O$ (+heat) $\rightarrow CO + 3H_2$

Water-Gas Shift reaction (WGS): $CO + H_2O \rightarrow CO_2 + H_2$ (+small amount of heat)
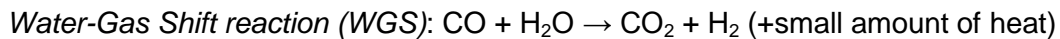
This process is known for being economical and its efficiency is among the highest of current commercially available hydrogen production methods (65-75%). Furthermore, natural gas is a convenient and easy to handle hydrogen feedstock with a high hydrogen-to-carbon ratio. On the other hand, the cost of hydrogen produced by SMR is highly dependent on natural gas price which is nowadays a non expensive source but if the demand of natural gas in other market sectors continues to grow, the natural gas reserves would decrease and the supply, and so the price, will be compromised. Another drawback is the big amount of CO_2 production which makes the expensive process of separation and carbon sequestration necessary to have the pure hydrogen.

Electrolysis

Electrolysis consists in the dissociation of water into hydrogen and oxygen by means of an electric current that passes through the water. The reactions involved are:

Anode: $\quad\quad 2\ H_2O_{(l)} \rightarrow O_{2(g)} + 4\ H^+_{(aq)} + 4e^-$ $\quad\quad\quad E^o_{ox} = -1.23\ V$

Cathode: $\quad\quad 2\ H^+_{(aq)} + 2e^- \rightarrow H_{2(g)}$ $\quad\quad\quad\quad\quad E^o_{red} = 0.00\ V$

The total reaction is endothermic, and the voltage indicated (1.23 V) is the minimal value to make this reaction thermodynamically favored at room temperature. It is necessary the addition of an electrolyte to the water in order to increase the conductibility, which for pure water is very low (0,055 μScm^{-1}).

These electrolytes should satisfy features such as low cost, high solubility and not to compete for the H^+ and OH^- species. In general making hydrogen from water by electrolysis is one of the most energy-intensive methods and it is also associated with considerable losses. Moreover, these electrolytic systems need costly materials such as the electrolyte membrane and noble metal-based electrocatalysts [3]. Therefore, this process is normally used when a higher purity of hydrogen is required. An advantage of this route is that it could be a zero emission technology if a renewable energy source, like a wind turbine or solar energy is used to produce the energy required for the process.

All the hydrogen production methods have variety of costs, benefits and challenges to overcome regarding the environmental impact, security, and economy. In this work the proposed method to produce hydrogen is the called "steam-iron" which is interesting now that it implies the inherent separation from the carbon oxides and moreover because renewable feedstock as bio-alcohols can be used. Next session is dedicated to this particular process.

1.2 Steam-Iron and the "chemical loop" concept

The so called "Steam Iron" is an old process which allows producing, store and releasing pure hydrogen. It was developed in the late 19th century to produce hydrogen from gasified coal (mainly for use in aerial navigation) [4]. The use of cheap and low reactive iron ores made the process unviable in those early years and thus this method was quickly replaced by the more efficient and economical natural gas reforming.

However, the steam-iron process is nowadays subject of renewed interest because of its simplicity, feedstock flexibility (including renewable energy sources) and the purity of the obtained hydrogen which is especially important for the use in hydrogen fuel cells [5].
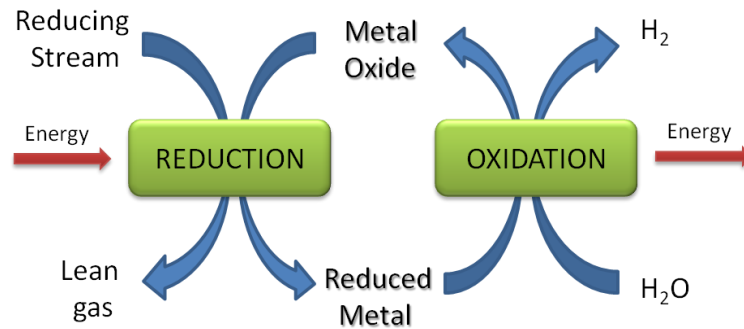
Figure 1.2—1. Scheme of a thermochemical cycle using a reducing fuel

The principle of this process is a chemical-loop that separates the hydrogen production from the feedstock oxidation (as illustrated in Figure 1.2—1) so the reaction consists in two temporarily separated steps, reduction and oxidation. During the reduction step, a metal oxide (mainly iron-based) is put in contact with a reducing stream which is thus converted into carbon oxides and water, producing a lean gas. In the subsequent oxidation step, the reduced catalyst is re-oxidized by water vapor yielding a hydrogen rich fuel gas and restoring the original oxidation state of the metal oxide [6]. This type of thermochemical cyclic process for water cleavage has been studied for a variety of materials. A more generic schematization could be written as
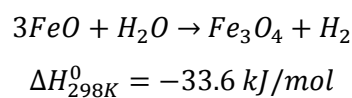
$$A\text{-}O \rightarrow A + \tfrac{1}{2}O_2$$

$$A + H_2O \rightarrow H_2 + A\text{-}O$$
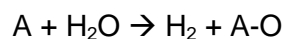
Where *A* can also be a combination of different compounds. The most relevant cycles are presented in Table 2 [7], from this data it can be noticed the high operation temperatures which makes them difficult to implement commercially. Another drawback is that the compounds involved in some of the cycles are toxic and/or corrosive (H_2SO_4, HCl) and for this reason the research in this area is also aimed at finding new and highly resistance materials required because of the combination of high temperatures, high pressures and corrosive compounds.

Table 2. Thermochemical cycles currently under consideration

Thermal Cycle	Steps	Maximum Temperature (°C)	Efficiency (%)
Sulfur cycles			
Hybrid Sulfur (Westinghouse, ISPRA Mark 11)	2	900 (1150 without catalyst)	43
Sulfur-iodine (General Atomics, ISPRA Mark 16)	3	900 (1150 without catalyst)	38
Volatile metal oxide cycles			
Zinc/zinc oxide	2	1800	45
Hybrid cadmium		1600	42
Non-volatile metal oxide cycles			
Iron oxide	2	2200	42
Cerium oxide	2	2000	68
Ferrites	2	1100-1800	43
Low-temperature cycles			
Hybrid copper-chloride	4	530	39

Among the various thermo-chemical cycles, those using pure and mixed iron oxides are considered the most feasible ones due to the availability, performance and low cost of this kind of catalysts. The "steam-iron" cycle, originally proposed by Nakamura in 1977 [8], uses magnetite (Fe_3O_4) which is then reduced to wustite (FeO) and afterwards re-oxidized with water to give hydrogen:

$$Fe_3O_4 \rightarrow 3FeO + {}^1\!/_2\,O_2 \qquad > 1600\,°C$$
$$\Delta H^0_{298K} = +319.5\ kJ/mol$$

$$3FeO + H_2O \rightarrow Fe_3O_4 + H_2$$
$$\Delta H^0_{298K} = -33.6\ kJ/mol$$
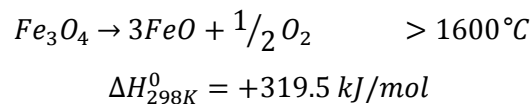
Nowadays the studies are pointing towards the decrease of the operative temperatures. There are different approaches in the effort to improve this cycle:

a) Modification of the catalyst
b) The use of a reducing agent in the first step
c) Reactors and devices design

Next session presents a general description of the former two since they are the ones explored in this research work but focusing mainly in the first one because there is a need for more efficient catalysts, especially for the first step since the reduction of the metal-oxide by the feedstock is endothermic and will determine probably the highest temperature required for the whole process

1.2.1 Steam-iron process: Modified materials

Ferrites properties

Magnetite is a ferrimagnetic mineral with chemical formula Fe_3O_4 that belongs to the *spinel* group whose general formula is $A^{2+}B_2^{3+}O_4^{2-}$. To be more precise, this compound presents the *inverse* spinel structure in which the Fe^{2+} occupies octahedral sites and the Fe^{3+} occupies both octahedral and tetrahedral sites, a representation can be seen in Figure 1.2—2 (adapted from [9]). The spinel class of oxides belongs to the space group $Fd3m$ and to the O_h^7 point group. The lattice is cubic and consisting of 8 molecules within the unit cell, for a total of 56 atoms. The positions of the oxygen atoms are more or less fixed but the arrangement of the cations varies considerably within certain limits [10].

$Fe^{3+}_{(Th)}$ $Fe^{2+,3+}_{(Oh)}$ $O^{2-}_{(Close-Packing)}$
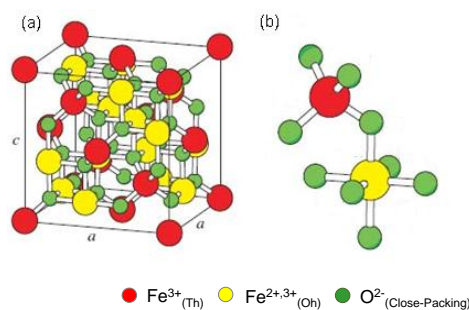
Figure 1.2—2. (a) Face-centered cubic spinel structure of magnetite. (b) Magnification of one tetrahedron and one adjacent octahedron sharing an oxygen atom.

Mixed-Ferrite cycles

The idea of the steam iron cycle is first to reduce magnetite (Fe_3O_4) to wustite (FeO) but this reaction takes place only at temperatures higher than 1600 °C. However, if the composition is modified with other transition metals like Cu, Ni, Co, Zn, Mn and so on, it could help to decrease the operational temperatures of this first step in the thermo-chemical cycle. Those materials with the same structure and similar composition to magnetite are the ones known as *ferrites.* In most of the cases the modified materials have a lower reduction temperature but on the other hand sometimes the reoxidation step is more difficult than for the pure Fe_3O_4.

Figure 1.2—3 shows an example on how the free energy of the oxidation and reduction of Co_3O_4, Mn_3O_4 and Fe_3O_4 are related to the composition [7]. In this case, Co_3O_4 is the material showing the lower temperature for thermal reduction but it presents thermodynamic limitations regarding the reoxidation step with water. The opposite is true for the Fe_3O_4. From this, it can be stated that the redox properties of this spinel type mixed oxides are strictly related to both the chemical composition and some morphological properties.

$$A:\ Me_3O_4 \rightarrow MeO + O_2$$
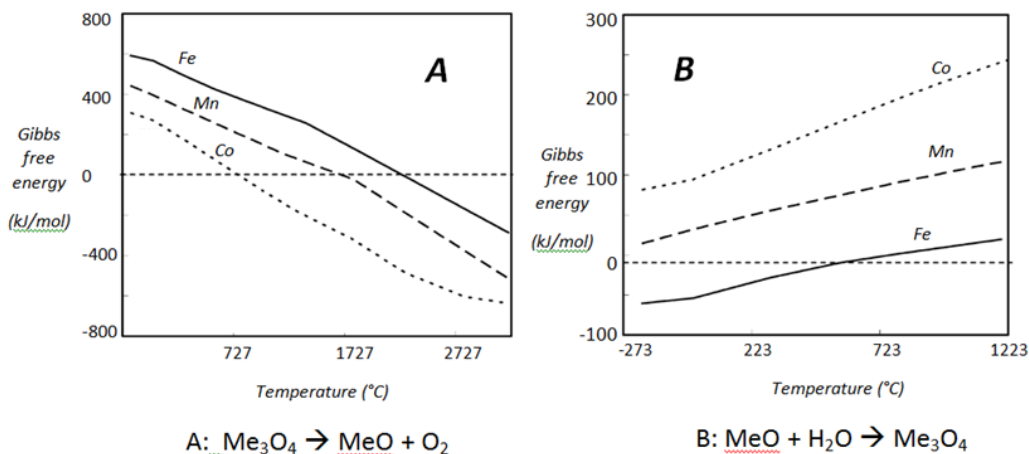
$$B:\ MeO + H_2O \rightarrow Me_3O_4$$

Figure 1.2—3. Gibbs free energy of the two reactions of the chemical loop for Co, Mn and Fe spinel-type oxides: (a) thermal reduction (b) water reoxidation.

In order to develop the more active catalysts some modifications to the original composition have been proposed, for example, the replacement of the iron 2+ in Fe_3O_4 by other transition metals, such as Mn, Ni or Co, to form mixed metal oxides $(Fe_{1-x}M_x)_3O_4$ could help to make easier the oxygen transfer to the reagents. This type of oxides called ferrites and their behavior in the ethanol oxidation are the subject of the present study.

In the literature there are some reports about modified ferrites and that present promising features for their use in this type of reaction. For example, Fresno et al., studied some commercially available mixed oxides ($NiFe_2O_4$, $Ni_{0.5}Zn_{0.5}Fe_2O_4$, $ZnFe_2O_4$, $Cu_{0.5}Zn_{0.5}Fe_2O_4$ and $CuFe_2O_4$) by carrying out the reduction step at 1723°C and in this case $NiFe_2O_4$ showed the lowest temperature for the thermal reduction and the highest net hydrogen production for the oxidation step [11].
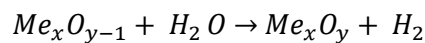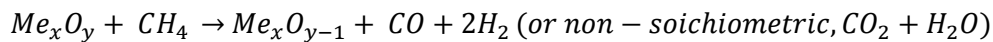
In another work, Kodama et al studied $CoFe_2O_4/ZrO_2$ and compared it with the $MnFe_2O_4/ZrO_2$ reported also by them before. They performed the thermochemical cycle in an inert atmosphere at temperatures starting from 1400 °C for the reduction step and around 1000 °C for the oxidation with water. They concluded that In most of the runs, Co-ferrite displayed higher reactivity than the Mn(II)-ferrite [12]. In a related paper the performance of the Ni-ferrite is reported under the same conditions and as a conclusion they stated that the $NiFe_2O_4/ZrO_2$ was found to be a very promising working material for the cycle and that the reactivity of this material could be reproduced in the repeated cycle with even a better performance than the obtained with the $CoFe_2O_4/ZrO_2$ [13].

1.2.2 Steam-iron process: Using reducing fuels

The high temperatures needed for the thermal reduction are mainly attributed to the high activation energy for releasing the oxygen in lattice so the addition of a chemical reaction with a reducing agent can lower the reaction temperature and this is another approach in the attempt to improve this process: the study of the reducing fuel used in the first step. Among the options available, the most commonly used are:

Hydrogen: The aim of using hydrogen in the first step is for chemical storage since the hydrogen can be later released in the moment when it is needed. For example, as a fuel in a car the reduced material can be charged (metallic iron for instance) and then water can be added to finally produce the hydrogen. The practical limitation for this approach is the amount of hydrogen that can be stored (less than 4,8%) [14].

Methane: The redox cycle based on methane as a reducing agent is as follows:

$$Me_xO_y + CH_4 \rightarrow Me_xO_{y-1} + CO + 2H_2 \ (or \ non-soichiometric, CO_2 + H_2O)$$

$$Me_xO_{y-1} + H_2O \rightarrow Me_xO_y + H_2$$

This particular process is attractive since is an alternative to the classical SMR+WGS+PSA process used for the production of high purity hydrogen [15]. Besides, as mentioned before, methane is nowadays a rapidly available feedstock. The drawback is that it is still hydrocarbon-based. Other publications use syngas as the reducing stream, derived from the reforming of light hydrocarbons; this approach is similar to that from methane because the real reducing agents are CO and H_2 obtained from methane decomposition (as previously discussed) [16].

Pyrolysis oil: The use of pyrolysis oil in the steam-iron process facilitates transportation and simplifies gasification and combustion processes of the feedstock before being processed to hydrogen as exposed by Bleeker et al [17]. The same authors mentioned the fact that coke deposition on the catalyst could be a drawback but they suggested that C can also be used as a reducing material.

Biomass gasification gas: The gasification of biomass yields the so-called biosyngas that contains amounts of CO and H2 depending on the applied process, oxidation medium, temperature processes and so on as studied by Wiebren et al., [18]. On the other hand low-temperature (<1000°C) gasification processes yields a product gas that contains significant amounts of hydrocarbon compounds. In most of the cases the biomass-derived gas produced is purified in a tar extractor and then used in the steam-iron process but doing so then there is the possibility of integrating the gasification part and the hydrogen production with fuel cell final application as explained in [19].

Bio-Alcohols: Bio-ethanol is produced by fermentation of biomass materials. When oxygen is insufficient for normal cellular respiration, anaerobic respiration takes place by yeasts, converting glucose into ethanol and carbon dioxide. Using bio-ethanol and bio-methanol to produce hydrogen by autothermal and steam reforming is currently an active research field [20]. The technology to produce these bio-alcohols, especially ethanol, from biomass is already accessible but it is still developing very fast so in the future the availability of this feedstock will be even higher. The advantages of using bio-ethanol as feedstock include its low toxicity, ease of deliverability and its potential for production from many different sources, ranging from cellulosic biomass to algae [21]. For these reasons, in the present research work ethanol was chosen as the probe molecule.

1.3 Infrared studies of the interaction alcohol-catalyst

In the field of heterogeneous catalysis, the main goal is the understanding of surface chemistry phenomena and Infrared spectroscopy (IR) has been successfully applied for it since the early 20th century when Buswell et al., reported the spectra of water adsorbed on montmorillonite [22]. Further developments related to IR, as Fourier transform instruments and diffuse reflectance attachments, have made this technique one of the most widely used for the characterization of solid surfaces.

The advantages of using this technique include the relative low cost of the instrumentation and accessories needed to study catalysts surfaces, moreover, it is relatively easy to adapt the IR apparatus for *in-situ* studies making possible to apply it in the mechanistic studies of heterogeneous catalyzed reactions. Next session gives a brief description of the principle of infrared spectroscopy. A detailed explanation is not the purpose of this handout.

Principle

Energy levels in a molecule, include the electronic, vibrational and rotational levels as depicted in Figure 1.3—1 [23]. At absolute zero all polyatomic chemical species are at the ground state but they can be promoted to a higher level if they adsorb radiation of the

adequate intensity. In the case of infrared radiation, the energy is of the order of transitions between vibrational states, this means that when infrared light hits a sample it mainly causes vibrational motions of the atoms like stretching, bending, wagging, rocking and so on. If the movement causes a variation of the dipole moment along the vibrational coordinate of the molecule, then it is said to be infrared active.

The most important IR bands arise from the simplest distortions of the molecule called "normal modes" and here the molecule is going from the ground state to the first excited level. In some cases, "overtone bands" are observed when the absorption of a photon leads to an excited vibrational state which is not necessarily the first one. Such bands appear at approximately twice the energy of the normal mode. There are also some other possible phenomena as the "combination modes" that involve more than one normal mode and the "hot bands" which appear when the transition starts in a vibrational state which is not the ground state. The phenomenon of Fermi resonance can arise when two modes are similar in energy; Fermi resonance results in an unexpected shift in energy and intensity of the bands.
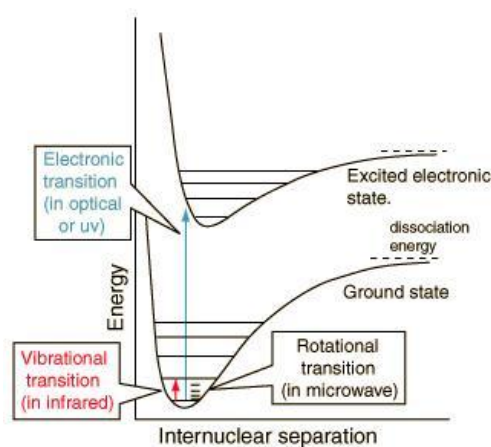

Figure 1.3—1. Energy levels of a molecule.

The number of potentially occurring normal vibrations depends on the degree of freedom of the system. In the case of a single molecule consisting of N atoms, there are 3N-6 degrees of vibrational freedom (3 for each atom, minus 3 rotational and 3 translational movements of the entire molecule in the 3D space). Linear molecules have 3N-5 degrees of vibrational freedom, because the rotation around the main molecule axis does not produce any change of rotational energy.

The possible modes of vibrations in a solid differ from the ones in the gas or liquid phase now that in the former case the atoms are not free to translate and rotate. Instead, they vibrate in a collective way giving rise to modes give rise to lattice vibrations ('frustrated translations and rotations') and acoustic modes [24]. Therefore, for a solid, the number of vibrational modes is in total 3N-3 where N is the number of atoms present in the smallest (primitive) Bravais cell, and minus three because those are the number of translations of the cell as a whole in the 3D space.

Experimental setup

There are a several ways in which the IR technique may be implemented for the study of the vibrations of adsorbates on surfaces. The most common ones include:

Transmission/Absorption IR Spectroscopy: This configuration is by far the most used. It follows the well known Beer-Lambert law: $A = \log(I_0/I_1)$ where I_0 and I_1 are the intensities of radiation before and after transmission through the sample (like in Figure 1.3—1).
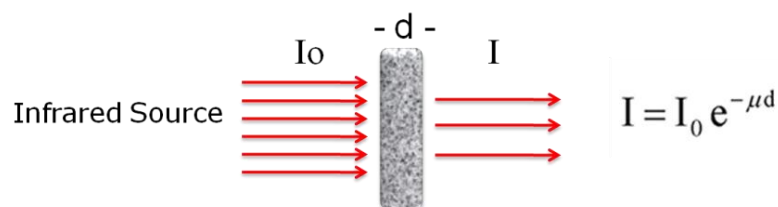

$$I = I_0\, e^{-\mu d}$$

Figure 1.3—2. Infrared absorption/transmission optical path

The solid sample must, of course, be able to transmit part of the IR radiation which is sometimes not the case for some of the common catalysts which are highly absorbent and in any case as normally the sample is prepared in the form of a pressed disk, it can have some mass transport limitations for the adsorption of molecules on it. This is often used for studies on supported metal catalysts where the large metallic surface area permits a high concentration of adsorbed species to be sampled.

Reflection-Absorption IR Spectroscopy (RAIRS): In this case the IR beam is specularly reflected from the front face of a highly-reflective sample, such as a metal single crystal surface (see Figure 1.3—3, [25]). In this configuration vibrations can only be detected if they are perpendicular to the surface. One major problem is that the signal is usually very weak owing to the small number of adsorbing molecules. Typically, the sampled area is around 1 cm^2.
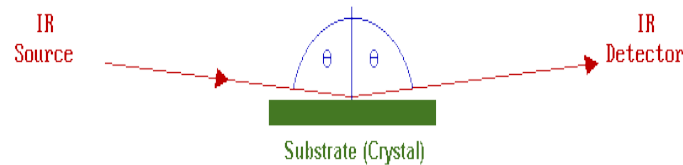

Figure 1.3—3. Infrared reflection-absorption optical path

Attenuated Total Reflection (ATR): Also known as Multiple Internal Reflection Spectroscopy (MIR). Here the IR beam is passed through a thin, IR transmitting sample in a manner such that it alternately undergoes total internal reflection from the front and rear faces of the sample. At each reflection, some of the IR radiation may be absorbed by species adsorbed on the solid surface [26].
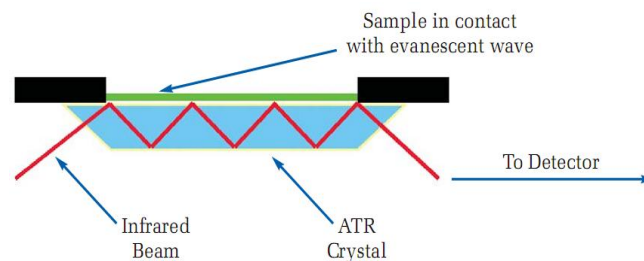

Figure 1.3—4. Infrared Attenuated Total Reflection optical path

Diffuse Reflectance IR Spectroscopy (DRIFTS): in which the diffusely scattered IR radiation from a sample is collected, refocused and analyzed. This modification of the IR technique can be employed with samples that are not sufficiently transparent to be studied in transmission. Next session is dedicated to this particular experimental setup since it was the one employed during the present work.
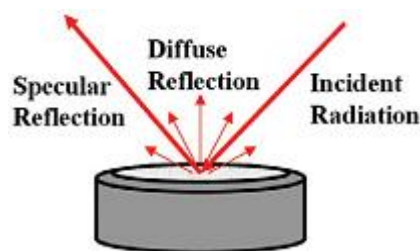
Figure 1.3—5. Infrared diffuse reflectance optical path

Applications (IR+Ethanol adsorption)

Nowadays approximately 80% of the processes in the chemical industries require the use of catalysts. Most of the catalytic processes are heterogeneous in nature, which means that the catalyst is in a different phase than the reagents [27]. Therefore, the study of the chemistry about the interactions developing on those interfaces is of great interest. Supported noble metals and transition metal oxides represent the majority of the solids used for catalysis. When performing in a reaction, these solids are able to absorb and transform the initial molecules to the desired products according generally to the following sequence:

- *Diffusion of reactants to the active surface*
- *Adsorption of one or more reactants onto the surface*
- *Surface reaction*
- *Desorption of products from the surface*
- *Diffusion of products away from the surface*

The above scheme not only takes into account the adsorption process but also its reverse - namely desorption. The adsorption and transformation of ethanol over metal oxides surfaces has been extensively studied [28-31] but even when ethanol seems to be a simple molecule, the range of possible products and the pathways followed are not a simple matter. Next paragraphs present examples where the infrared spectroscopy was useful to understand the adsorption and transformation of ethanol over different catalysts surfaces.

Ni/MgO

Busca et al. [32] performed reactivity and FTIR studies of this system and concluded that ethanol decomposition occurs on catalyst surface through formation of acetaldehyde, which is converted to acetates and then to carbonates (detected by IR), or decomposes to CO_2, C and H. They proposed the following pathway:
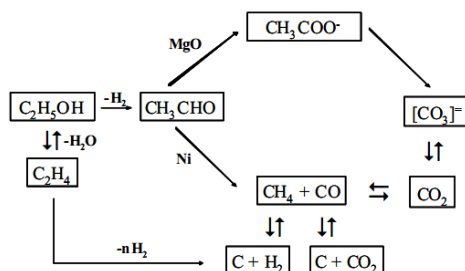

Figure 1.3—6. Main reaction steps in the ethanol-acetaldehyde dry decomposition over Ni/MgO

TiO₂, Au/TiO₂

In the study by Nadeem et al. [33], the TPD/FTIR results of the titania support and the support impregnated with gold showed significant differences and allow them to propose the route followed in each case. The detection of crotonaldehyde by infrared gave them a hint to suggest the route for the formation of benzene which was the main product over the gold containing catalyst.
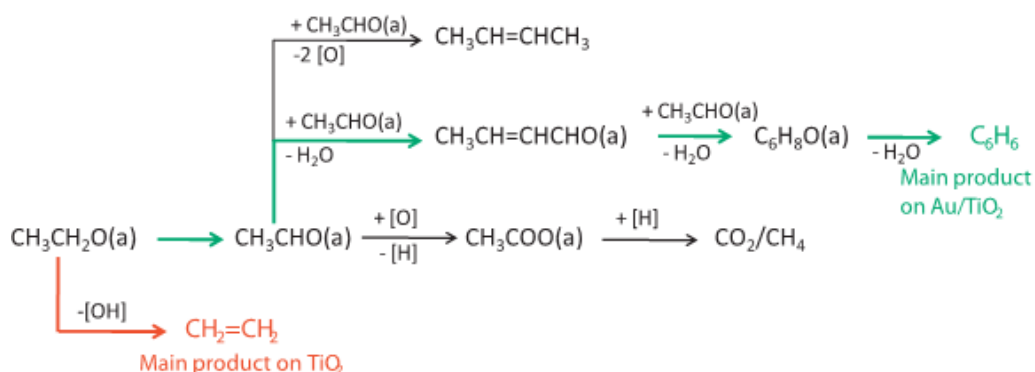

Figure 1.3—7. Main reaction steps in the ethanol decomposition over TiO₂ and Au/TiO₂

Pt/Al$_2$O$_3$, Pt/SiO$_2$

Petkovic et. al [34] used a combination of in situ DRIFTS analysis and first-principles DFT-based calculations to study the ethanol oxidation on Pt-containing catalysts. They found that Pt nanoparticles trap and accumulate oxygen at their surface and perimeter sites and play the role of sites that burn ethanol molecules and their partially oxidized derivatives to the "final" products. With respect to the support, they stated that alumina provides higher mobility of the fragments of ethanol molecules than the silica surface and hence increases the conversion rate of ethanol.

Pd/CeO$_2$, Pt/CeO$_2$, Rh/CeO$_2$

In the work reported by Idris [35] the comparison of ethanol adsorption over the three different ceria-supported noble metal catalysts was studied mainly by DRIFTS/TPD experiments and he found that ethanol dehydrogenation to acetaldehyde was facilitated by the presence of Pt or Pd; at higher temperatures the acetaldehyde condensed to other organic compounds, such as crotonaldehyde. By contrast, in the presence of Rh only traces of acetaldehyde or other organic compounds were seen on the surface, and detectable amounts of CO were found upon ethanol adsorption at room temperature. This, according to the author, indicates the powerful nature of Rh in breaking the carbon-carbon bond in ethanol. At the end he proposed the following general route depending on the metal.
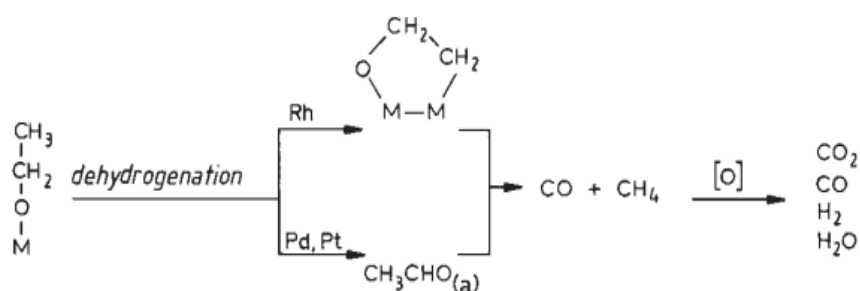

Figure 1.3—8. Adsorption and decomposition pathways of ethanol over Rh, Pd or Pt supported catalysts

Ni–Co–Zn–Al mixed oxides (from hydrotalcites)

The research presented by Busca and co-workers [36] shows a complete picture of the catalysts for the ethanol steam reforming system since they performed infrared characterization of the precursors (hydrotalcites) and the corresponding mixed oxides in combination with an infrared study of the species adsorbed and those on the gas phase (Figure 1.3—9). Besides, reactivity studies were also performed. Roughly, the remarks of the research are that the presence of cobalt increases the selectivity to H_2 and CO and decreases selectivity to methane in the low temperature range and that the most relevant fact influencing the selectivity is the evolution of surface acetate species (observed by infrared).
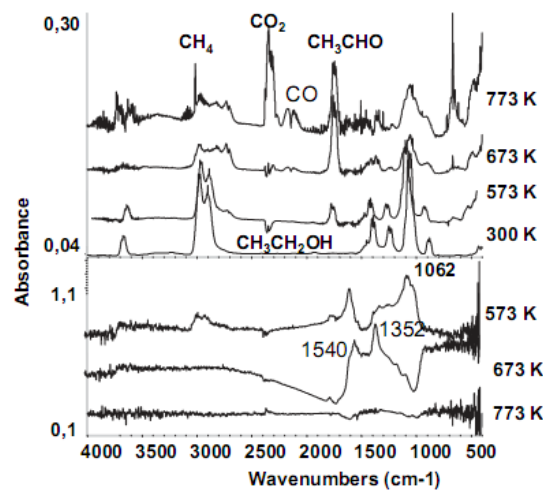

Figure 1.3—9. IR spectra of the adsorbed species (down) and of the gas phase (up) upon adsorption and conversion of ethanol

Pt/ZrO$_2$, Pt/CeO$_2$ and Pt/CeZrO$_2$

In the study carried out by De Lima et al. for this system [37] the authors proposed two routes for the formation of acetates when using the CeO_2 support (Figure 1.3—10). They observed that addition of Zr strongly increased the density of oxygen vacancies of the support due to the high oxygen mobility of the CeO2–ZrO solid solution formed. Therefore, the density of Type II bridging OH can be higher and it favors the pathway for the conversion of ethoxy to acetate species involving this group (Similar to Figure 1.3—10 (B))
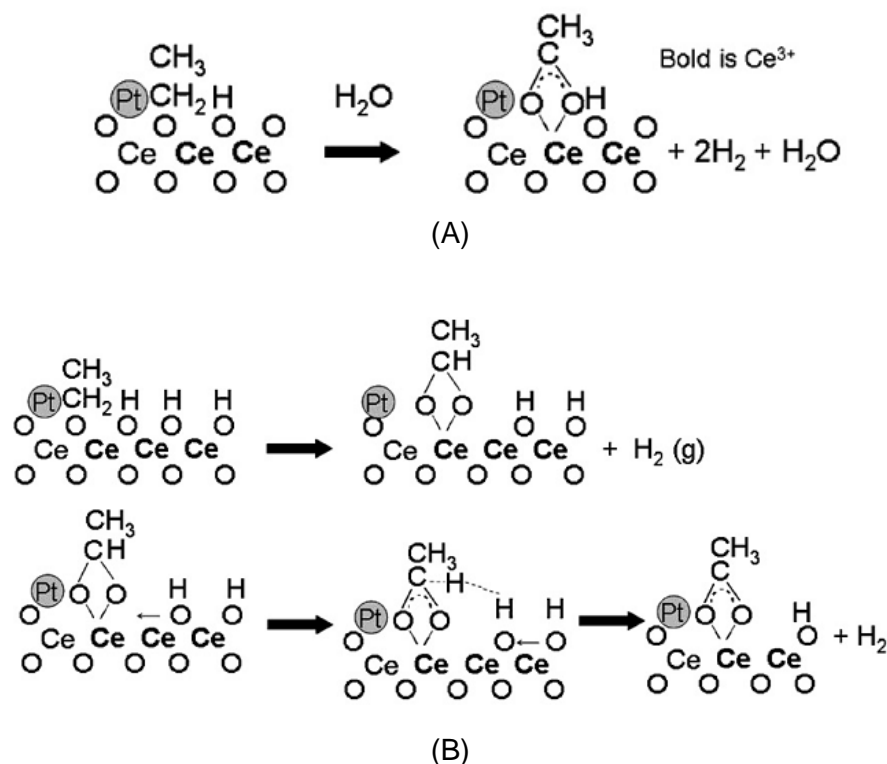
(A)

(B)

Figure 1.3—10. Acetate formation by two routes: (A) the hydroxyl route (without changing Ce oxidation state) and (B) via type II OH groups

Ni/Ca-Al₂O₃

The authors (Choong et al., [38]) compared the DRIFTS and TPD spectra of the support and the material promoted with Ni and they observed that Ni has a good capability to break the C^{α}-H and C-C bonds as well as high WGS activity. About the addition of Ca to the support, they stated that is useful since it promotes water adsorption providing abundant OH groups adsorbed that can participate along with Ni in the conversion of adsorbed intermediate species such as CH3CO and CH3CO into CH3COO at lower temperatures and that it reduces the dehydration reactions because Ca addition reduces the density of acidic sites on the alumina surface as seen by DRIFTS of the alumina with and without added Ca (see Figure 1.3—11).
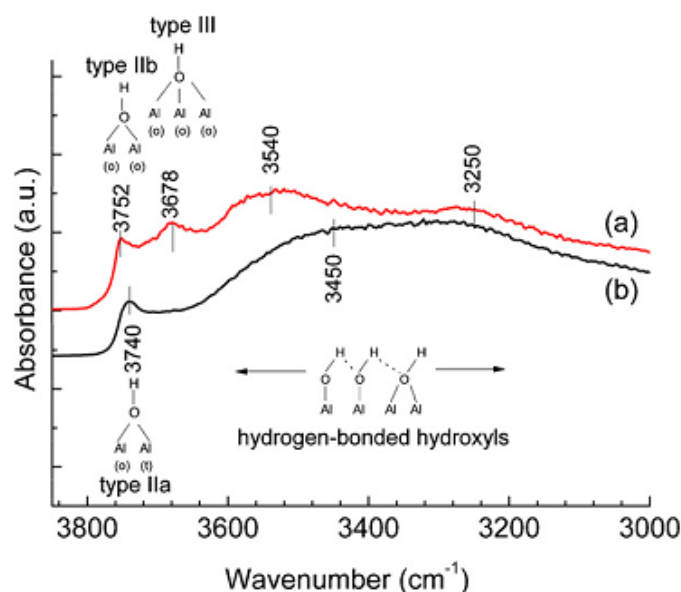
Figure 1.3—11. DRIFT spectra of the catalyst support in the OH region

There are many more examples in the literature of this kind of studies since ethanol adsorption is the key step in several reactions of interest, including steam reforming and partial oxidation. Nevertheless, until now no reports were founds of in-situ DRIFTS (or transmission) spectroscopy for the adsorption of ethanol over ferrites which is the topic explored on the present research.

1.3.1 Diffuse Reflectance Infrared Fourier Transform Spectroscopy (DRIFTS)

When an infrared beam reaches a sample, the incoming light can be reflected, scattered or transmitted. Only the part of the beam that is scattered within a sample and returned to the surface is considered to be diffuse reflection. As the light that leaves the surface has passed through a thin layer of the material, the intensity of the incident wavelength will be modified and this will give the structural information about the substrate. The principle of this technique is illustrated in Figure 1.3—12.

In DRIFTS the light intensity scattered at a given wavelength from an "infinitely thick" closely packed catalyst layer is compared with that scattered of a non-absorbing (white) reference. The light scattered is then collected in an integration sphere and detected.
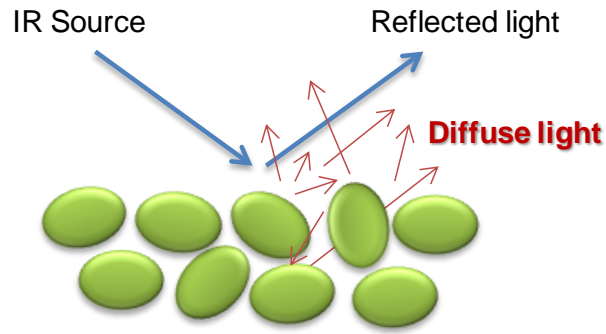
Figure 1.3—12. DRIFTS principle illustration

A more complete view of the experimental configuration can be observed in Figure 1.3—13 (adapted from [39]). Here the infrared source is collimated and directed to the paraboloid (P) that focuses the beam onto the sample (S) trough a small hole. The specular reflected light returns to the paraboloid but the diffuse one is collected by the ellipsoid (E) and directed to the detector.
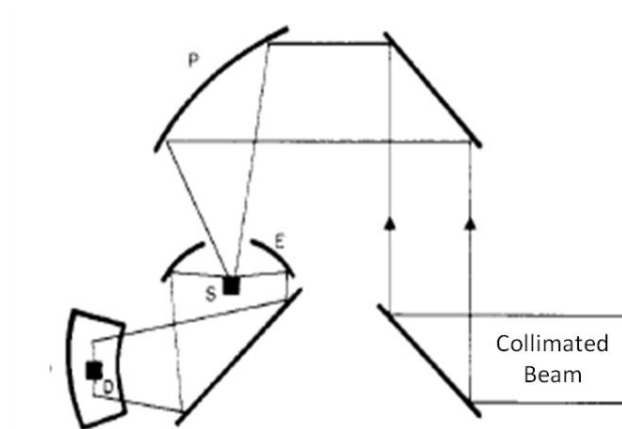

Figure 1.3—13. Example of configuration of the optics allowing the diffuse light to be collected.

Regarding the intensity of the scattered light collected, generally the Kubelka-Munk theory is accepted. It provides a correlation between reflectance and concentration expressed with the Kubelka-Munk formula:

$$F(R) = (1-R)^2/2R = k/s = Ac/s$$

Where,

R = reflectance

k = absorption coefficient

s = scattering coefficient

c = concentration of the absorbing species

A = absorbance

The original theory has some limitations since it assumes infinite sample dilution in a non-absorbing matrix, a constant scattering coefficient and an "infinitely thick" sample layer. However, with proper sample preparation diffuse reflectance spectroscopy can provide ppm sensitivity and high quality results. It is also stated by G. Busca in his review about infrared of organic molecules adsorbed on metal oxides [40] that the performances obtained using the transmission/absorption technique and those with the diffuse reflectance technique are today quite comparable.

Among the different experimental setups for infrared spectroscopy, diffuse reflectance is maybe the one giving the easiest access to the study of the surface of materials. One of the great advantages of this technique is that it does not require a complicated sample preparation, the catalyst powder is directly put in the sample holder and diluted with KBr if needed, and this avoids the mass transport limitations that are usually a drawback when using pressed discs (as in transmission) for kinetic studies for example.

Another characteristic that makes this technique attractive is the possibility to perform *in-situ* and even *operando* studies of reactions. The former term refers to the study of the catalyst under controlled atmosphere including the actual reaction mixture. Operando definition requires besides, the simultaneous measure of the conversion or a reaction rate alongside the spectroscopic data on the same cell and catalyst bed [41]. However, this last aspect is still under development since is the determination of an intrinsic reaction rate would require the careful consideration of the chemical engineering aspects of the reactors when designing the spectroscopic cells since normally they are not ideal reactors.

1.4 Aim of the thesis

The present research work was carried out in order to understand the interaction of ethanol with spinel-like catalysts having different composition and under different experimental conditions. The study was focused in the characterization of the species adsorbed on the surface of the materials by means of diffuse reflectance infrared Fourier transformed spectroscopy (DRIFTS). The parent project which is the frame for this study is the production of hydrogen by the steam-iron process here illustrated:
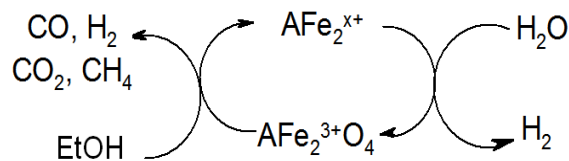
$$CO, H_2 \quad CO_2, CH_4 \quad EtOH \quad AFe_2^{x+} \quad AFe_2^{3+}O_4 \quad H_2O \quad H_2$$

Figure 1.4—1. Steam-iron process with Ethanol (A=Fe, Ni, Co, Cu)

The reduction of the ferrite by the ethanol is the first step of the cycle that, due to its endothermic nature, is crucial when choosing the operative temperature of the process. In order to optimize this step, it is necessary to understand the mechanism involved in the reduction process of the catalyst and how it is related to the structure, composition and/or to morphological characteristics. In this regard, in situ DRIFT spectroscopy combined with mass spectrometry is a powerful tool since it allows the identification of the species adsorbed on the surface of the catalyst and those desorbed as product of the reaction. This information can help to understand the differences in the reactivity of the catalysts and their product distribution which at the same time should guide the development of a more efficient catalyst for this important process.

The set of catalyst chosen to perform this study were modified ferrites with a general formula $A^{2+}Fe_2^{3+}O_4$ since they have showed good performance in the thermal reduction followed by hydrogen production. However, the idea in this case is also to use ethanol as a reducing stream which could help to decrease the operative temperatures and produce a lean gas that could have different uses depending on the composition. In order to compare and correlate the behavior of the different materials they were first characterized by means of x-ray diffraction (XRD), Raman spectroscopy, temperature programmed reduction (TPR) and surface area measurements.

2. Experimental methodology

2.1 Catalysts set

The aim of the parent research project is to find a catalyst able to perform efficiently the ferrite cycle with ethanol as reducing fuel, using for the reaction conditions as soft as possible. This particular research was focused on the characterization of the catalysts and in the study of the interaction of the ethanol with them. Materials investigated include $CoFe_2O_4$, $NiFe_2O_4$, $CuFe_2O_4$ and Fe_3O_4 (magnetite); these materials are expected to be good O^{2-}/electrons carriers and thus helpful for the cyclic reforming of ethanol.

2.1.1 Synthesis

The four catalysts were synthesized using a co-precipitation method. For the $CoFe_2O_4$ catalyst 250ml of a 2M solution of NaOH were added dropwise to 50 ml of a solution 1M of $Fe(NO_3)_2 \cdot 6H_2O$ and 0.5M of $Co(NO_3)_2 \cdot xH_2O$ at 50°C and pH>10. Afterwards the solution was kept under vigorous stirring for 3h and the precipitate was finally washed with water and filtered under vacuum. Same method was used for the other catalyst using $Ni(NO_3)_2 \cdot 6H_2O$ as the Ni^{2+} source and $Cu(NO_3)_2 \cdot 2,5H_2O$ for the Cu^{2+}. For the magnetite, the supplies used were $FeSO_4 \cdot 7H_2O$ (for the Fe^{2+}) and $FeCl_3$ (for Fe^{3+}).

The powders were dried at 120°C for 4h (for the magnetite the drying temperature is 80°C in order to avoid the oxidation of Fe^{2+} to Fe^{3+}). These compounds are the precursors of the final mixed oxides. In order to obtain the catalysts, these precursors are annealed in static air at 450°C for 8h (N_2 flow was used in the thermal treatment of the magnetite). Catalysts are labeled as shown in Table 3.

Table 3. Labels used for the different materials

M^{2+}	Precursor	Catalyst (after thermal treatment)
Co	CFp	CF450
Ni	NFp	NF450
Cu	CuFp	CuF450
Fe	FFp	FF450

2.1.2 Characterization

X-ray diffraction (XRD)

From the famous Brag-law it is known that diffraction of x-rays occurs at all the angles of 2θ simultaneously in powder samples. In order to obtain a diffraction pattern, the detector (in most designs) rotates to various 2θ angles to measure diffraction from the sample. Figure 2.1—1 is a schematic diagram of a powder X-ray diffractometer, showing the rotating detector [42]. The most common source of X-rays is the Cu or Mo X-ray tube.
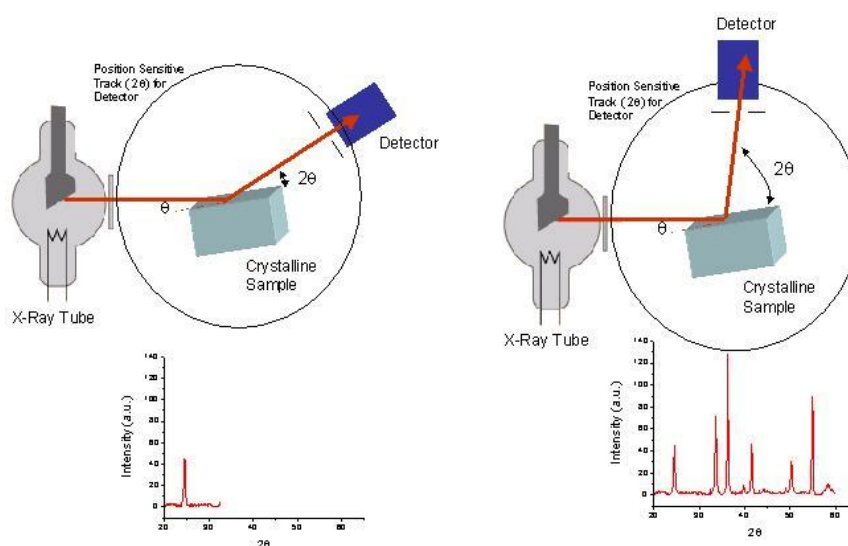

Figure 2.1—1. X-ray diffraction experimental setup scheme

In the present research this technique was used to determine if the synthesized catalysts had the expected inverse-spinel structure. XRD patterns in the range 10°<2θ<80° were recorded with a Philips PW 1050/81 apparatus controlled by a PW1710 unit (λ=0.15418nm (Cu), 40kV, 40mA). The scanning rate was 0,05°/s and step time of 1s.

The Debye-Scherrer equation was used for the calculation of crystallite dimensions, which is related to the FWHM (Full Width at Half Maximum) through the formula:

$$\tau = \frac{K\lambda}{\beta \cos \theta}$$

Where:

K is the shape factor which is dimensionless and has a typical value of about 0.9, but varies with the actual shape of the crystallite, λ is the x-ray wavelength, β is the line broadening at half of the maximum intensity (FWHM) in radians, θ is the Bragg angle and τ is the mean size of the ordered (crystalline) domains.

Surface area

The specific surface area was measured applying the single point BET method. The instrument used for this analysis was a Carlo Erba Sorpty 1700. The BET method (Brunauer Emmet Teller) calculates the surface area of the sample from the volume of the gas corresponding to the monolayer adsorption. The single-point approximation consists in the measurement of the pressure of adsorption and the corresponding gas volume adsorbed. The equation correlating this with the monolayer gas volume is:

$$\frac{P}{V(P_s - P)} = \frac{1}{V_m} \cdot \frac{P}{P_s}$$

Where P is the pressure, P_s is the surface tension of the adsorbed gas (nitrogen in this case), V is the adsorbed gas volume and Vm is the monolayer gas volume. The percent error that derives from these approximations is about 5% on values over 3 m^2; below this limit, the surface area calculated cannot be considered reliable.

In the analysis around 0.5g of the sample was placed inside the sample holder and then heated at 150°C under vacuum (4 Pa) in order for it release the water, air or other molecules adsorbed. Afterwards the sample was put in liquid nitrogen and the adsorption of the gaseous N_2 was carried out.

Temperature Programmed Reduction (TPR)

Temperature-programmed reduction (TPR) is a widely used tool for the characterization of metal oxides, mixed metal oxides, and metal oxides dispersed on a support. TPR is a method in which a reducing gas mixture (typically 3% to 17% hydrogen diluted in argon or nitrogen) flows over the sample. A thermal conductivity detector (TCD) is used to measure changes in the thermal conductivity of the gas stream. The TCD signal is then converted to concentration of active gas using a level calibration. Integrating the area under the concentration vs. time (or temperature) yields total gas consumed. Figure 2.1—2 shows an example of a TPR profile.
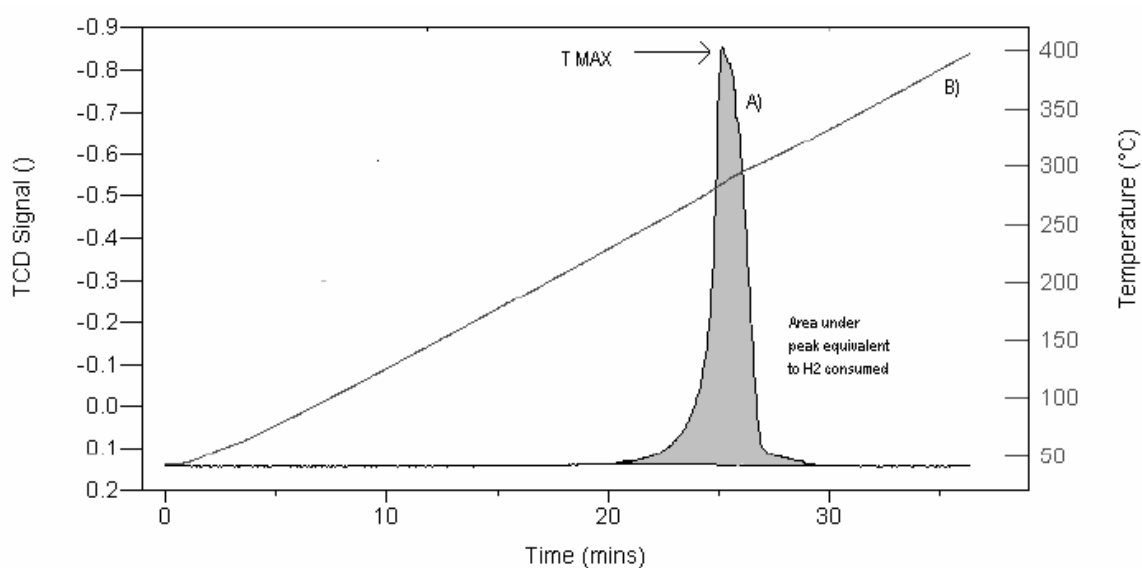

Figure 2.1—2. Temperature-programmed reduction profile for a metal oxide. Trace A displays the TCD signal output as a function of time. Trace B displays the temperature as a function of time during a 10 °C heating rate from ambient to 400 °C.

The figure illustrates a TPR spectrum where the peak maximum indicates the temperature that corresponds to the maximum rate of reduction. The TPR method provides a qualitative, and sometimes quantitative, picture of the reproducibility of the catalyst surface, as well as its high sensitivity to chemical changes resulting from promoters or metal/support interactions.

This analysis is important and attractive because it does not depend of a specific property of the catalysts besides having reducible specie. This technique is not restricted to the study of metal oxides but almost all data existing are related to this type of solids. The reaction of a metal oxide with hydrogen can be expressed as follows:

$$MO_{(s)} + H_{2(g)} \rightarrow M_{(s)} + H_2O$$
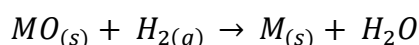
For most part of the oxides this reaction has a negative free standard energy. But even with positive energies it could be carried out if the value of the water vapor partial pressure is small enough now that in this case the term $\log\left(\dfrac{P_{H_2O}}{P_{H_2}}\right)$ would be negative and eventually can overcome the positive ΔG° in the equation:

$$\Delta G = \Delta G° + R * T * \log\left(\frac{P_{H_2O}}{P_{H_2}}\right)$$

The instrument used for this analysis was the TPD/R/O 1100 catalytic surface analyzer of Thermo Quest Company. The reducing gas was 5% H_2 in Ar. The temperature program started at 50 °C and then the temperature was increased at a rate of 10 °C/min until 650 °C were it was hold for 60 min.

Raman Spectroscopy

Using Raman spectroscopy is possible to observe the differences in the vibrational modes of the samples with respect to the composition which causes local distortions that are not seen by x-ray diffraction. Raman spectra were recorded using a Ranishaw spectrometer with a 514.5 nm Ar^+ ion laser source equipped with a microscope (50X lens was used). The power was 12.75 mW using 20 second exposure and 15 accumulations. The configuration to acquire this kind of spectra is similar to the one in Figure 2.1—3.
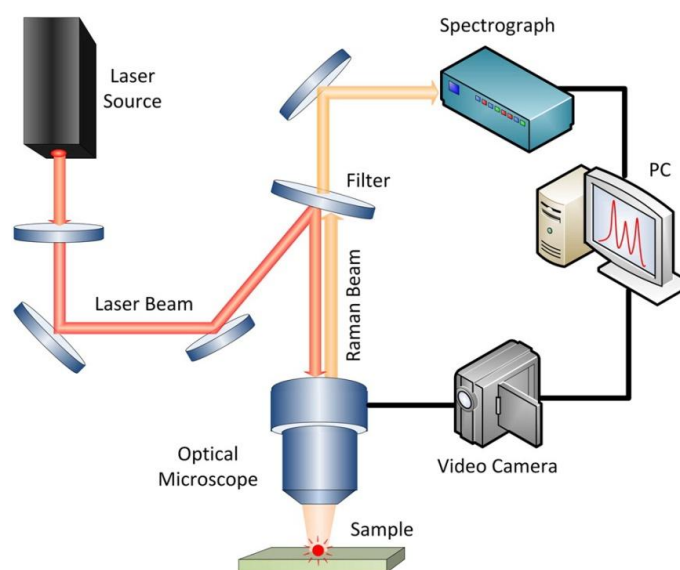

Figure 2.1—3. Raman spectrometer scheme

Diffuse Reflectance Infra-red Fourier Transform Spectroscopy (DRIFTS)

This technique was used to study the interaction of the ethanol with the different catalysts. The experimental setup is depicted in Figure 2.1—4. DRIFT-MASS scheme. First the sample is loaded in the sample holder and the cell is closed and inserted into the DRIFT apparatus. In order to feed the ethanol a system was adapted to the apparatus where the alcohol is loaded in a syringe which is pushed by a pump at the desired constant rate.

Subsequently, ethanol is vaporized in the heating jacket and mixed with the carrier gas flow (Ar); finally, this gas mixture reaches the inlet of the diffusion reflectance cell and passes through the catalysts. The outlet in this case is connected to a quadrupole mass analyzer.

During a standard procedure, the sample was heated at 450°C with an Ar flow (4.5 ml/min) for 45 min in order to remove molecules eventually adsorbed on the material. Then the sample was cooled down to room temperature and the IR background was collected. Right after, ethanol was fed until saturation was reached (as seen by IR and MS, around 15 min) and then Ar was left to flow until the weakly adsorbed ethanol was evacuated. When the mass and DRIFT spectra were not changing, the temperature was increased to 200 °C for 1.5 min and then cool down to 30 °C to record the spectra. This last step was repeated for the other temperatures (200, 250, 300, 350 and 400°C).
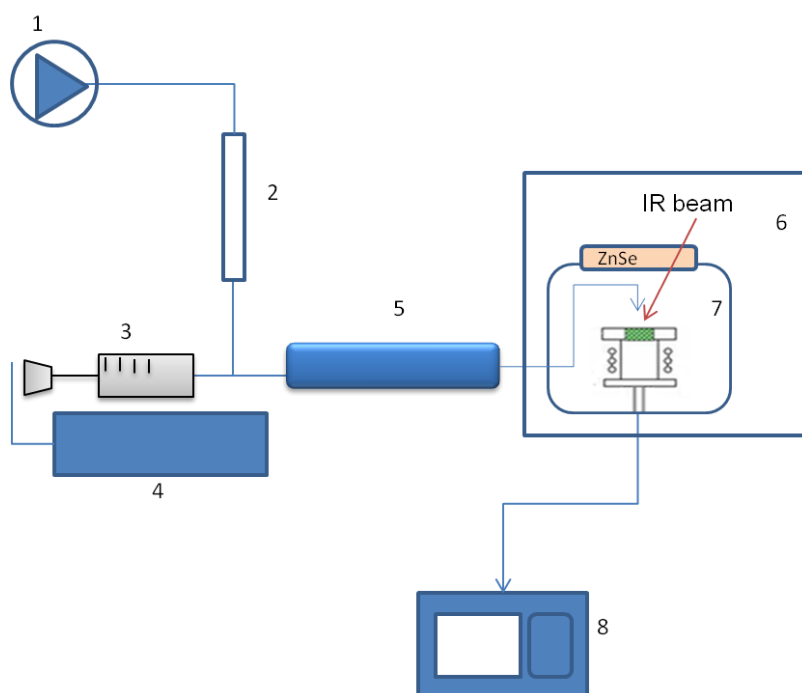

Figure 2.1—4. DRIFT-MASS scheme

1. Inert feed (Ar).
2. Bubble flow meter.
3. Syringe for liquid feed.
4. Syringe pump.
5. Heating stripe.
6. DRIFT apparatus
7. High temperature cell
8. MASS analyzer

Regarding the mass analysis, selected ions at the outlet of the DRIFTS apparatus were followed with time. Table 4 shows the m/z values detected and the correspondent characteristic products.

Table 4. Ions followed for the outlet of the DRIFTS

M/Z	Main Compound	Other compounds
2	Hydrogen	
16	Methane	
25	Ethylene	
28	Carbon monoxide	Ethylene, Ethane
29	Acetaldehyde	Ethanol, Ethyl ether
30	Ethane	
31	Ethanol	Ethyl ether
40	Argon	
41	Crotonaldehyde	Butene
43	Ethyl acetate	Acetaldehyde, Acetic acid Acetone
44	Carbon dioxide	Acetaldehyde
45		Ethanol, Ethyl ether, Acetic acid
56	Butene	
58	Acetone	
59	Ethyl ether	
60	Acetic acid	
61	Ethyl acetate	

3. Results

3.1 X-ray diffraction (XRD)

Cobalt-ferrite

Figure 3.1—1 shows the XRD pattern for the cobalt ferrite catalyst after calcination at 450 °C. From this pattern it can be deduced that the desired $CoFe_2O_4$ spinel phase was obtained and there is not segregation or transformation to other crystalline phases. The patter on the bottom, shown as a reference, is the calculated one for magnetite [43].
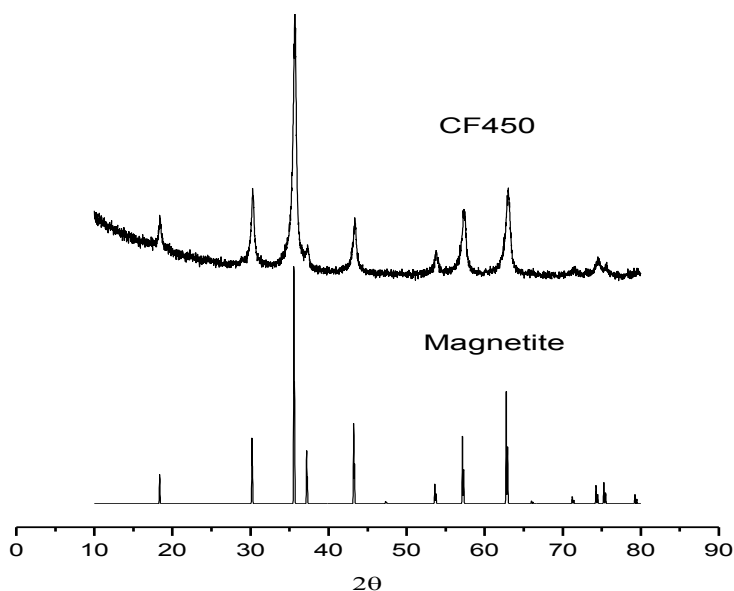

Figure 3.1—1. XRD pattern for the cobalt-ferrite catalyst calcined at 450°C (CF450) and the corresponding reference pattern for a ferrite spinel (magnetite).

Nickel-ferrite

The XRD pattern of the nickel-ferrite catalyst calcined at 450 °C is shown in Figure 3.1—2 also compared to the magnetite structure. It can be observed that is less crystalline than the one for the cobalt-ferrite but still it has the spinel structure and it does not show the presence of other phases.
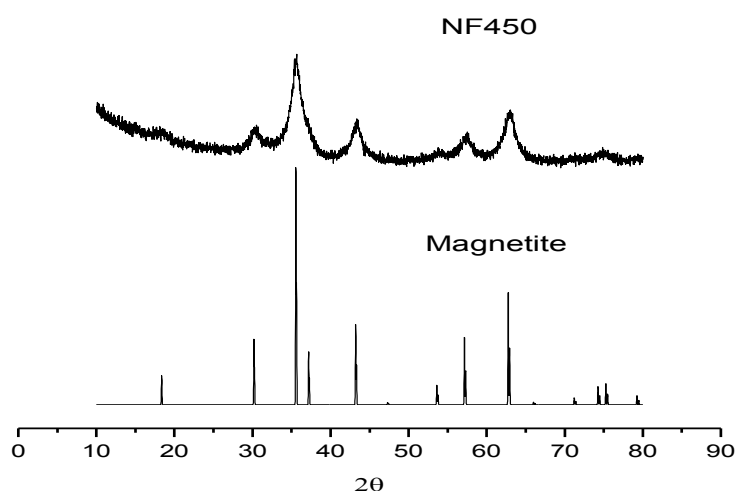
Figure 3.1—2. XRD pattern for the nickel-ferrite catalyst calcined at 450°C (NF450) and the corresponding reference pattern for a ferrite spinel (magnetite).

Copper-ferrite

The XRD pattern (Figure 3.1—3) of the copper-ferrite shows that the spinel phase was obtained. However, there is an extra peak in the XRD pattern that indicates that in this case part of the Cu is not incorporated into the structure. The peak was ascribed to CuO (Tenorite) whose calculated pattern is also shown for comparison [43]. The segregation of the copper oxide can be due to the differences in ionic radii of the Cu^{2+} with respect to the Fe^{2+} (see Table 5) and also to the distortions caused by the Jahn-Teller effect. For this reason, this kind of spinel is normally synthesized with *harder* methods as solid state reaction above 1000 °C obtaining crystalline materials but with low surface area.

Table 5. size and mass of the different divalent ions

Catalyst	O_h ionic radii[1]	Atomic mass
CF450	0.65	58.9
NF450	0.69	58.7
CuF450	0.73	63.5
FF450	0.61	55.8

[1]For the divalent metal in the $A^{2+}_{Oh}B^{3+}_{2(Oh,Th)}O^{2-}_4$ general formula of an inverse spinel [44]
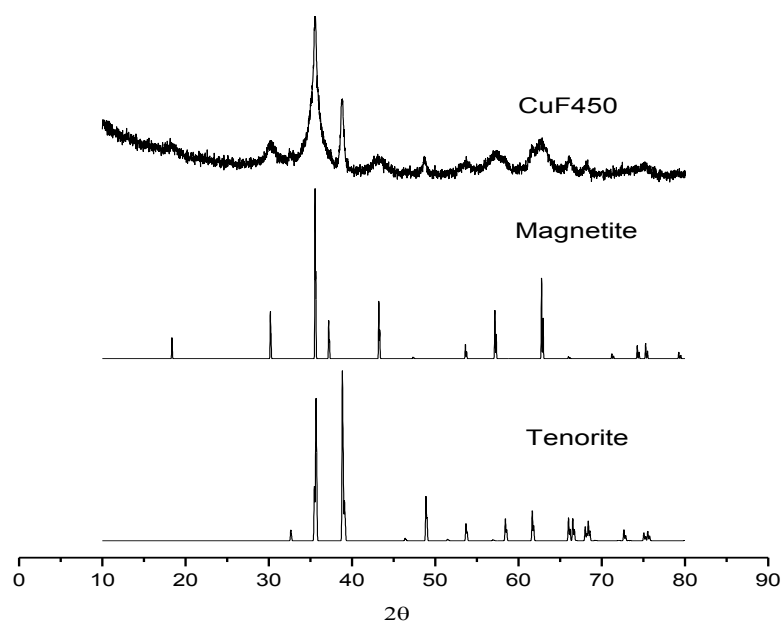
Figure 3.1—3. XRD pattern for the copper-ferrite catalyst calcined at 450°C (CuF450) and the corresponding reference pattern for a ferrite spinel (Magnetite) and copper oxide (Tenorite).

Magnetite

Figure 3.1—4 shows the XRD pattern for the unmodified ferrite catalyst after calcination at 450 °C. Also in this case the spinel phase was obtained.
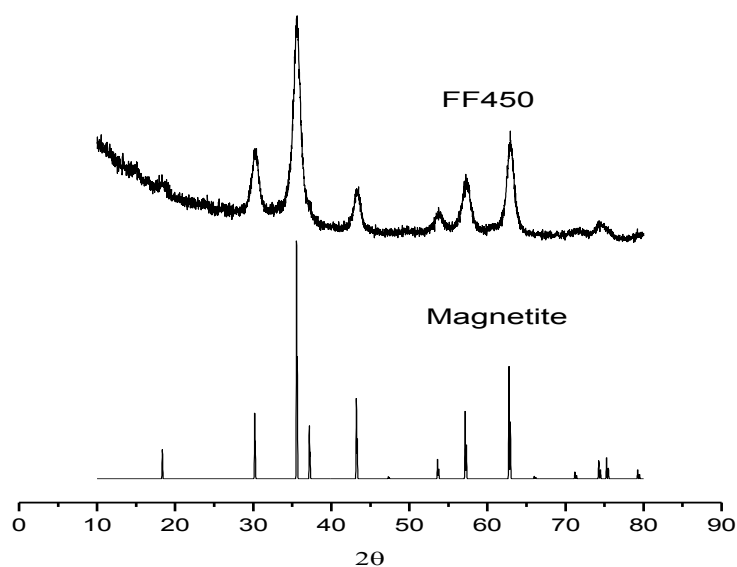

Figure 3.1—4. XRD pattern for the magnetite calcined at 450°C (FF450) and the corresponding literature reference pattern for this material.

3.2 Surface area

Table 6 shows the result of the surface area measurements for the fresh and calcined catalysts. The results show that all the ferrites have high surface area even after the thermal treatment. They all present similar SSA and crystallite size, which gives the possibility to compare the chemical differences without contribution from these morphological features. The results reported in Table 6 show a trend indicating that there is an inverse proportional relationship between the surface area and the crystallite size.

Table 6. Surface area and crystallite size results for the ferrites

Catalyst	Precursor Surface Area (m^2/g)	Catalyst surface area[a] (m^2/g)	Crystallite size[a] (nm)
CF	180	70	12
NF	197	94	7
CuF	177	75	8
FF	164	85	10

[a]For the material annealed at 450 °C 8h

3.3 Temperature programmed reduction (TPR)

From Figure 3.3—1 it can be deduced that the reduction profile is highly dependent on the ferrite composition. As a general fact it is observed that the presence of the different cations (Ni^{2+}, Co^{2+} and Cu^{2+}) has a positive effect on the reducibility with respect to the pure magnetite which agrees with the thermodynamic comparison previously discussed. Among them, CuF450 has a superior degree of reduction at lower temperature. However, as shown by x-ray diffraction, this sample is not a pure spinel but this first peak at low temperature could be assigned to the reduction of Cu, both in the spinel and in the segregated CuO according to the studies of Khan et al., in similar materials (spinel $Fe_{2.73}Cu_{0.27}O_4$ and CuO) [45].
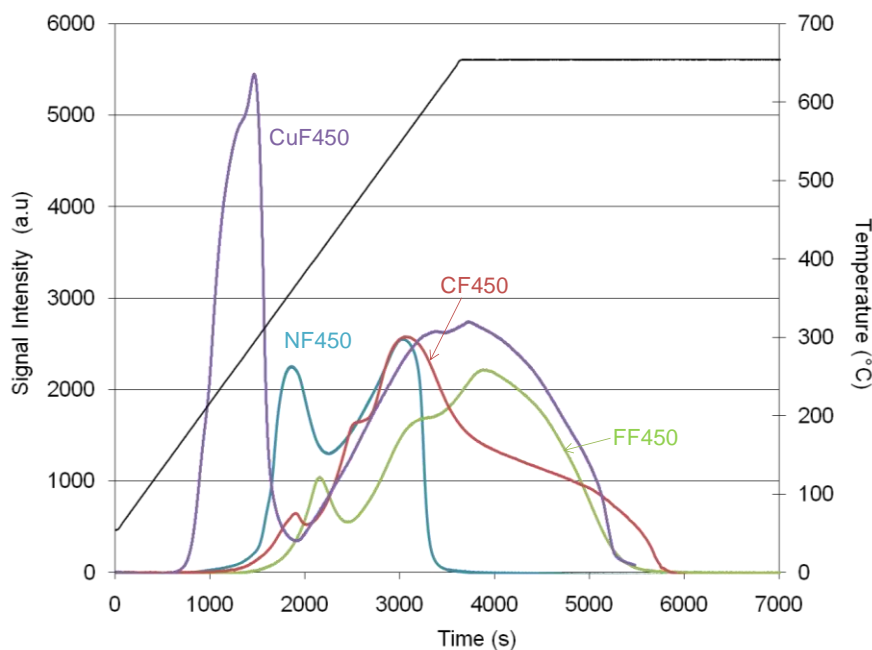
Figure 3.3—1. TPR profile upon hydrogen adsorption for the different catalysts

3.4 Raman Spectroscopy

Next paragraph describes the possible assignments of the normal modes of vibrations in ferrites according to the information collected by Hosterman [46]. In this assignment the main assumption is that the simplest unit of the spinel $(A^{2+}_{(Oh)}B^{3+}_{2(Oh,Th)}O^{2-}_4)$ is composed of two AO_4 tetrahedra and one B_4 tetrahedra as proposed by Waldron [47].

A_{1g}: Involves mainly oxygens moving away from the tetrahedral cation.

E_g: Symmetric bending motion of O anions within the AO_4 unit.

$F_{2g(1)}$: Complet translation of the AO_4 unit within the spinel lattice.

$F_{2g(2)}$: Translation along one direction of the lattice with the cation and oxygen moving in opposite direction.

$F_{2g(3)}$: Either antisymmetric AO_4 breathing or asymmetric bending motion of the oxygen bonded to the tetrahedral ion.

Even thought this assignment does not take into account the motion of the octahedral cation many researchers use it in assigning the vibrational modes [48-50]. However, taking into account that every oxygen atom is bound to three octahedral cations and only one single tetrahedral cation even if the cation remains at rest, the bonding force between octahedral cations and the oxygen atoms must be relevant for determining phonon energies.

This part of the characterization could help in this disclosure since in the structure of inverse spinels the tetrahedral cation should be the Fe^{3+} and the one changing is the octahedral one. However, this kind of study should be carried out much more carefully now that the spinels not necessarily have ideal cation distribution. Here, this technique was used just as an identification tool. Figure 3.4—1 shows the Raman spectra obtained for the catalysts annealed at 450 °C. The bands observed are collected and assigned in Table 7. The values are in agreement with previous reports in the literature for this type of materials [51-53].
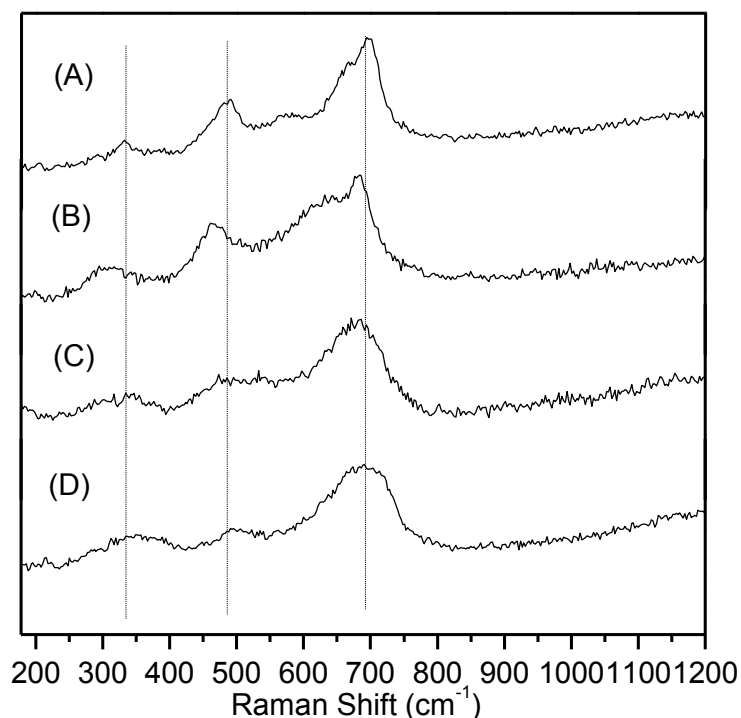

Figure 3.4—1. Raman Spectra for the catalyst calcined at 450 °C: NiF450 (A), CF450 (B), CuF450 (C), FF450 (D).

In the literature, there is not a general agreement regarding the assignment of the specific atomic motions within the spinel lattice during the Raman-active vibrations, especially in the inverse structure since they sometimes show active modes additional to the five predicted by group theory. Besides, the transition metal added can cause local distortions of the crystal lattice which usually are not detected by x-ray diffraction. Those local distortions of the structure respect to the pure magnetite depend upon the mass of the cations, the bonding forces, and the ionic radii. The idea with this type of studies on the differences of one structure with different composition helps to have an idea of which are the atoms involved in the vibration and their coordination.

Table 7. Assignation of the Raman-active vibration for the different catalysts

Catalyst	$F_{2g(1)}$	E_g	$F_{2g(2)}$	$F_{2g(3)}$	A_{1g}
NF450	204	330	485	582	694 670 sh
CF450	199	295	461		685 645 sh
CuF450	175	346	476	532	672
FF450	214	350	495		690

As observed from the graph and the table, the most intense mode of vibration is the A_{1g} and it is supposed to be related to the AO_4 stretching which means that it should be the same for all the samples since is the Fe^{3+} the one occupying this tetrahedral sites, so the small shift among them is an indication that in fact the ion in octahedral coordination has also influence in this mode. This mode of vibration has a shoulder in the case of the NF450 and CF450 which has been interpreted as the result of the distinct AO6 and BO6 octahedral units within the inverse lattice. The magnetite on the other hand does not present these two features but this is due to the fast electron transfer between the Fe^{3+} and Fe^{2+} cations occupying the octahedral sites. As a result, a valence of $Fe^{+2.5}$ is often quoted for the octahedral site of Fe_3O_4 [46].

On the other hand, the shift observed for the $F_{2g(2)}$ mode is bigger so it might be that this one is more sensitive to the divalent cation in the octahedral coordination which has not been documented in detail in the literature. For the other vibrational modes the intensity is not enough to make an unambiguous assignment. A deeper study on the assignment of the vibrational modes is beyond the scope of this research but following the shifts in frequencies of some Raman-active modes while the metal cations within the spinel lattice are exchanged gives information about the dependence of the lattice vibrations on the tetrahedral and octahedral coordination and this could be helpful in a future in-situ study of the reaction by Raman spectroscopy.

For the ferrite modified with Ni, the Raman spectra was taken for the samples calcined at 320, 450 and 750 °C as presented in Figure 3.4—2. From there it is evident that an increase in the thermal annealing temperature produces more intense bands without any significant shift of the frequencies for the different vibrational modes. Thus, morphological factors as crystallite size and surface area should not affect the position of the main vibrational modes if the structure and the composition remain the same.
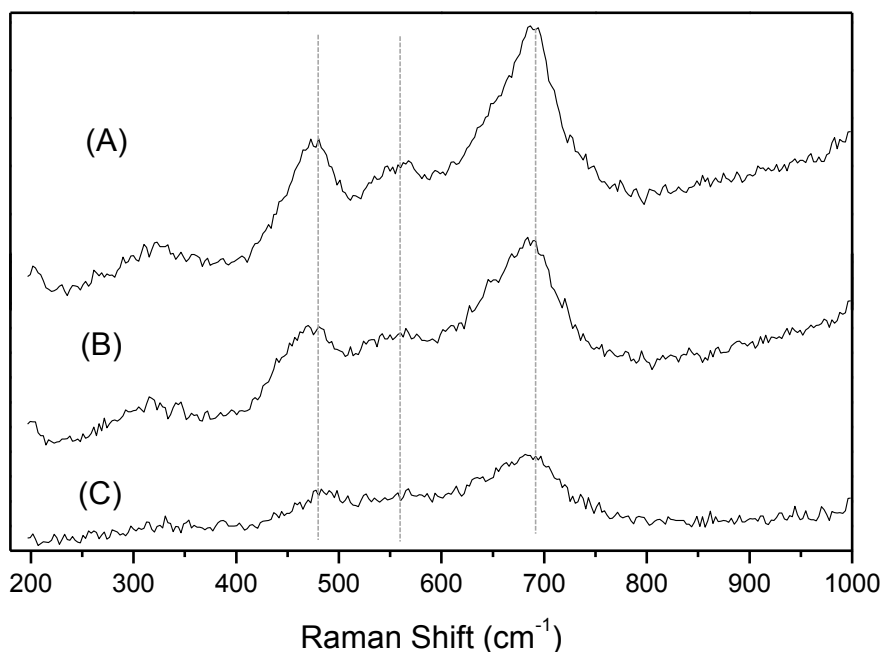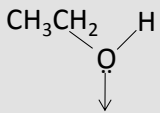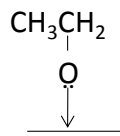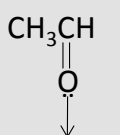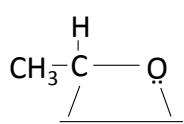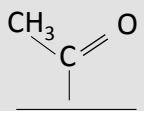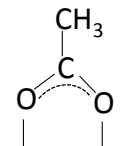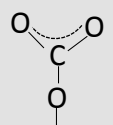

Figure 3.4—2. Raman spectra for the NiFe$_2$O$_4$ annealed at 750°C (A) 450 °C (B) and 320 °C (C)

3.5 Diffuse Reflectance Infrared Fourier Transform Spectroscopy (DRIFTS)

The adsorption of alcohols over metal oxides can lead to different kind of adsorbed species depending on the surface properties of the material under study. Table 8 shows the most representative intermediates and collects the characteristic infrared bands for the adsorption of ethanol according to the literature [54-56] and the observations during this research. In general there is an agreement on the way that ethanol adsorbs at low temperature which is mainly as an ethoxide.

Table 8. Common species upon adsorption of ethanol on catalysts surfaces

Specie		Characteristic frequency (cm^{-1})
Adsorbed ethanol	CH_3CH_2 — H, O	3200-3700 OH ν 1380 CH_3 δ 1270 OH δ
Adsorbed ethoxide	CH_3CH_2, O	2970 CH_3 $\nu_{(as)}$ 2930 CH_2 $\nu_{(as)}$ / CH_3 $\nu_{(s)}$ 2875 CH_2 $\nu_{(as)}$ 1107 CO $\nu_{(as)\ monodent}$ 1065 CO $\nu_{(as)\ bident}$ / CC $\nu_{(as)}$
η^1-Aldehyde	CH_3CH, O	1650-1700 CO ν
η^2-Aldehyde	CH_3—C(H)—O	2755 CH ν 1348 CH_3 δ 1275 CO ν 1148 CC ν 972 CH_3 ρ
Acyl	CH_3—C=O	2978 CH_3 $\nu_{(as)}$ 2901 CH_2 $\nu_{(as)}$ / CH_3 $\nu_{(s)}$ 1636 CO ν
Acetate	CH_3—C—(O, O)	1547 OCO $\nu_{(as)}$ 1445 OCO $\nu_{(s)}$ 1338 CH_3 $\delta_{(s)}$
Carbonate	O—C—(O, O)	1547 OCO $\nu_{(as)}$ 1318 OCO $\nu_{(s)}$

However, the species formed and the pathway followed when increasing temperature is more related to the surface chemistry of each catalyst and there is not a general rule. The next sessions are the discussion of the species observed during the ethanol adsorption and transformation with the temperature over the 4 materials studied and at the end there is a comparison of the products detected and the proposition of the route followed in each case.

3.5.1 Session I: Room temperature adsorption of ethanol and its transformation + temperature programmed desorption (TPD)

The idea of this part of the research is to extract information on the way ethanol interacts with the different materials. The reason why this kind of experiments are performed at lower temperature with respect to the normal ones used during the reaction is because at high temperature the equilibrium favors the desorption, on the contrary, working in this way some intermediates can be "caught" and it is possible to observe them as explained by Busca et. al in a review about infrared studies of the mechanisms of activation of C-H bonds on oxidation catalysts [57]. Moreover, this experimental condition is useful since it gives a picture of the reactivity of the "clean" surface, without any coke accumulation which is the aim when developing a catalyst since coke is the main cause of deactivation.

DRIFTS: The sample was pretreated under Ar at 450 °C for 1h. Next, the sample was cooled down to room temperature (30 °C) and the ethanol was fed at 0.6 μl/min until saturation was reached (as seen by IR and MASS) and then the sample was flushed for around 40 min with Ar to remove the weakly adsorbed ethanol. Afterwards the temperature was increased to 150 °C for 2 min and then cooled down again to 30 °C to take the spectra. The same procedure is subsequently performed for the other temperatures, going back to room temperature every time to take the spectra (adapted from [33]).

TPD: The adsorption of ethanol was done in the same way than for the DRIFTS measurements but desorption was done at a constant rate of 5°C/min until 450 °C and hold at this temperature for around 30 min more.

NF450

Figure 3.5—1 shows the resulting DRIFT spectra for the NF450 catalyst. The spectra on the bottom corresponds to the adsorption of ethanol at room temperature (T=30 °C) here the observed bands correspond to H-bonded ethanol (mainly broad absorption between 3000-3500 cm^{-1} for the OH stretching, 1383 for the δCH$_3$ deformation and a weak band at lower frequency –around 1270- for the δOH) and bands of ethoxides (as the product of ethanol dissociation including the C-C and C-O stretching around 1056 cm^{-1} and 1100 cm^{-1}). Also those bands at 2970, 2926 and 2865 cm^{-1} are the characteristic CH bands associated with ethoxides (CH$_{3v(a)}$, CH$_{2v(a)}$ and CH$_{3v(s)}$) [58].
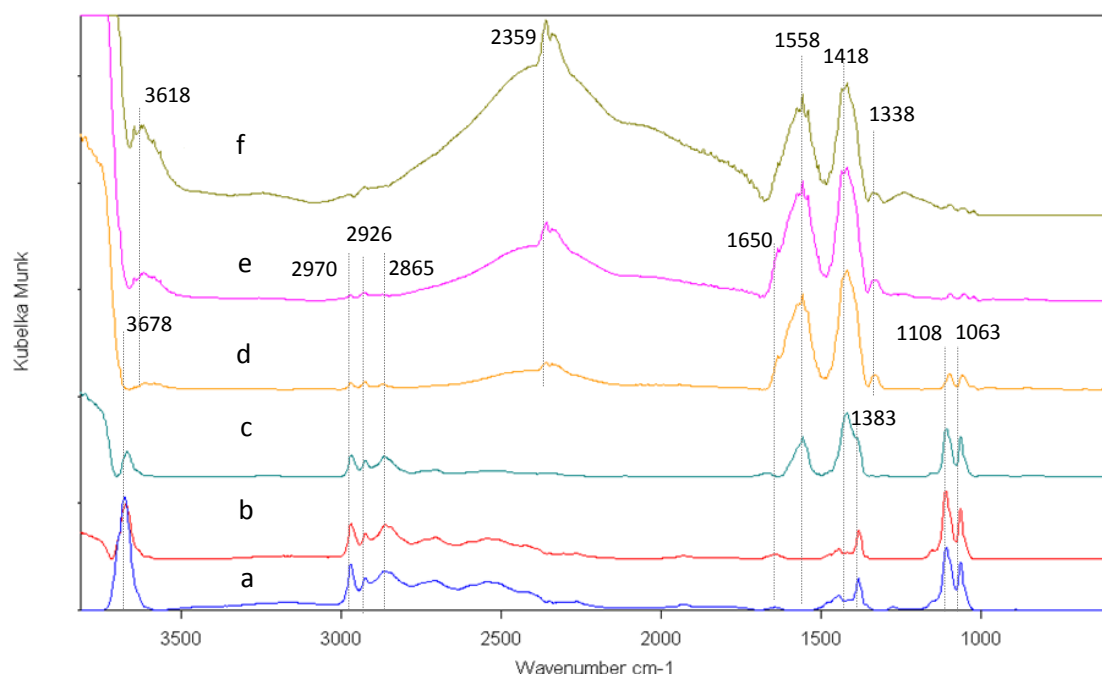

Figure 3.5—1. DRIFT spectra for the NF450 catalysts after ethanol adsorption at 30 °C (a) and desorption at 150 (b), 250 (c) 300 (d) 350 (e) and 400 °C (f).

When increasing the temperature some bands at 1338, 1418, and 1558 cm^{-1} reveal (very broad the last two). These bands can be assigned to the vibrational modes of acetate species (δCH$_3$, OCOv$_s$ and OCOv$_{as}$ respectively) [59]. The broadening of the band at 1558 cm^{-1} suggest carbonate formation which also would have the OCO stretching at this wavenumber [60].

These species could further produce CO_2 which is seen through the band around 2359 cm^{-1}. The shoulder around 1700-1650 cm^{-1} can be assigned to the C=O stretching of acetaldehyde, which can be rapidly oxidized to acetate species, as suggested earlier by Yee et al. [30]. The very broad feature formed in the range 3000-1800 in spectra d-f may be indicative of partial reduction of the catalyst resulting in electronic absorption [40].

The temperature programmed desorption (TPD) of ethanol for this catalyst is presented in Figure 3.5—2. As discussed before, ethanol adsorbs either forming an hydrogen bond or it can be dehydrogenated to form ethoxy species (Eq. 1) in both forms it can be reversibly desorbed as observed when the temperature increases until almost 300 °C. Acetaldehyde is also observed at low temperature, its formation can be due to ethanol oxidative dehydrogenation (Eq. 2) (water is also observed in this temperature range). Also in the low temperature range it is worth to notice that ethane appears and that its trend is similar to the acetaldehyde so this could be an indication of an ethanol disproportionation into acetaldehyde and ethane like a sort of self-Meerwein-PV reduction by ethanol (a reaction that might be catalyzed by the "basicity" of the spinel) (Eq. 3).
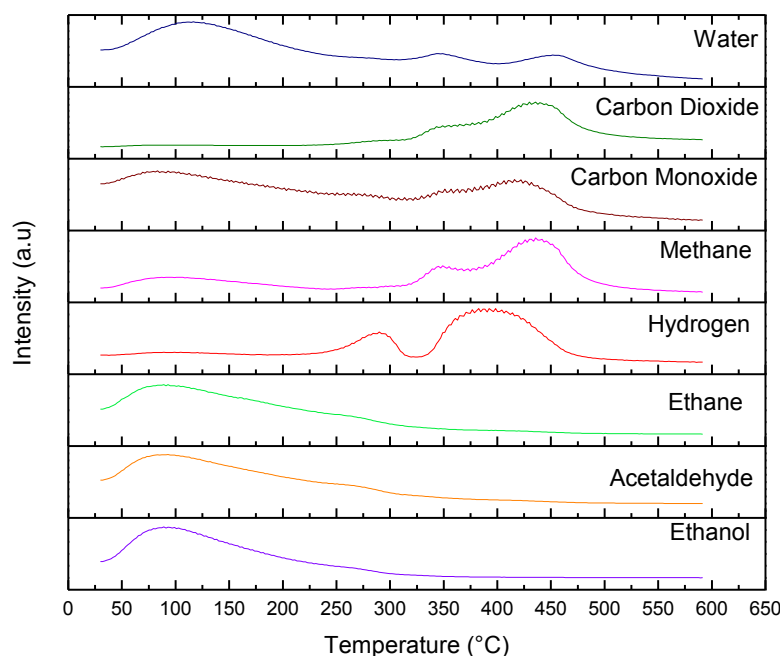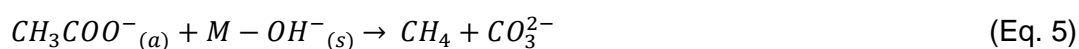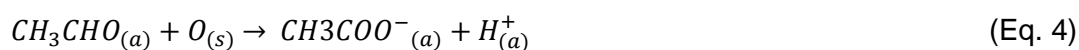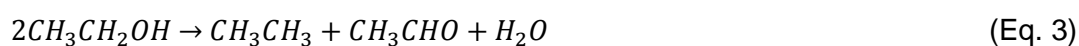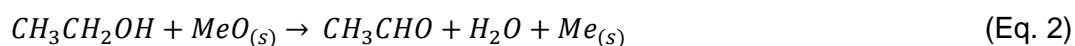

Figure 3.5—2. Ethanol TPD for the NF450 catalyst

The figure also shows that around 230 °C there is a desorption of hydrogen that could correspond to the release of the hydrogen produced during acetaldehyde formation. In this T range, DRIFT experiments highlight also the formation of acetates; the oxidation of acetaldehyde into acetates occurs by reaction of the aldehyde with the oxygen from the solid (Eq. 4). After 315 °C there is desorption of methane that could be related to the formation of the carbonate species from the acetates that is observed also by the DRIFTS (Eq. 5). The very similar trend of CO_2 and CH_4 supports this hypothesis. A similar behavior is also shown by CO, which indicates that also acetaldehyde is being decomposed into methane and CO. As mentioned before, the carbonate species can be further transformed to carbon dioxide.

The desorption in different steps of CO_2, CH_4, H_2, CO and H_2O, indicates that the formation of such products involve several reactions, they can include reverse and direct water gas-shift reaction (Eq. 6) which is a reversible reaction but being slightly exothermic, the direct way is not so favored at high temperature; but also reactions like methane reforming and CO oxidation can be involved (Eq. 7 and 8)[1].

$$CH_3CH_2OH \rightarrow CH_3CH_2O^-_{(a)} + H^+_{(a)} \qquad \text{(Eq. 1)}$$

$$CH_3CH_2OH + MeO_{(s)} \rightarrow CH_3CHO + H_2O + Me_{(s)} \qquad \text{(Eq. 2)}$$

$$2CH_3CH_2OH \rightarrow CH_3CH_3 + CH_3CHO + H_2O \qquad \text{(Eq. 3)}$$

$$CH_3CHO_{(a)} + O_{(s)} \rightarrow CH3COO^-_{(a)} + H^+_{(a)} \qquad \text{(Eq. 4)}$$

$$CH_3COO^-_{(a)} + M - OH^-_{(s)} \rightarrow CH_4 + CO_3^{2-} \qquad \text{(Eq. 5)}$$

$$CO + H_2O \rightarrow CO_2 + H_2 \qquad \text{(Eq. 6)}$$

$$CH_4 + H_2O \rightarrow CO + 3H_2 \qquad \text{(Eq. 7)}$$

$$CO + O_{(s)} \rightarrow CO_2 \qquad \text{(Eq.8)}$$

---

[1] In the series of equations the subscript (a) stands for adsorbed and (s) for solid

CF450

In the case of the catalyst modified with Co (CF450) the DRIFT spectra shows that at room temperature ethanol is H-bonded to the surface (band at 3253 cm^{-1}) and also the ethoxy bands appear (1102 and 1060 cm^{-1} for the C-O stretching and bands at 2972 and 2881 cm^{-1} for the $CH_{3v(a)}$, and $CH_{3v(s)}$) [58]). The band at 1682 cm^{-1} indicates the presence of adsorbed acetaldehyde as a product of ethanol oxidative (or direct) dehydrogenation and ethanol disproportionation as discussed before for the NF450 catalyst. When the temperature is increased it can be observed the decreasing in the intensity of the ethanol and ethoxy bands and the disappearance of the acetaldehyde signal. No acetate or other intermediate species were observed to be formed in the surface, indicating a different pathway than for the NF450 catalyst.
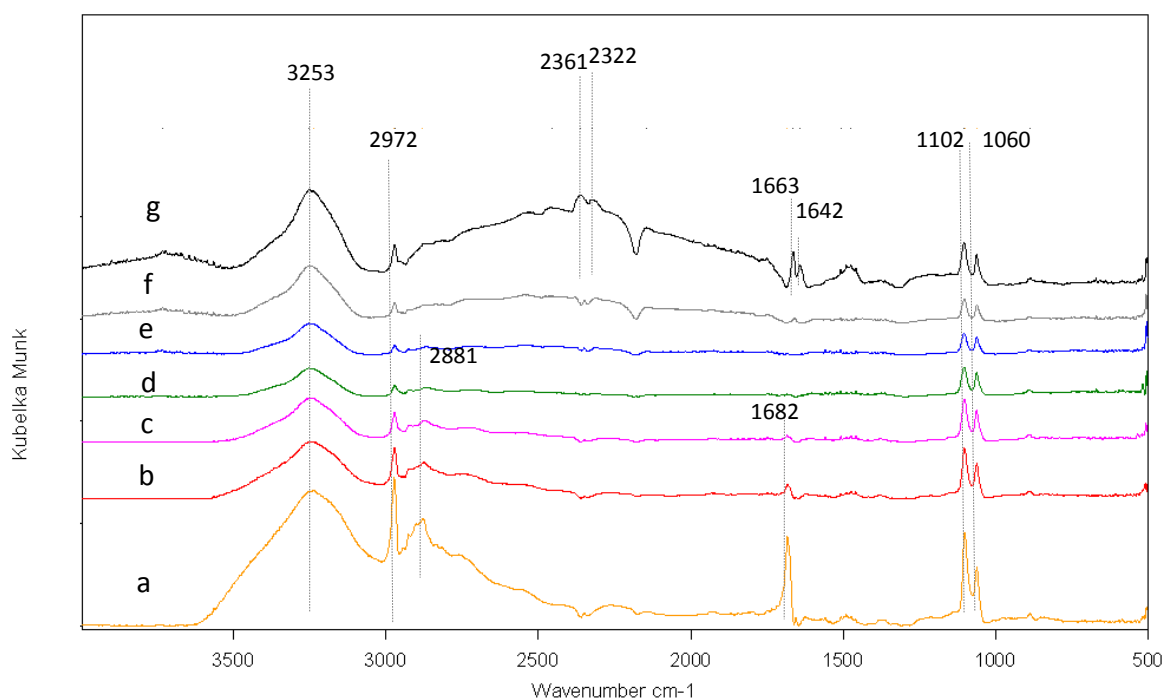

Figure 3.5—3. DRIFT spectra for the CF450 catalysts after ethanol adsorption at 30 °C (a) and desorption at 150 (b), 200 (c) 250 (d) 300 (e) and 350 (f) and 400 °C (g).

During the ethanol TPD for the CF450 catalyst (Figure 3.5—4) at low temperature some methane and CO are observed and this can be due to the decomposition of acetaldehyde as observed also for the NF450 catalyst.

There is also hydrogen release between 250-300 °C that might be formed by ethanol dehydrogenation into acetaldehyde (which occurs over the entire T range) but hydrogen remains adsorbed and is desorbed in this range as observed also by Noronha et al [61]. In the high temperature range (T > 300 °C) the event occurring is the formation and desorption of carbon monoxide, methane, carbon dioxide and water with the maxima around 452 °C. This indicates that the adsorbed species (ethanol, ethoxy and acetaldehyde) are being decomposed and oxidized but at higher temperature than for the NF450 catalyst.

It is worth noting that the DRIFT experiments highlighted that there was no formation of acetates; this agrees with the results of TPD experiments. In fact, the amount of methane and CO_2 formed with the CF450 catalyst (both products being formed by acetate decomposition) is lower than with the NF450 catalyst (see Figure 3.5—9). On the other hand, there was not H_2 desorption in the high temperature range. These observations indicate that with the CF450 spinel the acetaldehyde formed by ethanol dehydrogenation is more weakly bound to the surface than with the NF450. Therefore, with CF450 most acetaldehyde desorbs into the gas phase (in fact, the signal for acetaldehyde is bigger with CF450 than with the rest of catalysts as seen in Figure 3.5—9), whereas with NF450 the aldehyde is more strongly bound to the surface, and easily oxidized into acetates and finally decomposed in the high-T range.
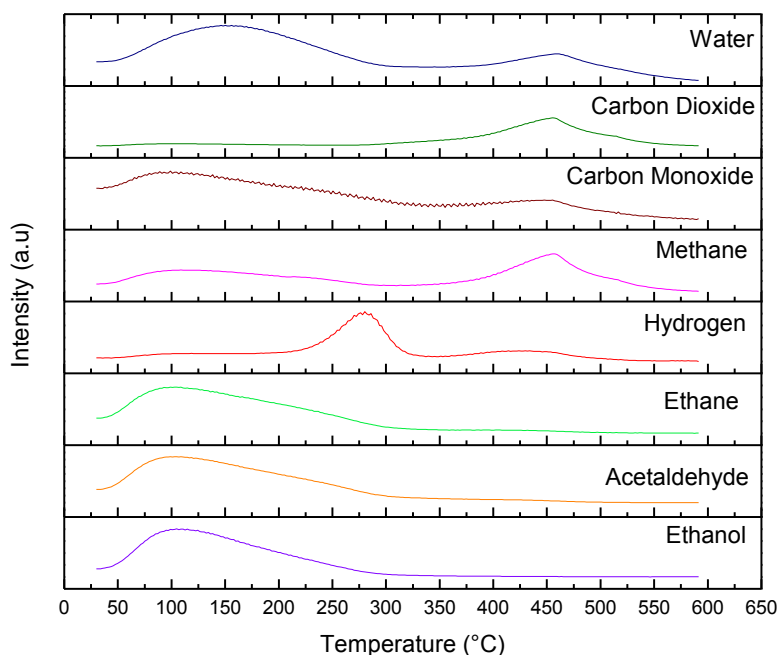

Figure 3.5—4. Ethanol TPD for the CF450 catalyst

CuF450

The DRIFT spectrum for the CuF450 catalyst is shown in Figure 3.5—5. Regarding the adsorption at low temperature, the behavior is not different from the other ferrites, meaning that ethanol is attached to the surface either in a molecular form or dissociated as an ethoxide seen at 1064 and 1106 cm^{-1}. Already at 250 °C there are new bands, the most prominent at 1252 cm^{-1} can be attributed to adsorption of acetaldehyde in the η^2 configuration which is favored over the partially reduced sample [62].

Afterwards (at 300 °C) it appears an important band at 1643 cm^{-1} and some small ones at 2126 cm^{-1} and 2182 cm^{-1} corresponding to the formation of acyl species and their decomposition product that includes CO and methyl species adsorbed (Eq. 9) which can recombine to release ethane. Formation of ethane was also observed by Padilla et al. [63], This assignment is in agreement with the TPD results performed for this sample (see Figure 3.5—6).

$$CH3CO_{(a)} \rightarrow CO_{(a)} + CH_{3(a)} \qquad\qquad \text{(Eq. 9)}$$

Regarding the TPD (Figure 3.5—6), the low temperature behavior of the CuF450 catalyst has a trend similar to the other catalysts but in the middle range temperature (200-350 °C) there is ethane released as expected according to the DRIFT spectrum interpretation. Moreover, in this temperature range all the other catalysts desorbed certain amount of hydrogen but it is not the case for the CuF450, on the contrary, the hydrogen signal starts to decrease. In the high temperature range (> 350 °C) mainly carbon dioxide and methane are observed, the last one possibly due to hydrogenation of the remaining CH$_3$ species.
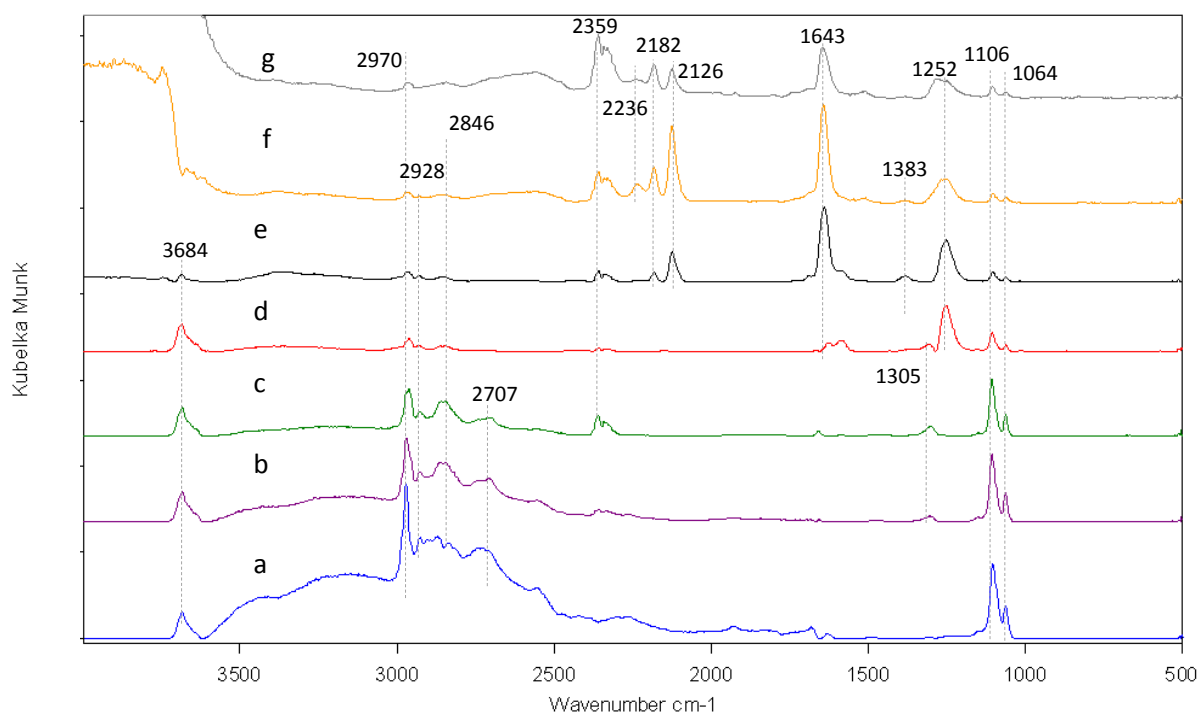
Figure 3.5—5. DRIFT spectra for the CuF450 catalysts after ethanol adsorption at 30 °C (a) and desorption at 150 (b), 200 (c) 250 (d) 300 (e) and 350 (f) and 400 °C (g).
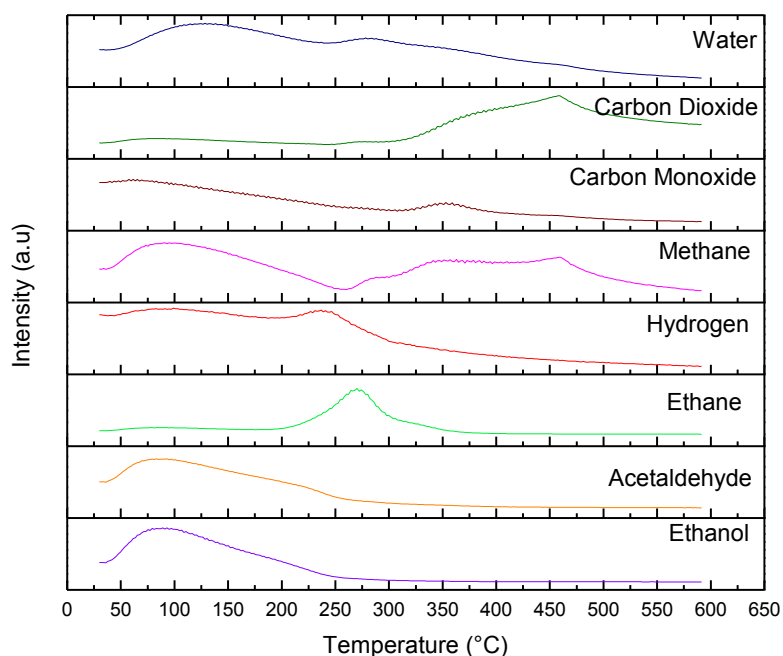

Figure 3.5—6. Ethanol TPD for the CuF450 catalyst

FF450

Adsorption of ethanol was also studied for the magnetite, the resulting spectrum is shown in Figure 3.5—7 and at room temperature once again the ethoxy-bands can be observed (1063 and 1109 cm^{-1} for the C-O/C-C stretching) together with the bands for undissociated ethanol (mainly 1380 cm^{-1} for δCH_3). When increasing the temperature the acetate bands start to be bigger (1342, 1421 cm^{-1} for the δCH$_3$ and OCOv$_s$) and at 300 °C there is a band at 1265 cm^{-1} that could indicate that aldehyde in the η^2 is being adsorbed. The main difference of this spectrum with the other ones is the very broad feature formed in the range 3000-1800 cm^{-1} that could be an indication of partial reduction of the catalyst.

This optical behavior for slightly reduced oxides has been attributed to electronic absorption and it is observed mainly when they become non-stoichiometric even due to simply outgassing at high temperature as stated by Busca [40]. It is also at this temperature (> 300 °C) where the oxidation products appear in the TPD experiments (Figure 3.5—8).
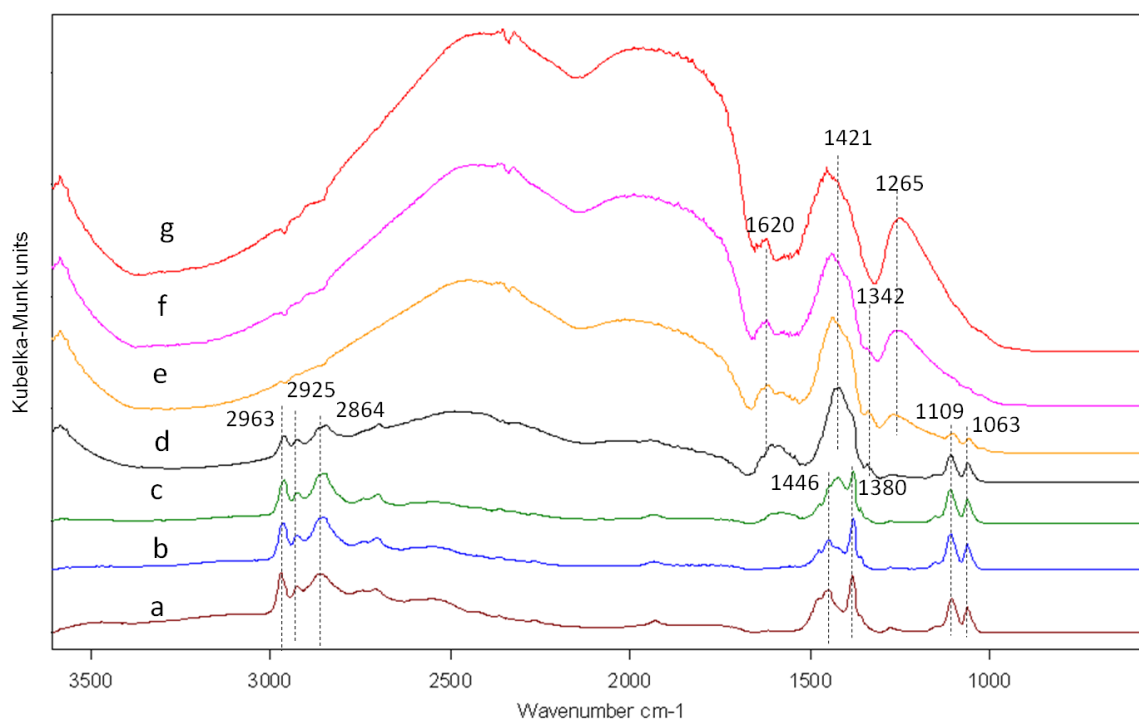

Figure 3.5—7. DRIFT spectra for the FF450 catalysts after ethanol adsorption at 30 °C (a) and desorption at 150 (b), 200 (c) 250 (d) 300 (e) and 350 (f) and 400 °C (g).

The behavior at low temperature for the TPD in this case is similar to the other materials discussed before with the hydrogen desorption around 272 °C due to ethanol dehydrogenation. At higher temperature there is a big desorption of CO_2 with a maxima around 340 °C which agrees with the observed reduction in the DRIFT spectra. Also methane, CO and water are observed in this temperature range and as in the case of the CF450 catalyst this can be explained by the decomposition of acetaldehyde and direct oxidation to CO_2 and water.
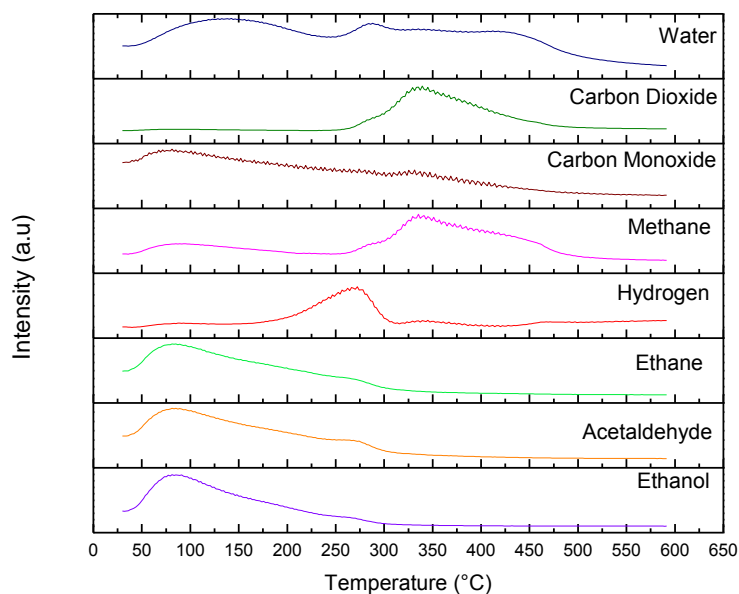

Figure 3.5—8. Ethanol TPD for the FF450 catalyst

Comparison

Figure 3.5—9 shows the desorption profile of each compound compared for the different catalysts. Several observations can be made from this comparison. About the NiF450 it can be observed that is the only one that forms hydrogen both in the low and high temperature range. Also the CO, CO_2 and CH_4 production are clearly separated in at least two steps suggesting that their formation comes from different reactions. In the case of CF450 catalyst, it seems that it adsorbs more ethanol than the others but it desorbs it mainly as acetaldehyde at low temperature. The decomposition and oxidation products start to appear at higher temperatures than for the other ferrites. For the CuF450 the most particular characteristic is the release of a high amount of ethane in the middle temperature range and also the fact that it does not desorbs hydrogen. Finally, the FF450 is the one producing more CO_2 and water and also some decomposition products even at lower temperatures than the rest of the materials studied.
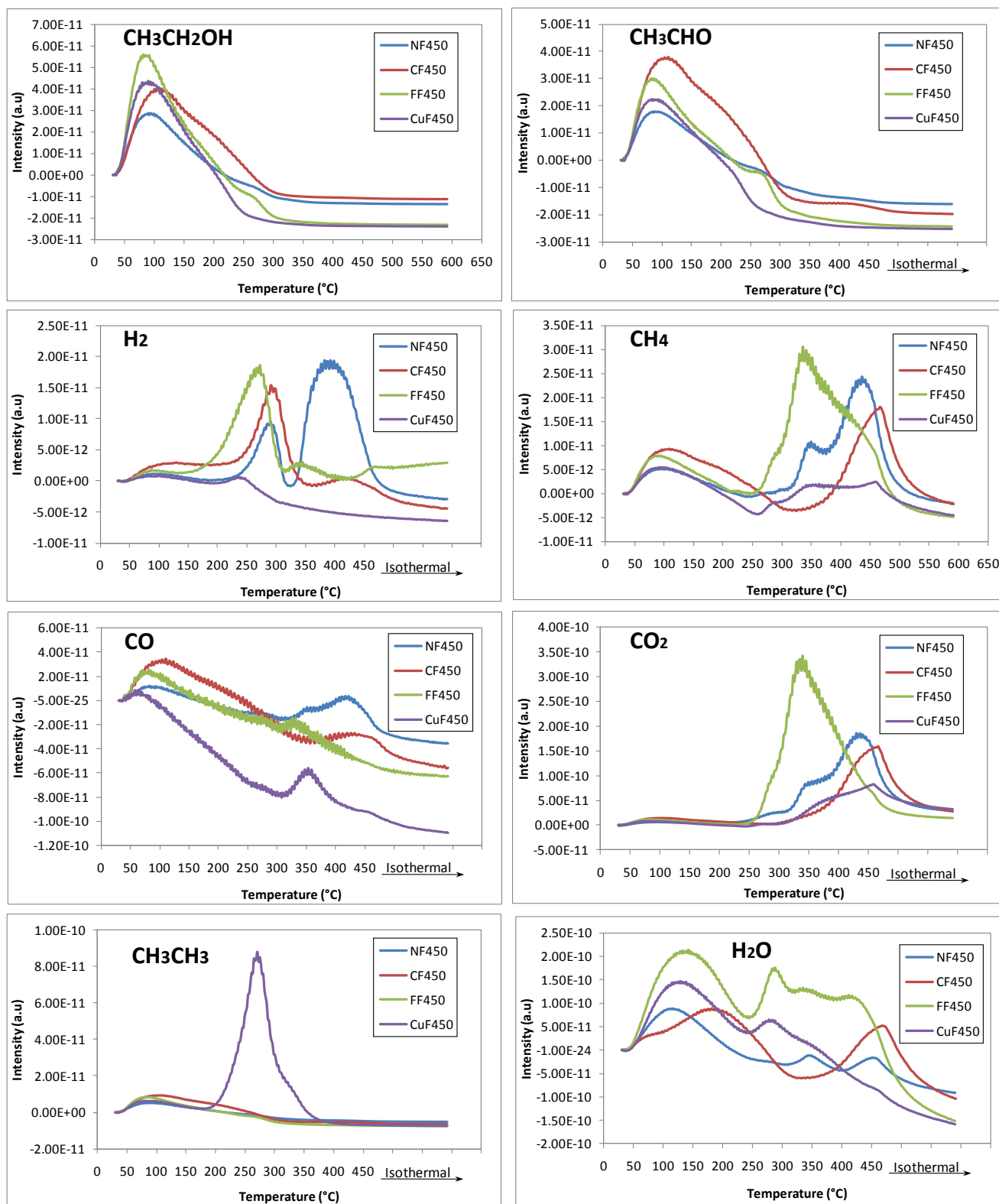
Figure 3.5—9. Desorption profile (TPD) of each product in the different catalysts

Proposed pathways

Figure 3.5—10 present the route proposed for the adsorption and transformation of the ethanol in the different catalysts according to information discussed before. The first part of the scheme corresponds to the low temperature range of reaction and is not delimited because is common for the set of materials. It includes the adsorption of ethanol as ethoxide and some disproportionation of it to give the ethane observed on the TPD. Then the acetaldehyde can be adsorbed in the η^1 or η^2 configuration being the first one less strongly bound to the surface and then easily desorbed or transformed (sometimes not even detected on the surface) and the second one can be observed at higher temperatures in the partially reduced surface of some catalysts.

A) NiF450: the acetaldehyde is easily oxidized into acetates as observed by the DRIFTS, the acetates are further decomposed to methane and carbonates that are released as CO_2. The formation of more CO_2 and hydrogen (which is only observed for this catalyst) could be due in some extent to the water-gas shift reaction or methane reforming and CO oxidation.

B) CF450: In this case the acetaldehyde is even observed at low temperature which means is not so reactive on this surface; only at high temperature the decomposition and oxidation products were observed. Also the ethoxides were more stable on this surface.

C) CuF450: For this catalyst it was possible to observe in the spectra the adsorption of acetaldehyde in the η^2 configuration and its transformation to acyl species that are further decomposed to CO and methyl species that recombine to form ethane which was detected by TPD and at higher temperature CO_2 and CH_4 were also observed and they had the same trend.

D) FF450: The acetate bands were also detected for this catalyst when increasing the temperature together with a band attributed to η^2-acetaldehyde. In contrast to the NF450 catalyst, in the high temperature range no carbonate bands were detected on the DRIFTS and no hydrogen release was observed in the TPD so it is more likely to be a direct oxidation and decomposition of both acetaldehyde and acetates.
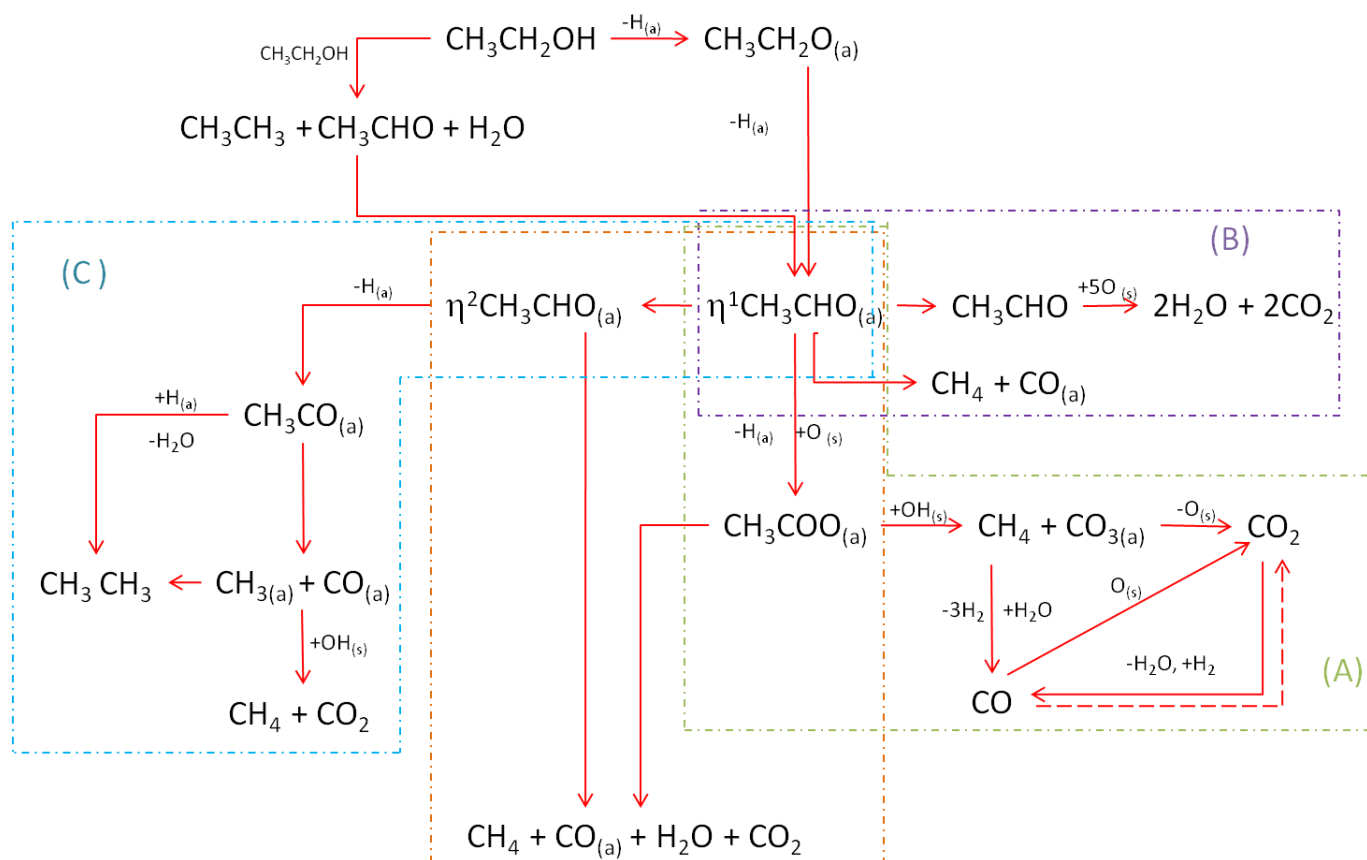
Figure 3.5—10. Ethanol adsorption and transformation over NF450 (A) CF450 (B) CuF450 (c) and FF450 (D).

Remarks: From the previous discussion, it is clear that the composition of the catalysts has a big effect in the way the ethanol is adsorbed and transformed. At this point it is possible to make some hypothesis on the behavior of each catalyst during the reductive step of the cycle.

For example, one of the problems of the cycle is to find a material which can offer a good compromise between the high temperature which is usually needed for the first (endothermic step), with the middle-low temperatures needed for the second reversible exothermal step; if the two T are not too different, then the cycle can be carried out more efficiently. In this respect, the FF450 sample seems to be the best (greater CO_2 produced at relatively low T) but for example the CF450 even when it works at higher temperatures it forms less intermediate species which sometimes can accumulate and cause the deactivation of the catalyst by coke formation for instance.

On the other hand, if a syngas (or anyway a reducing stream) is preferred as a gas exiting the first cycle (which can be used eventually for some other application, for example to feed a gas turbine), then the NF450 seems better. About the CuF450 it can be concluded that it could be useful in the transformation of ethanol to hydrocarbons which is indeed an interesting topic but not the goal of this particular project.

It should be also pointed out that the most part of the studies of ethanol adsorption on metal oxides and supported metals reported on the literature have been carried out for reduced samples since normally the aim is to evaluate the materials in steam reforming. Moreover, until now there are no reports of in-situ DRIFTS studies of adsorption on ferrites making the present research fully original as compared to the published data until now.

3.5.2 Session II: Room temperature adsorption of ethanol + water

In this part the experiments were performed in the same way than in the previous session but using ethanol with some water content (azeotropic mixture: 95.6% ethanol and 4.4% water). Figure 3.5—11 presents the results of such experiments for the NF450 catalyst. The general look of the spectra is similar to the one for pure ethanol (Figure 3.5—1) in the sense that acetate bands are clearly visible starting from 300 °C. These bands show a maximum at 350 and decrease after that. At higher temperature the ethoxy bands (1098 and 1057 cm^{-1}) are still present, also there are some extra OH stretching bands and in comparison with the previous test the very broad signal attributed to a partial reduction of the catalyst is not present so it can be assumed that water decreases the reduction degree of the catalyst.

In the figure also the evolution on time of the mass signal for the different products which is taken simultaneously is presented. The peaks observed correspond to the desorption by increasing the temperature but it is worth to remind that between two peaks the temperature is 30 °C since the procedure was to rise the temperature for 1.5 min and then go back to room temperature to take the spectra of the species that remained adsorbed. Even when it is not possible a direct comparison with the TPD performed after adsorption of pure ethanol (Figure 3.5—1) some observations should be pointed out.

For instance, at low temperature there is a big amount of desorbed ethanol, acetaldehyde and ethane with a very similar shape for the last two. This could be a further confirmation of the production of ethane at low temperature by disproportionation of ethanol. In the midle range again we observe desorption of hydrogen than after decreases and increases again at 400 °C. This two stages of Hydrogen desorption were also observed in the case of pure ethanol.

Regarding methane and carbon monoxide it can be seen that they are desorbed both at low and high temperature as expected from acetaldehyde decomposition (low range) and acetates oxidation and decomposition (high temp.). CO_2 is observed since 300 °C but the maximum is at 400 °C with some amount possibly produce by WGS reaction which was seen to be favored only in this catalyst.
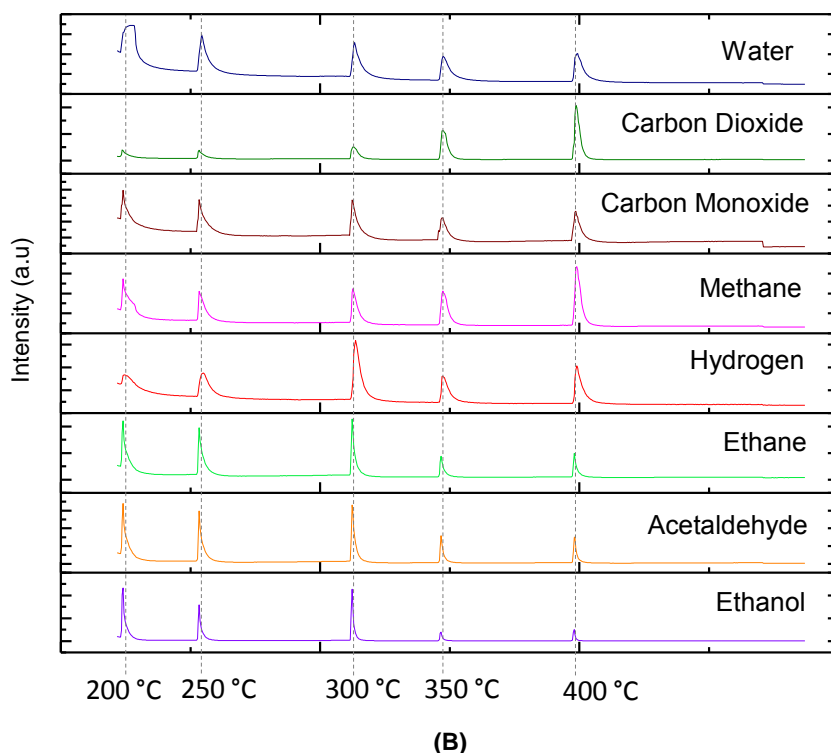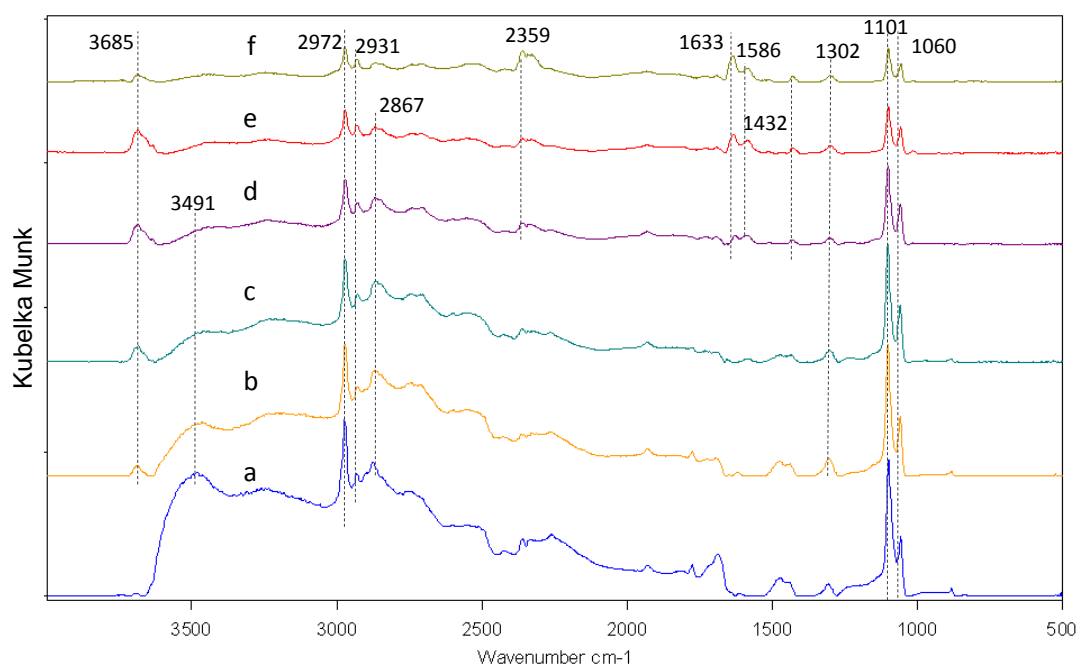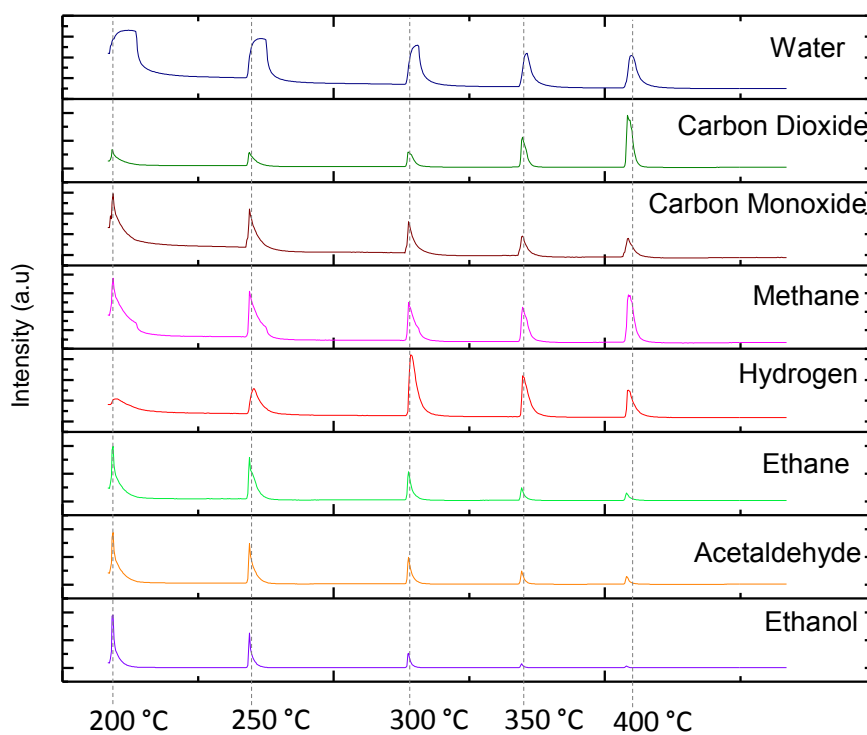

(A)

(B)
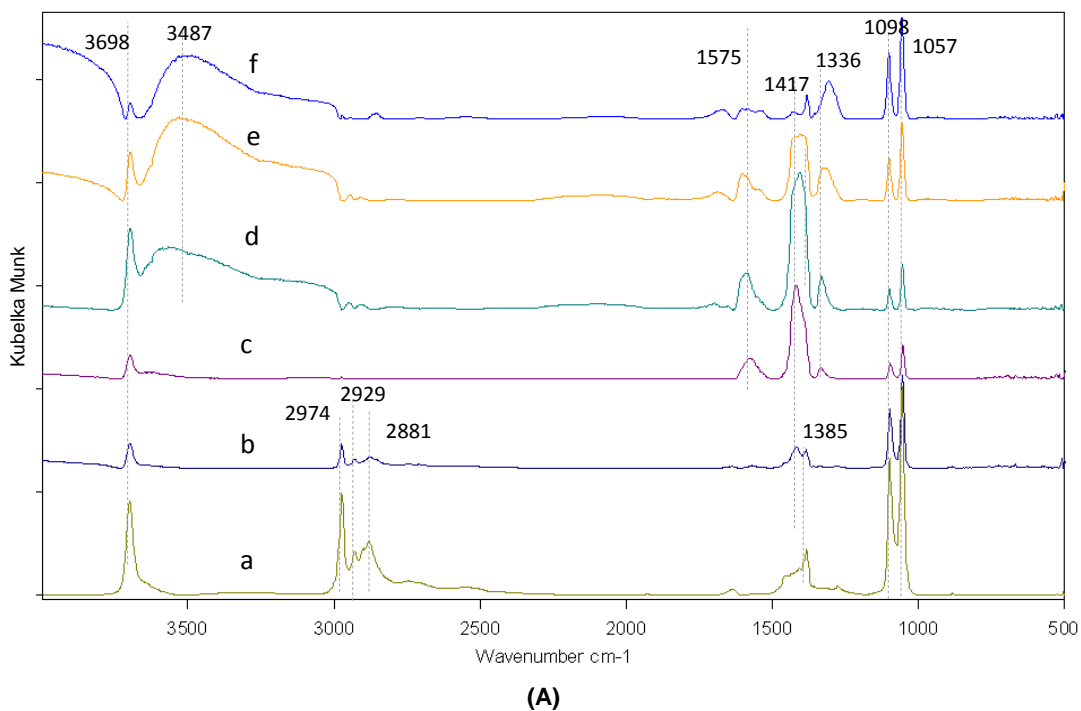
Figure 3.5—11. *(A)* DRIFT spectra for the NF450 catalysts after ethanol + water adsorption at 30 °C (a) and desorption at 200 (b) 250 (c) 300 (d) and 350 (e) and 400 °C (f). *(B)* Evolution of the mass signal for the different products (temp. hold for 1.5 min and then cool down to 30 °C)

In the case of the CF450 catalyst (Figure 3.5—11) also the spectra look similar to the ones without water content in the sense that only ethoxy species are clearly visible. There are some extra OH stretching bands (especially at low temperature) due to the presence of water, and at higher temperature it is seen the formation of bands corresponding to acyl and acetates but with small intensity.

Concerning the mass analysis, the trends are not very different from the results using pure ethanol: low temperature desorption of ethanol, ethane and acetaldehyde together with some carbon monoxide and methane as product of acetaldehyde decomposition. There is hydrogen released at 300 °C in agreement with the TPD using pure ethanol. At high temperature the oxidation and more decomposition products are desorbed.

(A)

(B)

Figure 3.5—12. *(A)* DRIFT spectra for the CF450 catalysts after ethanol + water adsorption at 30 °C (a) and desorption at 200 (b) 250 (c) 300 (d) and 350 (e) and 400 °C (f). *(B)* Evolution of the mass signal for the different products (temp. hold for 1.5 min and then cool down to 30 °C)
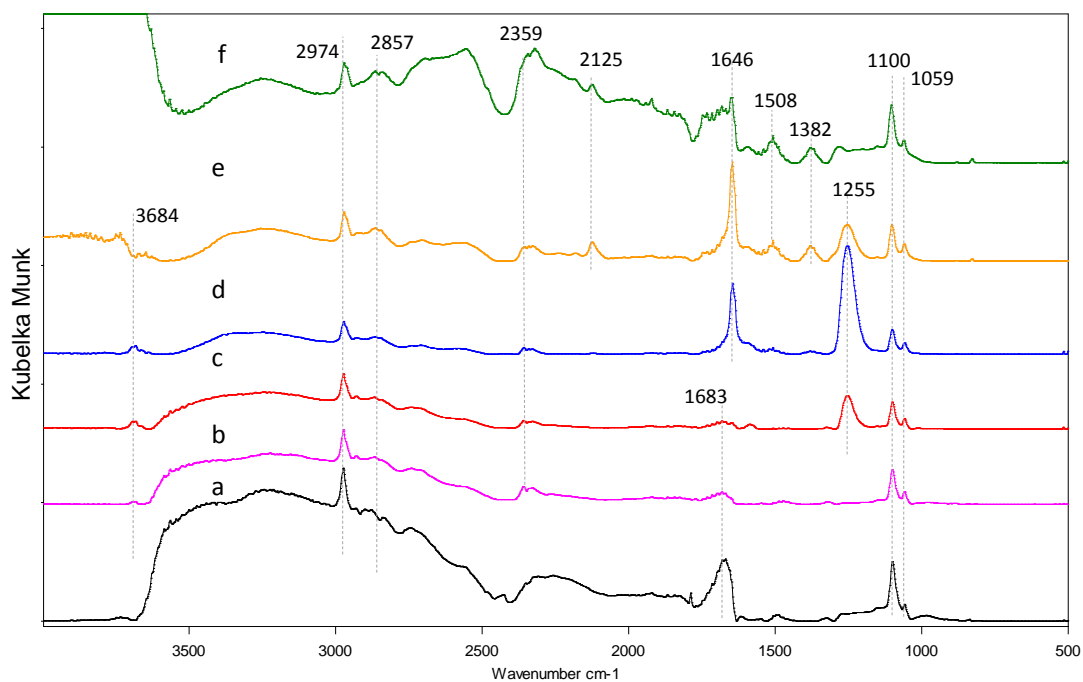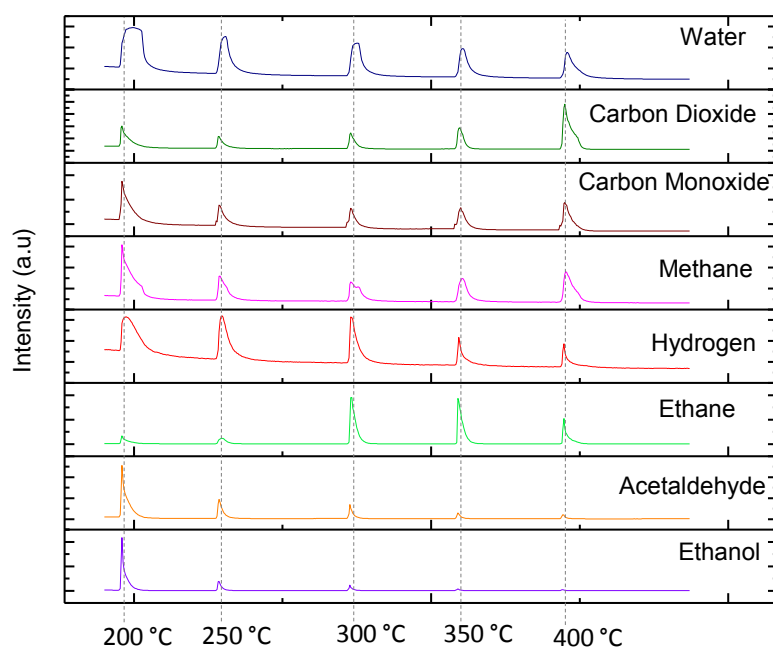
(A)

(B)

Figure 3.5—13. *(A)* DRIFT spectra for the CuF450 catalysts after ethanol + water adsorption at 30 °C (a) and desorption at 200 (b) 250 (c) 300 (d) and 350 (e) and 400 °C (f). *(B)* Evolution of the mass signal for the different products (temp. hold for 1.5 min and then cool down to 30 °C)

Figure 3.5—13A shows the spectra for the CuF450 in presence of water. It presents the bands corresponding to the η^2-acetaldehyde and acyl species like in the previous case. Here, the difference is that only a small CO band appears at 2125 cm^{-1} indicating that this decomposition is less effective when water is present. From the mass analysis (Figure 3.5—13B) it is evident the formation of ethane at temperatures around 300-350 °C in agreement with the TPD analysis performed before.

DRIFTS results for the FF450 catalyst are presented in Figure 3.5—14A and again they are pretty similar to the ones without the water content. Therefore with these results it can be stated that the presence of water (in small quantities) has few effect on the *adsorbed* species over the ferrites. On the other hand, Figure 4B presents the mass analysis of the products desorbed at each temperature. Even when a strict comparison with the TPD experiments of pure ethanol is not possible, here it is also evident that the FF450 produces the biggest amount of CO_2 and CH_4 around 350 °C. The apparent rising on the CO signal before 300 °C was due to a technical issue: one of the plastic lines was unplugged and the air, and so the N_2, were able to enter, as confirmed by the simultaneously increase in the m/z 14 signal (not shown).
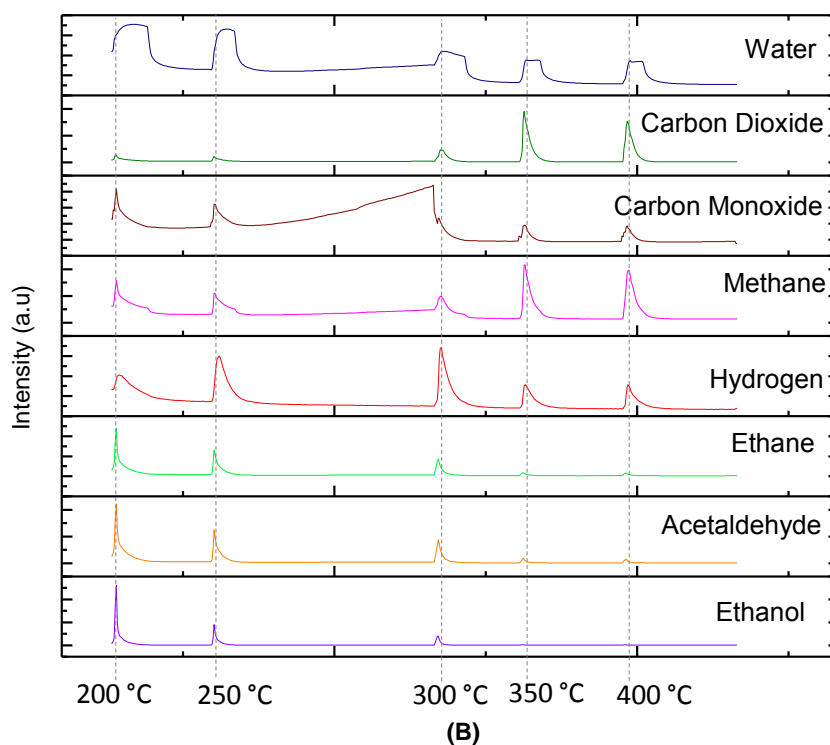

(A)
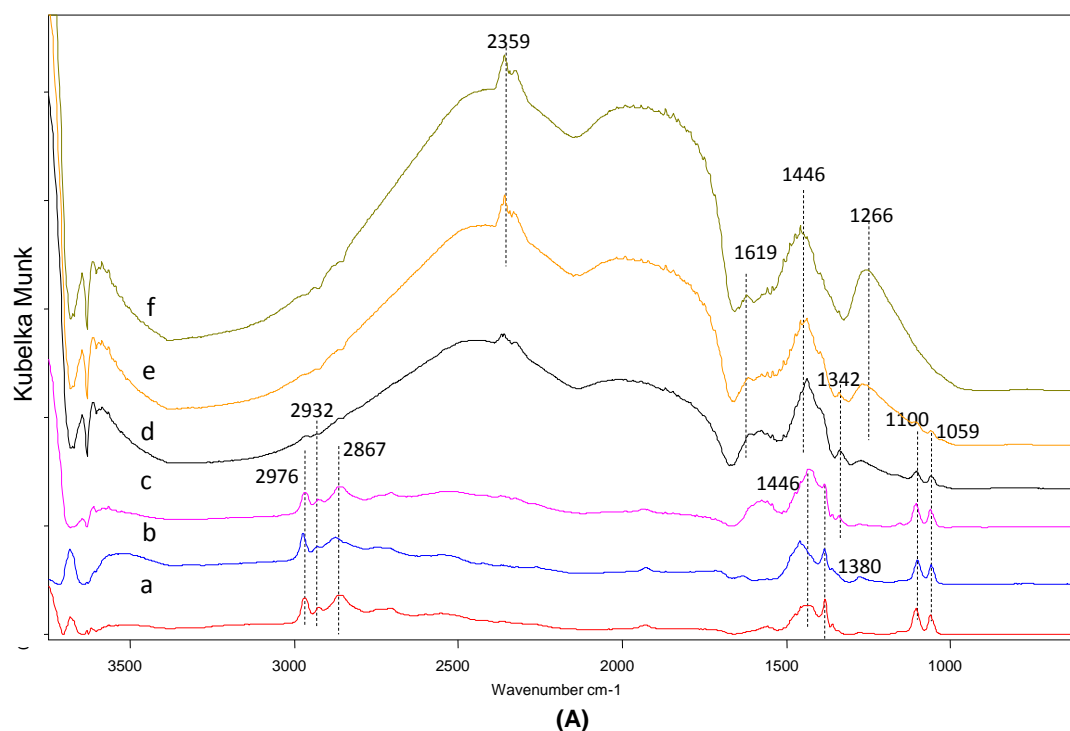
Figure 3.5—14. *(A)* DRIFT spectra for the FF450 catalysts after ethanol + water adsorption at 30 °C (a) and desorption at 200 (b) 250 (c) 300 (d) and 350 (e) and 400 °C (f). *(B)* Evolution of the mass signal for the different products (temp. hold for 1.5 min and then cool down to 30 °C)

Remark: Up to this point it can be concluded that the presence of small quantity of water has small effect on the behavior of the four catalysts which makes feasible the use of azeotropic ethanol for the reduction of the ferrites. This fact could be an economical relief when compared to the use of pure ethanol, the final initiative would be to use bio-ethanol as less processed as possible. Nevertheless, it is worth to remind that the second step of the cycle is the reoxidation of the ferrites with water so the two steps should have different temperatures optimized for each purpose.

3.5.3 Session III: Ethanol adsorption at different temperatures

In this session the DRIFTS experiments correspond to different experimental conditions with respect to the former two sessions since here the adsorption of ethanol was not limited to room temperature. First the sample was pretreated at high temperature (420 °C) flowing Ar to remove any adsorbed contaminant, and then again cool down to 30 °C. A background was recorded and then ethanol was pumped while recording spectra. When there is no change, the ethanol feeding was stopped and desorption spectra recorded. After, the catalyst was heated to the next temperature, taking a new background and feeding again ethanol. The rest of the procedure is repeated increasing the temperature every time by 50 °C. For simplicity only the spectra of 250 °C and 350 °C are shown now they are representative of the behaviors observed.
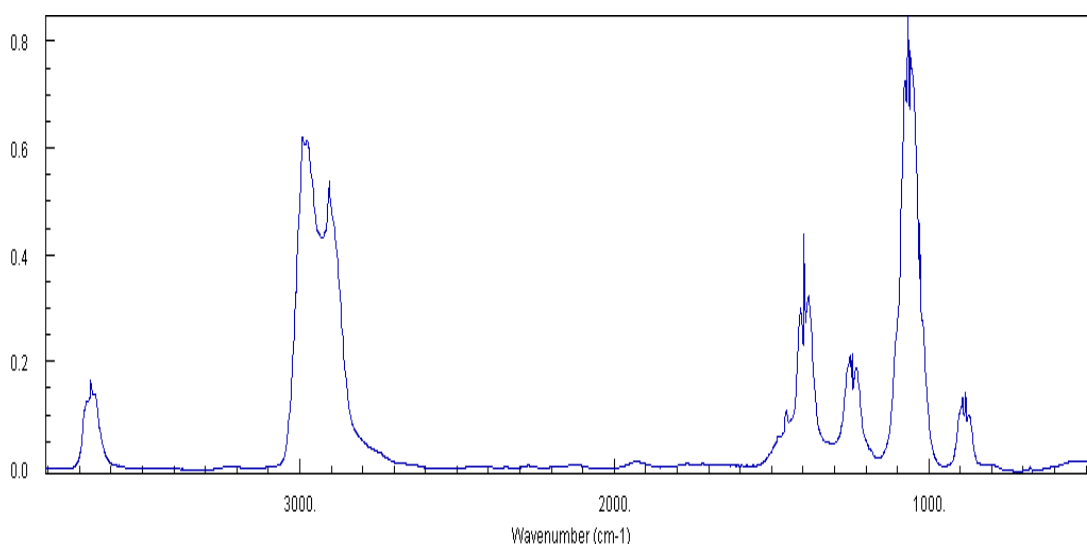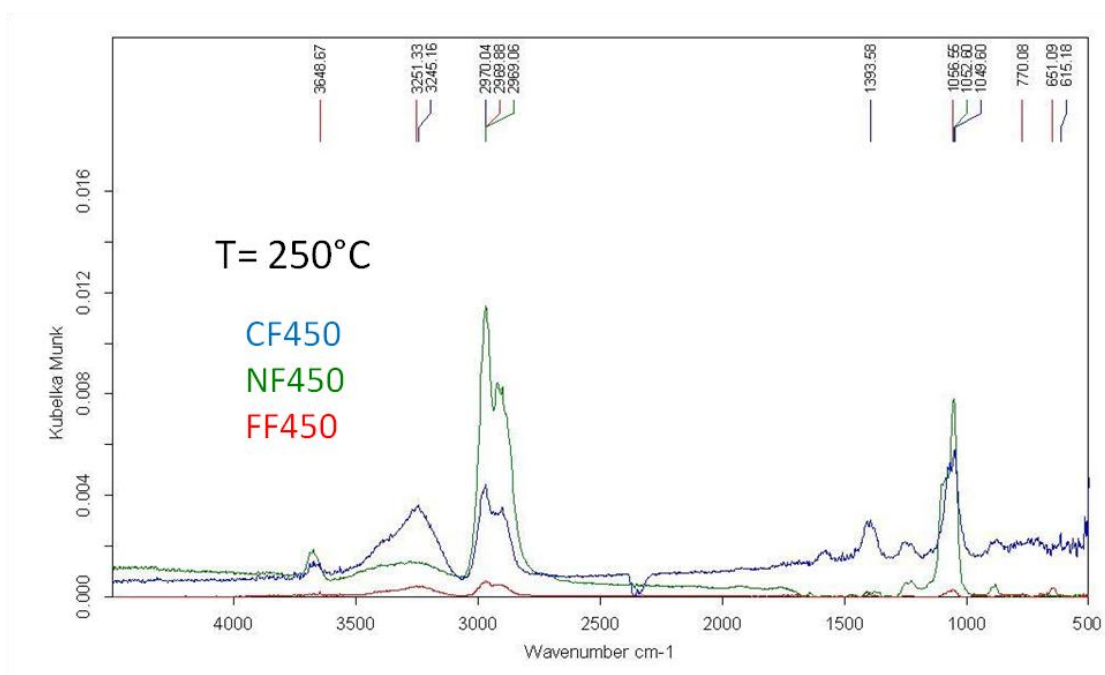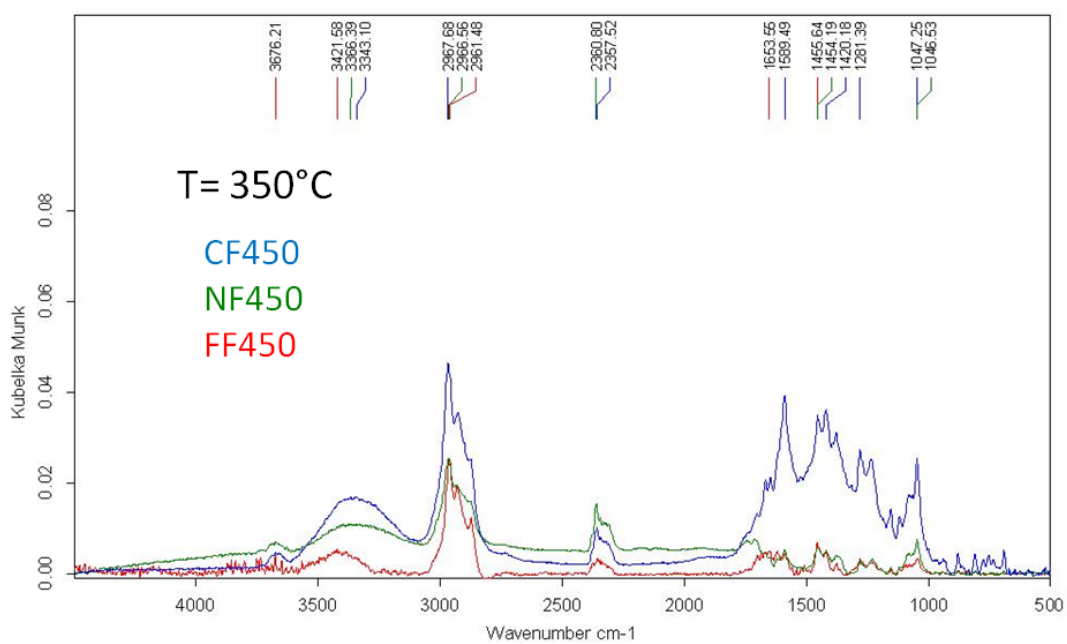

Figure 3.5—15. Gas phase ethanol spectra (taken from the NIST website)
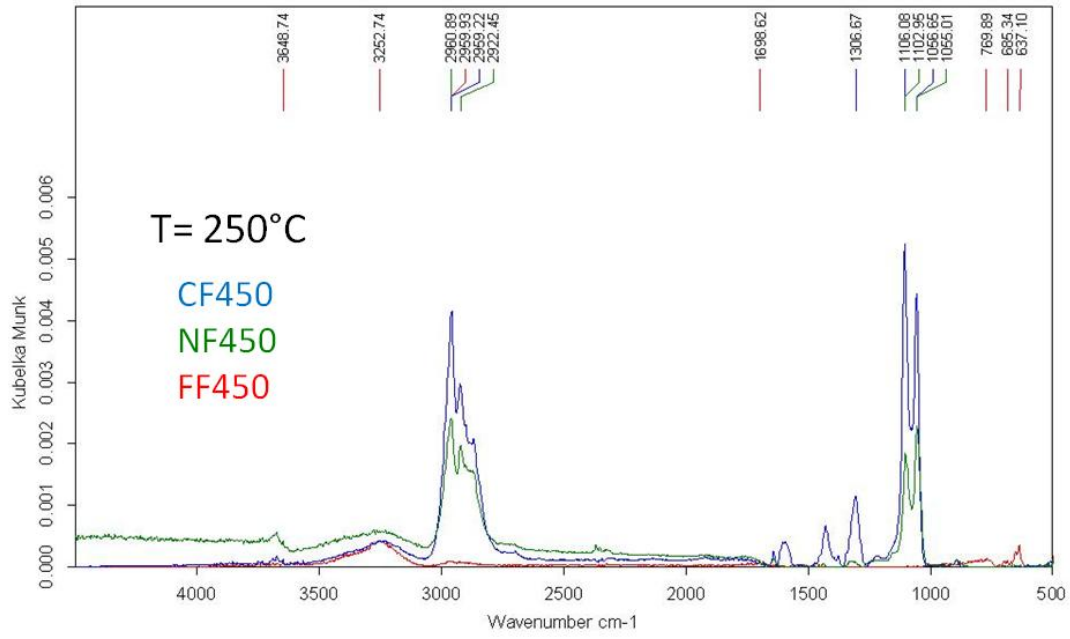
(A)

(B)

Figure 3.5—16. DRIFT spectra for the catalysts calcined at 450°C during adsorption of ethanol at 250 °C (A) and 350 °C (B)
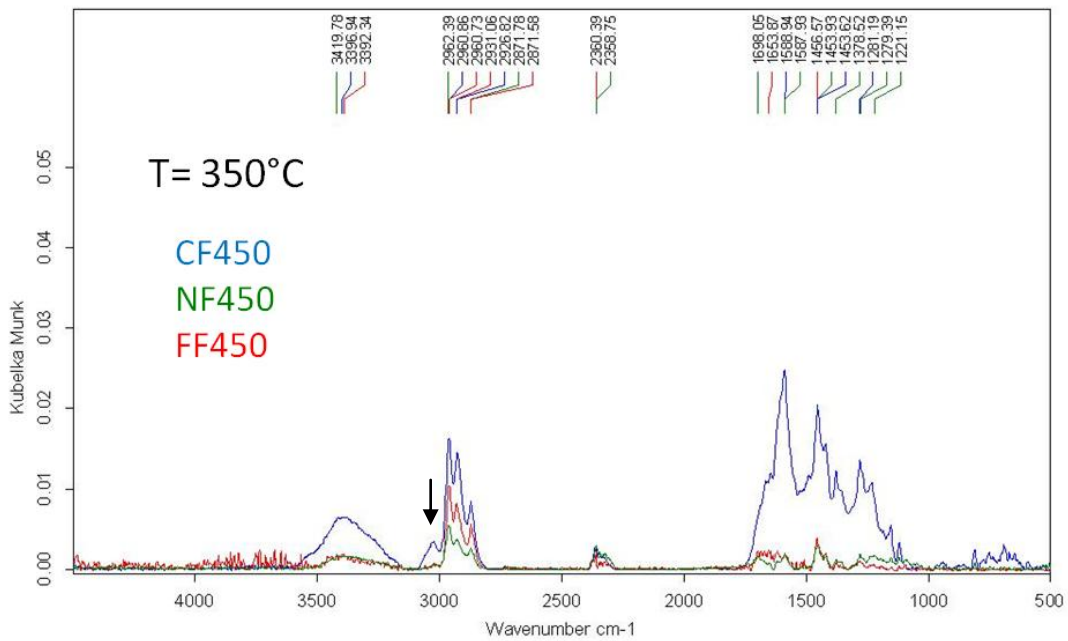
Figure 3.5—16 shows the spectra for the catalysts calcined at 450°C, (i.e. CF450, NF450 and FF450) *during the feeding* of ethanol at 250 and 350 °C. From the figure it can be observed that adsorption at 250 °C shows mainly the characteristic gas phase ethanol (shown as a reference in Figure 3.5—15) but also the broad band around 3200 cm^{-1} indicates that part of the ethanol is staying adsorbed on the surface. At 350 °C the adsorption is clearly different, here not only gas phase ethanol is detected but also it is possible to observe that part was adsorbed as ethoxide now that the characteristic bands for the C-O stretching are present for the 3 catalysts (around 1047 cm^{-1} and 1106 cm^{-1}).

On the other hand, when the ethanol feeding is stopped (but the Ar is still flowing), the excess of ethanol is being removed and only the chemisorbed species remain to be observed as presented in Figure 3.5—17. Here it is clear that at 250 °C the bands of ethoxides are present for the CF450 and NF450 (around 1056 and 1105 cm^{-1}, C-O and C-C stretching and also those between 2866-2960 cm^{-1} are the characteristic CH_3 bands associated with ethoxides). At this temperature (250 °C) only the CF450 presents bands at 1307 cm^{-1} 1429 cm^{-1} and 1603 cm^{-1} that are related to the vibrational modes of acetate-like species (δCH_3, $OCOv_s$ and $OCOv_{as}$ respectively) [58].

In the case of the FF450 no evidence of ethoxy species was found at 250 °C, only the band of H-bonded ethanol around 3250 cm^{-1}. This observations contrast with ones of the previous sessions in which the CF450 catalyst was the one forming less intermediate species but in this case the ethanol is being fed at each temperature so it might be an indication that the CF450 is able to keep adsorbing ethanol and transforming it to acetates whereas the NF450 and FF450 might be already saturated.

(A)

(B)

Figure 3.5—17. DRIFT spectra for the catalysts calcined at 450°C during the desorption of ethanol at 250 °C (A) and 350 °C (B)

At 350°C the products that remain adsorbed can include acetaldehyde, acetates and acyl species but compared with the spectra during the adsorption, the ethoxy bands are not present and there is a band above 3000 cm^{-1} which indicates the presence of an unsaturated product, probably ethylene since it was also observed in the mass analysis (see next session).

Mass analysis

While recording the IR spectra, the m/z signals of products at the outlet stream of the IR cell were also recorded. Figure 3.5—18 shows an example of the variation of the signal in the mass spectrometer with time. The broad features correspond to the stage of the ethanol feeding, after this, there is a desorption period and then when the temperature is increased the narrow feature appears and then when the system is *stable* the feeding starts again. For instance, ethanol corresponds to the m/z 31 which in the figure is the grey and the most intense signal.
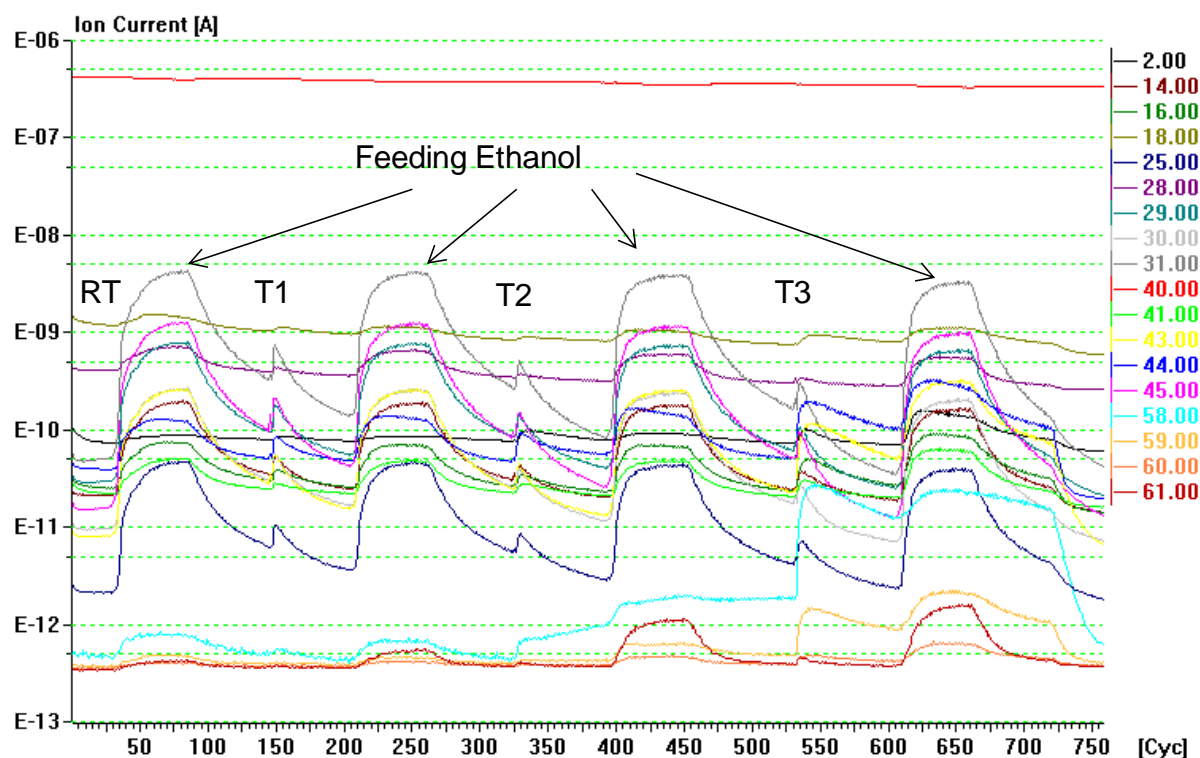

Figure 3.5—18. m/z signals recorded vs. time (cycles) [Y axe in Log scale]

In order to compare the different catalysts some representative data during the reaction with ethanol at each temperature were chosen. In this way, even if a quantitative assessment of each compound is not possible, comparisons can be made.

Figure 3.5—19 (part A and B) shows the major products obtained during the feeding at 250, 300 and 350 °C for each catalyst investigated compared with a blank performed without catalyst. In the very first figure, the ethanol signal is presented and in this case the signal is lower for all the catalysts compared to the sample holder alone which means that in presence of a catalyst ethanol is being converted more efficiently into different products. The signal of the blank experiment is also higher in the case of acetaldehyde, carbon monoxide, ethane and ethylene. This indicates that without catalyst the ethanol can be in part dehydrogenated to acetaldehyde and also decomposed to CO and CH_4 but also can be dehydrated to produce some ethylene which is not convenient since this is one of the precursors in coke formation by polymerization [5]. Among the catalysts, the CF450 is the one showing higher relative amounts of this unsaturated product which is consistent with the observation of the C-H alkene stretching band for this catalyst detected during the DRIFTS experiments.

On the other hand, for the catalysts, acetaldehyde can be further dehydrogenated and oxidized. In fact, hydrogen was produced in a bigger amount with the catalysts, especially at 350 °C. Only for the NF450 and FF450 some CO was present at high temperature but in few amounts. CO_2 trend was stable without catalyst which is a signal of lower oxidation. This is also true in the case of acetone and water which are also oxidation products. Gathering this information it can be inferred that among the samples tested under this conditions, the NF450 seems to be the more reactive specially at high temperature since the relative amounts of CO_2, CH_4, and even acetone are more significant for this catalyst specially at the highest temperature here tested (350 °C) whereas the FF450 seems to produce less oxidation and decomposition products.
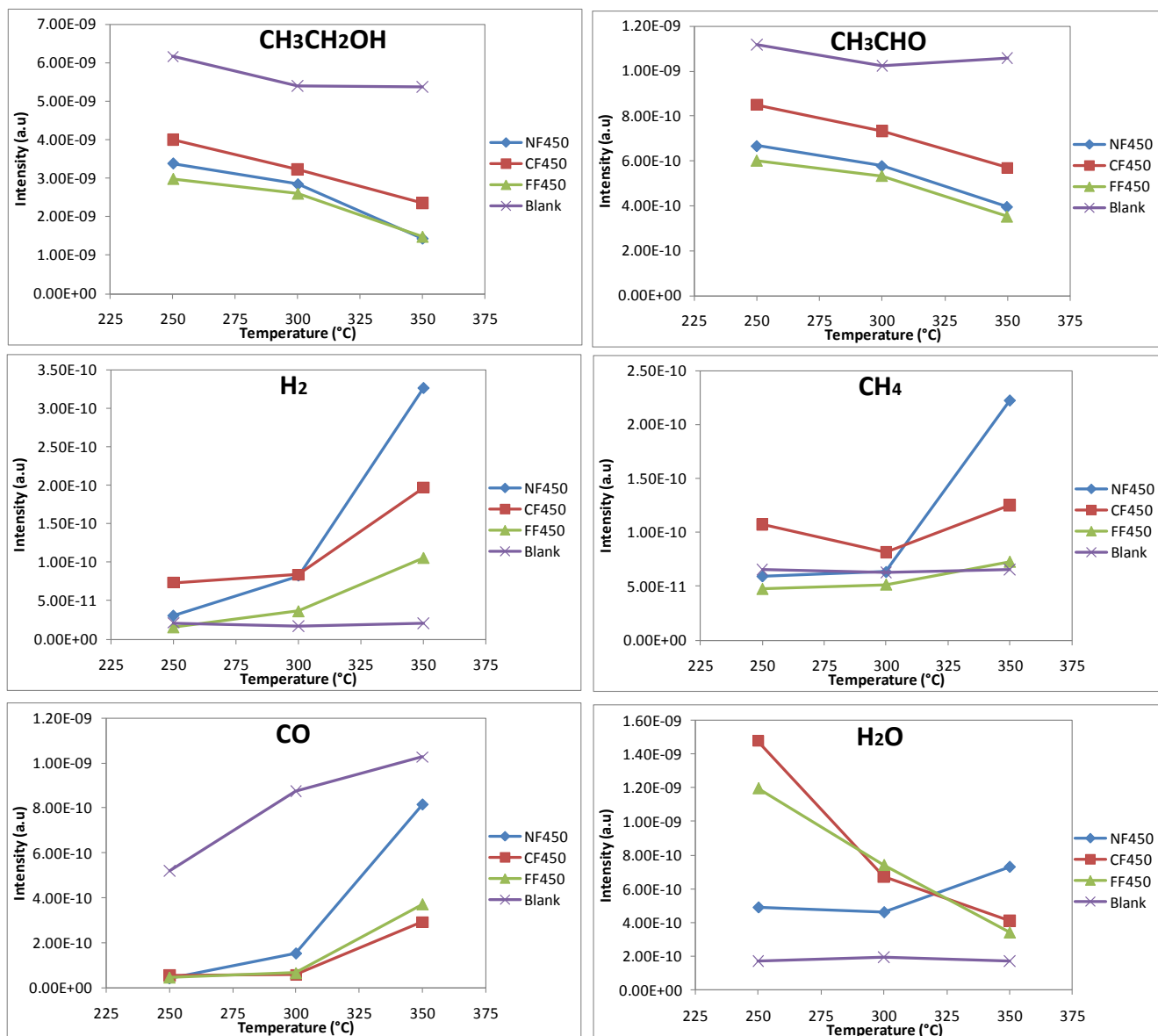
(A)

Figure 3.5—20. Mass analysis of the products of reaction with ethanol at different temperatures for the *A*-F450 catalysts (part A)
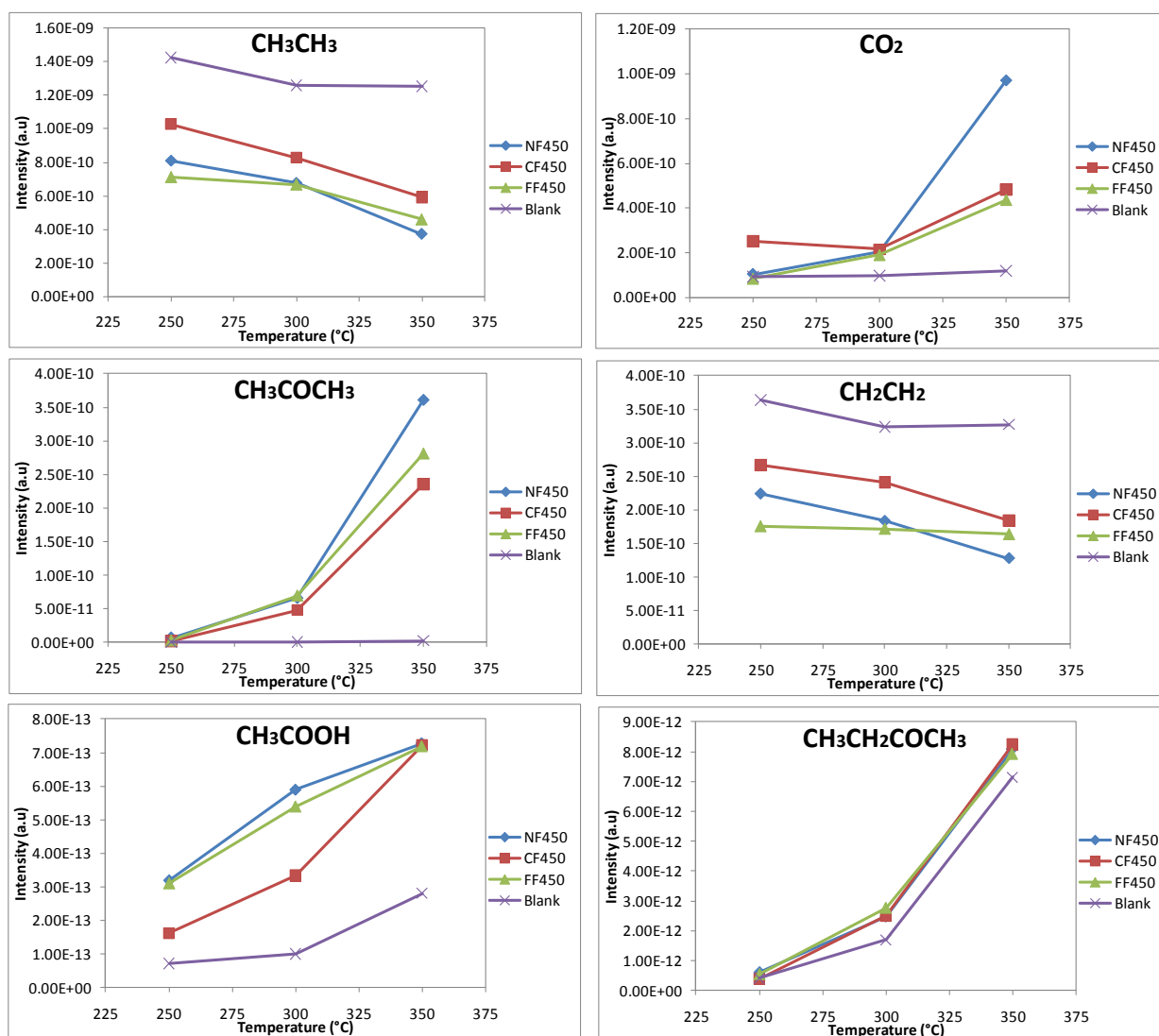
(B)

Figure 3.5—19. Mass analysis of the products of reaction with ethanol at different temperatures for the _A_-F450 catalysts (part B)

**Remarks:** The constant feeding of ethanol probably causes the saturation of the catalyst and the formation of more by-products which makes difficult the interpretation of this kind of data by diffuse reflectance spectroscopy; however the on-line mass analysis of the desorption products allowed to see some differences in the reactivity. Under these conditions the NF450 seems to be more oxidant, especially at high temperatures (350 °C) and produces less relative amounts of ethylene which is known to cause the deactivation of the catalyst during the reactions because of its polymerization to produce coke. However, the CF450 catalysts produces a lean gas with a better H2/CO ratio, so the choice of the catalyst depends on the characteristic desired of the produced gas.

3.5.4 Session IV: Influence of the annealing temperature of the precursors

In order to study the influence of the annealing temperature of the precursors, the Co-ferrite and Ni-ferrite were calcined at lower temperature (320°C) and then tested for ethanol adsorption at different temperatures. Figure 3.5—20 to Figure 3.5—22 show a comparison of the spectra after desorption for the CF320 and NF320 catalysts at different temperatures.

Already at 150 °C (Figure 3.5—20) the catalyst with Ni shows a band corresponding to adsorbed acetaldehyde or acetyl species due to ethanol dehydrogenation (1657 cm^{-1}, [54]) and both catalysts show the bands corresponding to ethoxy species between 1062-1103 cm^{-1} (C-O/C-C stretching) and 2864-2972 cm^{-1} (C-H stretching).
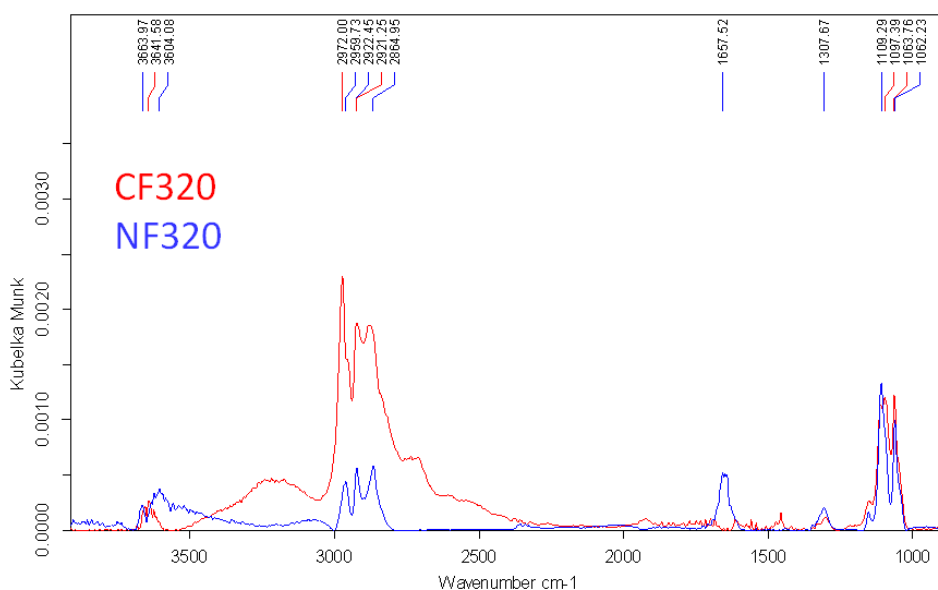
Figure 3.5—20. DRIFT spectra for the catalysts calcined at 320°C after desorption at 150 °C

Increasing the temperature to 200 °C a band for CO stretching is observed for both catalysts (1642 and 1653 cm^{-1}) and also the two of them show a band around 1300 cm^{-1} which could be attributed to δCH_3 but it is difficult to establish to which specie it belongs (acetaldehyde, acetate, acetone).
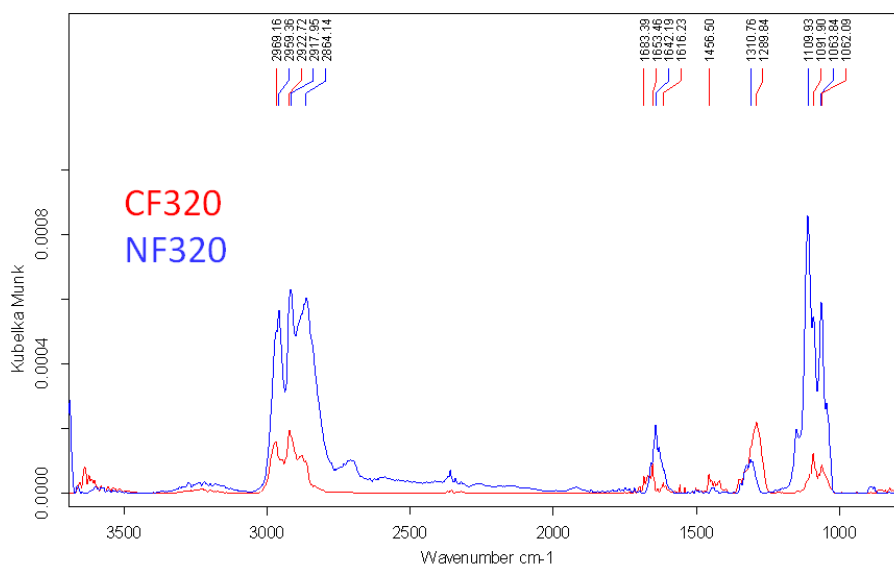
Figure 3.5—21. DRIFT spectra for the catalysts calcined at 320°C after desorption at 200 °C

For the spectra at 250 °C (Figure 3.5—21) it can be observed that the C=O band is present in both catalysts and is more intense than the bands for ethoxy species. Also absorbed CO_2 is observed by the band around 2358 cm^{-1}. These characteristics could be an indication of the formation of an oxidation product as acetone which has the characteristic bands in this position at least on SiO_2 (1699 cm^{-1}(υC=O) and 1372 cm^{-1} (δCH3) [64]).
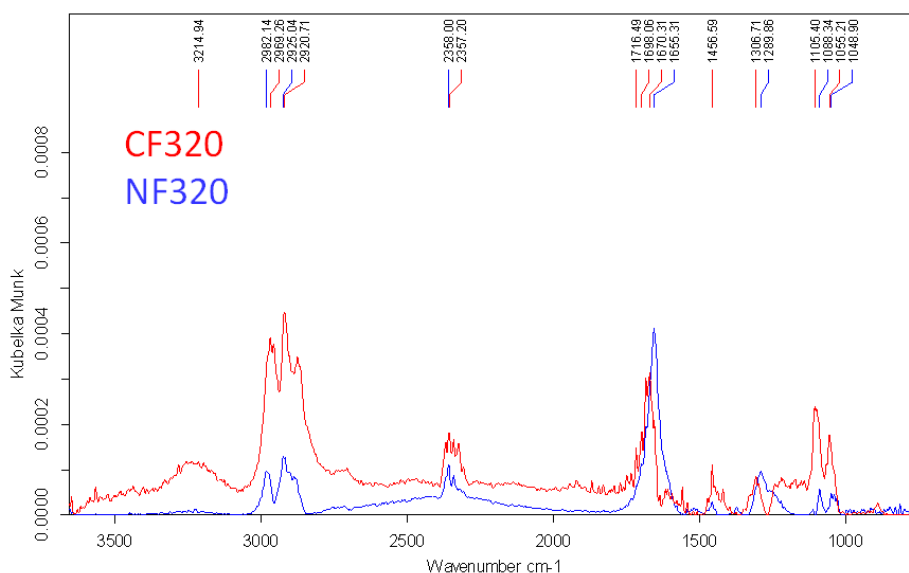
Figure 3.5—22. DRIFT spectra for the catalysts calcined at 320°C after desorption at 250 °C

Mass analysis

Figure 3.5—23 shows the evolution of the mass signal of ethanol with time. As previously describe (see Figure 3.5—18), the broad features correspond to the feeding of ethanol and the narrow ones to the moment when the temperature is increased. From there it is possible to see that the increase of the temperature produces a decrease in the ethanol signal which is therefore being transformed to the products.
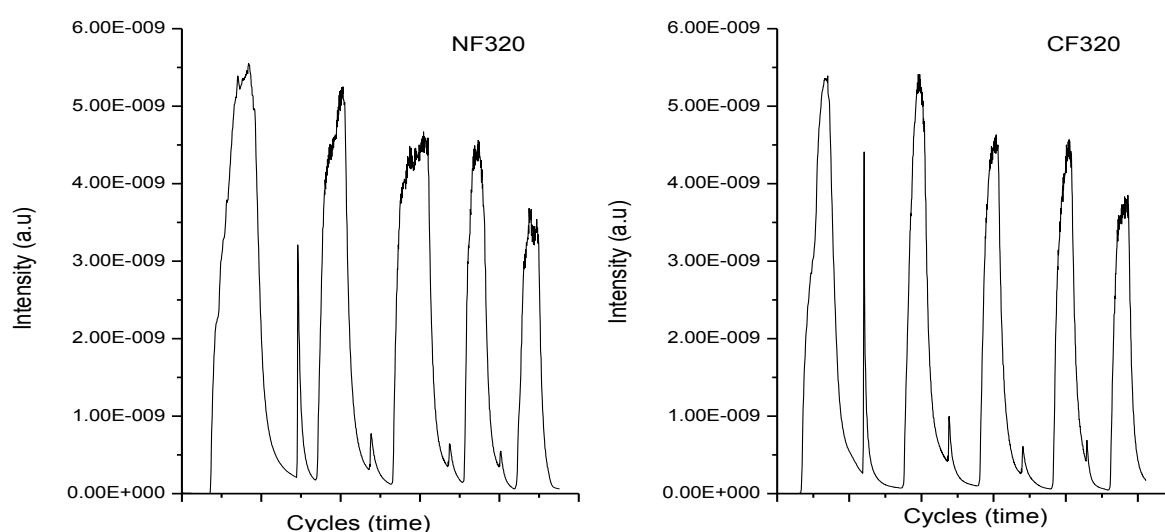
Figure 3.5—23. Evolution of the ethanol mass signal with time for the NF320 (left) and CF320 (right)

To have a clearer picture, the data corresponding to feeding at the different temperatures (maximum ethanol value during feeding) were extracted and are presented in Figure 3.5—24 together with the signal for the products at the same point. The figure contains a zoom in the zone between 150-300 °C in the low intensity region (taking out the ethanol signal).
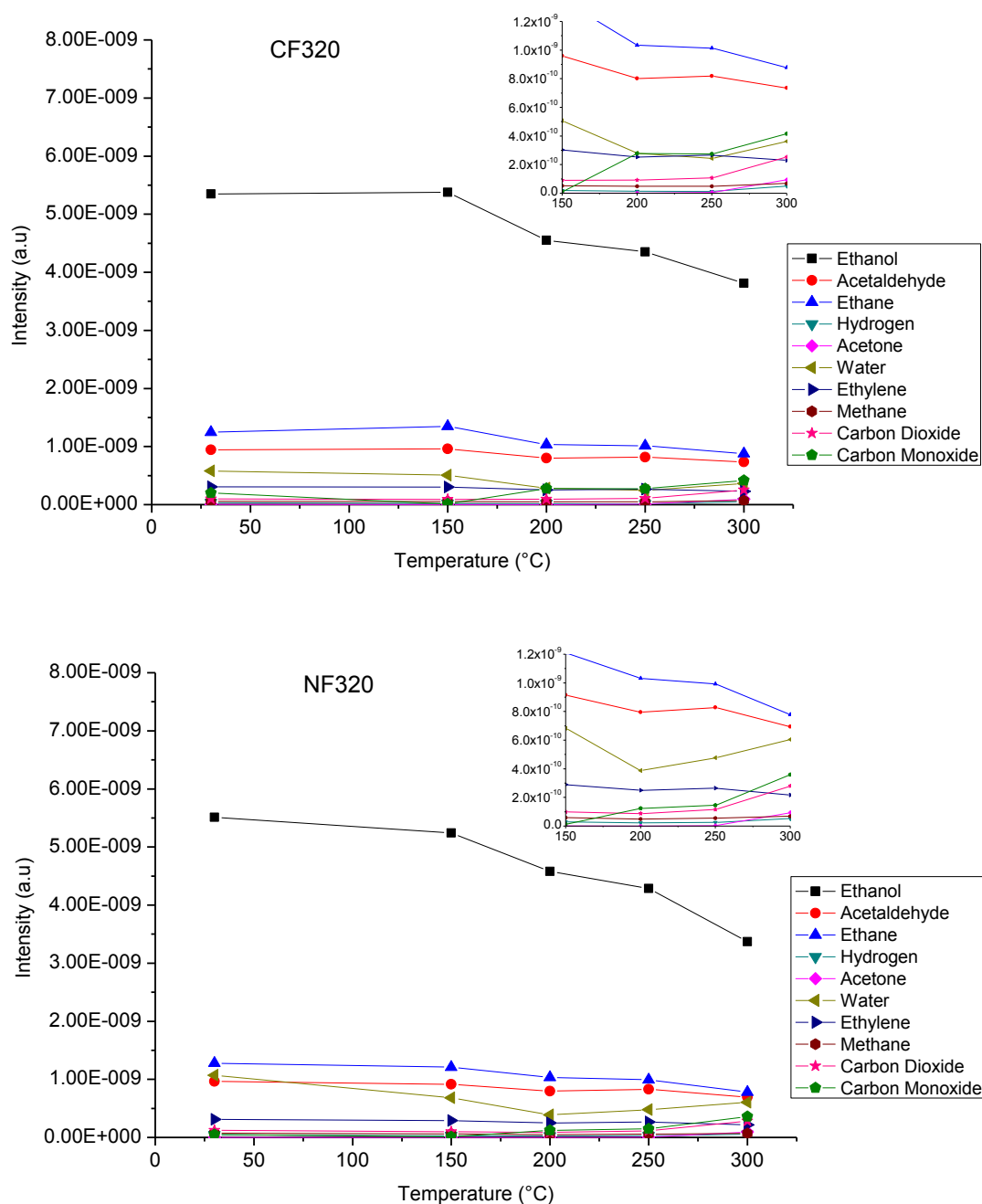
Figure 3.5—24. Products during the ethanol feeding at different temperatures (with an inset zoom between 150-300°C for the minor products) for the CF320 (Top) and NF320 (bottom)

From the figures it is possible to deduce that the main compound at each temperature is unconverted ethanol. The products of ethanol transformation include acetaldehyde, ethane and water probably formed by ethanol disproportionation and oxidative dehydrogenation.

This kind of disproportionation was observed in all the experimental conditions, especially at low temperatures but when the catalyst is calcined at lower temperature, the ethane becomes the main product, above aldehyde for instance. Some carbon monoxide and methane (decomposition products) and carbon dioxide and water (oxidation product) were also detected but only starting from 250°C. Acetone is detected in low quantities for both catalysts at high temperature (300 °C) which is in agreement with the observations in the DRIFT spectra that showed it characteristic bands appearing at 250 °C. However, as a general observation it is possible to say that for the samples calcined at lower temperature the composition has little effect in the product distribution.

For the Co-ferrite catalyst, further experiments were carried out annealing the catalyst at higher temperature (750 °C). The resulting spectra are presented and compared with the previous ones. Figure 3.5—25 correspond to spectra during the feeding and after evacuation of ethanol at 250 °C. During the absorption (Figure 3.5—25A) the general trend is that the catalyst calcined at lower temperature adsorbs more (this should be verified, from now it is only "visual"). After evacuation the presence of ethoxide species is evident for the CF320 and CF450. For the catalysts calcined at higher temperature (CF450 and CF750) acetate species are present (bands at 1576 and 1418 cm^{-1}). In the case of the CF750 the spectrum shows stronger bands attributed to H-bonded ethanol (broad band at 3245 cm^{-1} O-H stretching, 1393 cm^{-1} δCH3, 1242 cm^{-1} δOH) and this could be an indication that is less active in the transformation of ethanol. Table 9 shows the results of surface area measurements for the samples calcined at low, middle and high temperature. For the last two, also the crystallite size was measured and this appear to be bigger at 750 °C, probably due to sintering phenomena of the particles of the catalysts with this high temperature.

Table 9. BET Surface area analysis for the Co and Ni-ferrites calcined at different temperatures

Catalyst	Precursor	320 °C	450 °C	750 °C
CF	180 m^2g^{-1}	106 m^2g^{-1}	70 m^2g^{-1} (12nm)*	10 m^2g^{-1} (36 nm)*
NF	197 m^2g^{-1}	165 m^2g^{-1}	94 m^2g^{-1}	18 m^2g^{-1}

*Crystallite size as measured by x-ray diffraction

(A)

(B)

Figure 3.5—25. DRIFT spectra for the cobalt-ferrite catalyst calcined at different temperatures during the adsorption of ethanol at 250 °C (A) and after evacuation (B)

Figure 4 shows the comparison of adsorption and desorption of ethanol at 300 °C. For the absorption it can be noticed that the catalysts calcined at 750 °C has less affinity for ethanol adsorption. On the other hand the one calcined at 320°C shows bigger bands including the one for CO_2 but it also presents some negative features that can be due to some structural changes (now that the temperature is close to the one used to produce it) and this could be a drawback when using it in the reaction since working temperatures start around 300 °C.

For all the catalyst the ethoxy bands are present during the adsorption but basically disappear after evacuation which means this specie does not remain on the surface to be transformed and instead it is desorbed probably as ethanol.
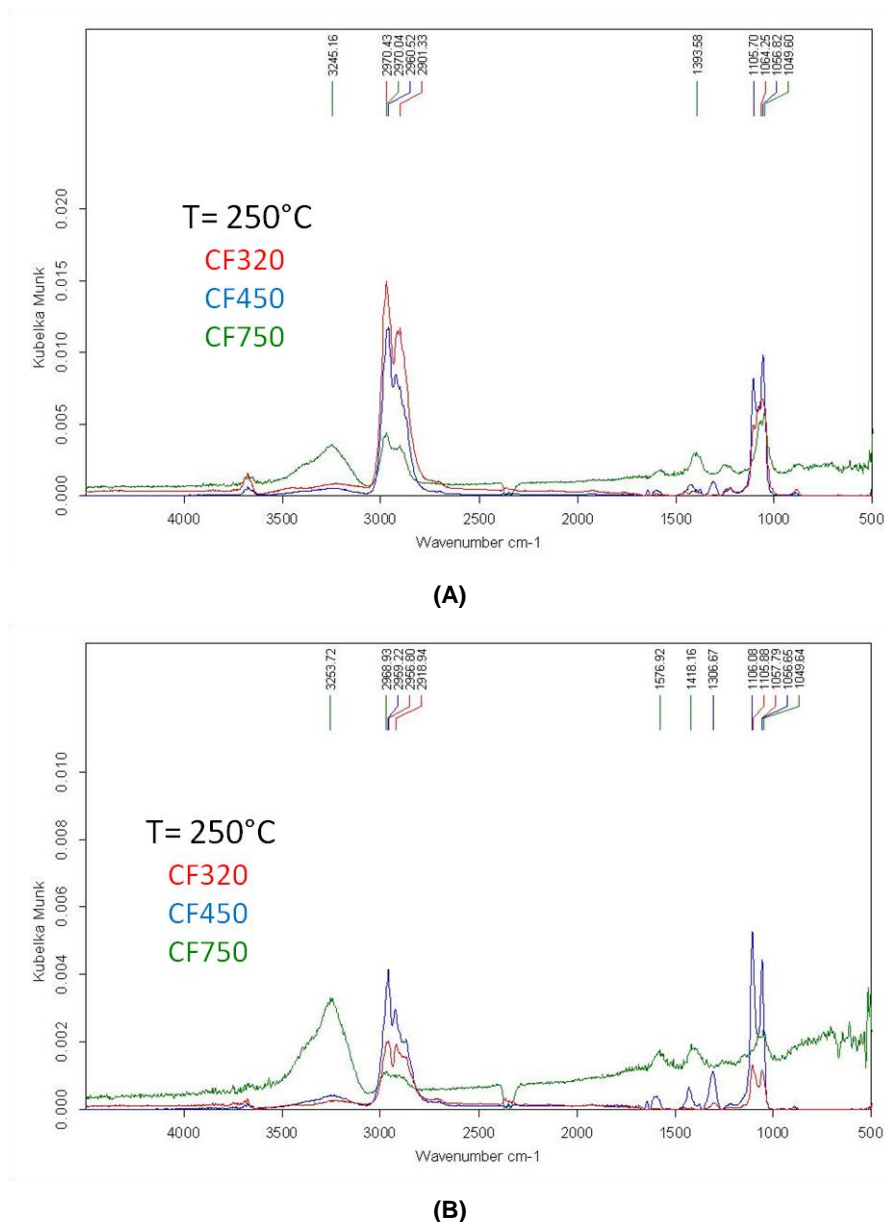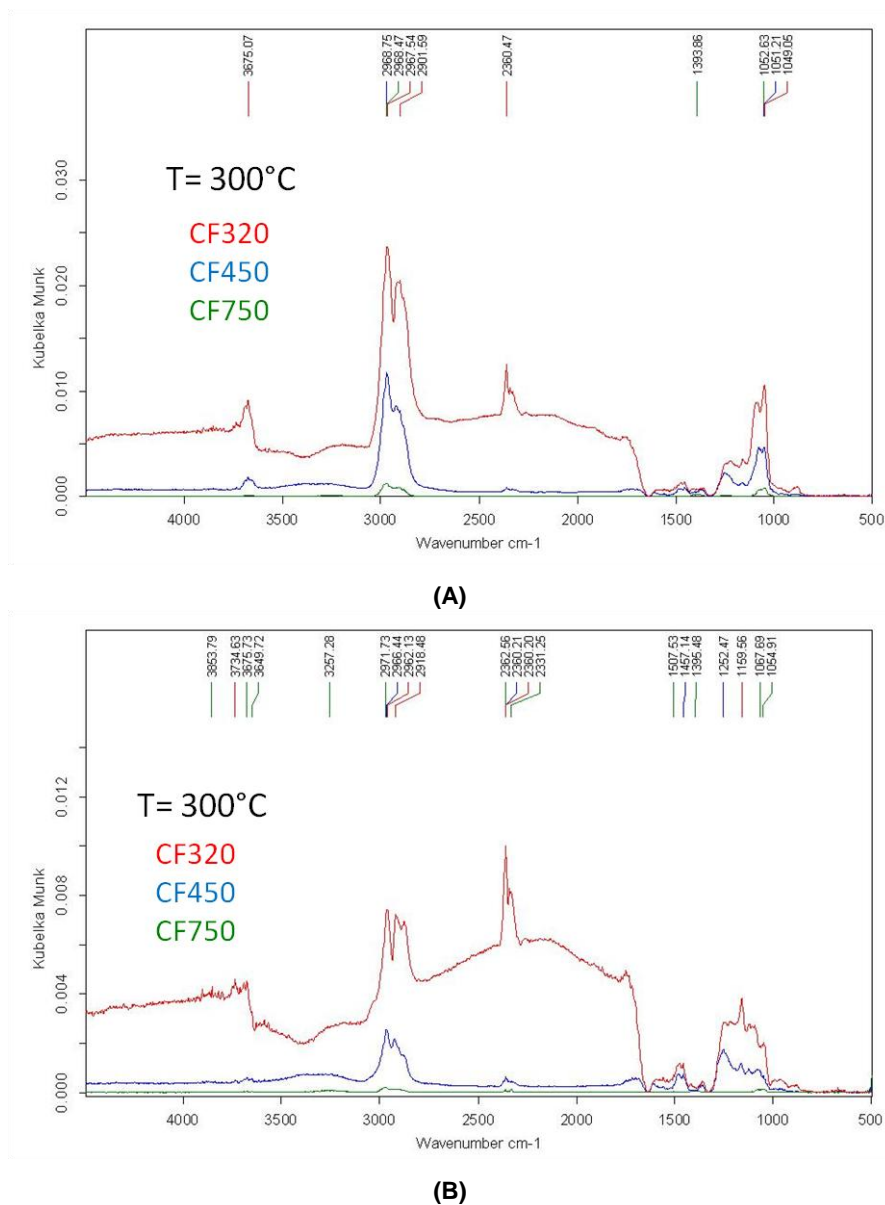

(A)

(B)

Figure 3.5—26. DRIFT spectra for the cobalt-ferrite catalyst calcined at different temperatures during the desorption of ethanol at 250 °C (A) and after evacuation (B)
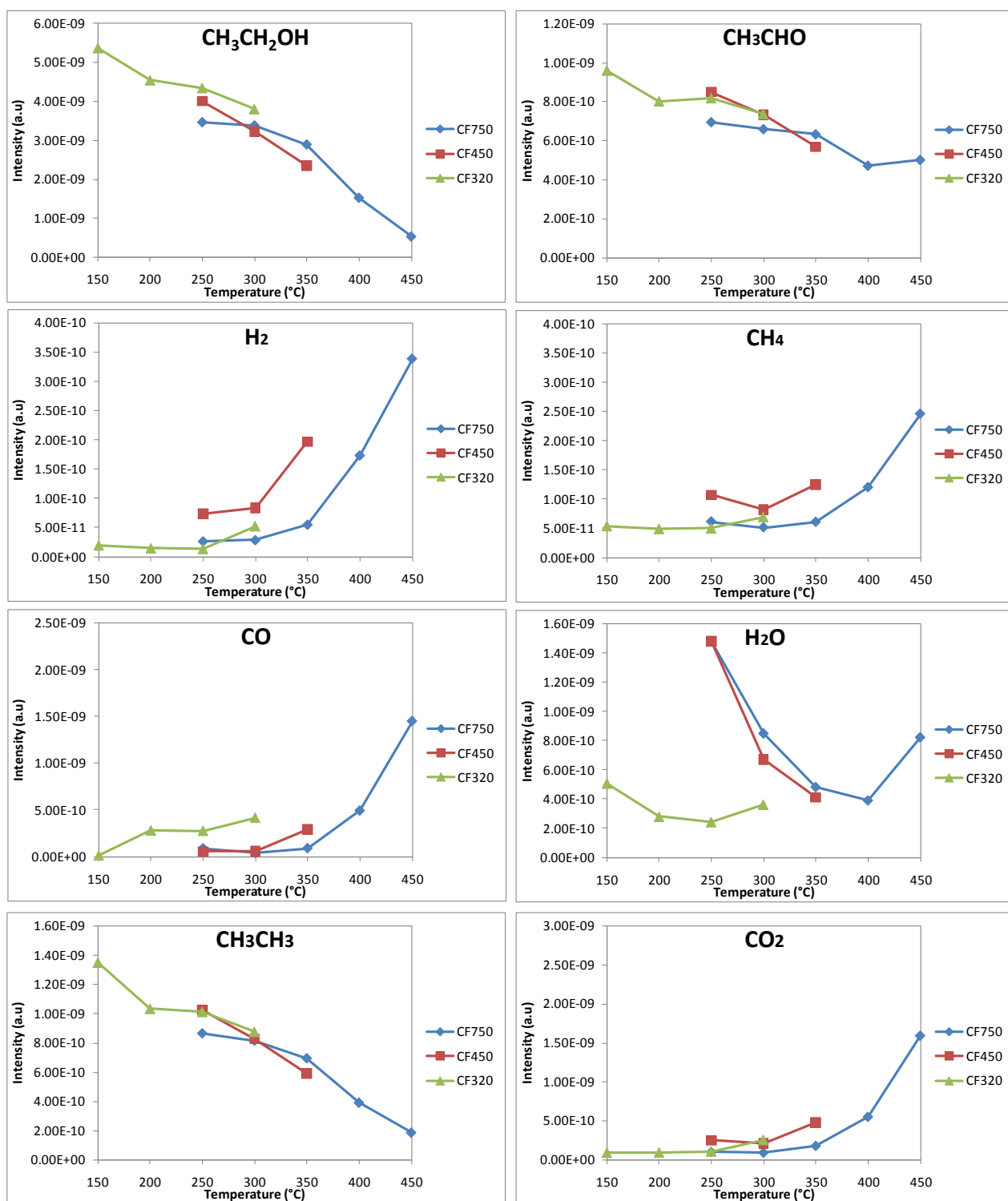
Mass Analysis

Figure 3.5—27 compares the main products after ethanol adsorption at different temperatures for the Co-ferrite calcined at 320, 450 and 750 °C. The very first figure shows the ethanol trend which is decreasing with the temperature for all the samples as expected since it is being converted to the products but as it can be observed the CF450 seems to convert more at least at 300-350°C. In the case of the acetaldehyde) it is formed in bigger amounts at low temperature since at higher temperatures it can be oxidized or decomposed.

Ethane was also observed to be formed in all cases. The trend shows that it decreases with temperature in a similar way than the acetaldehyde and the ethanol which could be an indication of the disproportionation of ethanol to give acetaldehyde, ethanol and water as proposed before (see Eq. 3, page 47). For the water the trends are not clear since water can be formed in several ways: desorption of OH and H previously adsorbed, oxidative dehydrogenation, disproportionation of ethanol, direct oxidation, etc.

The hydrogen formation increases with the temperature for the set of materials but is interesting to notice that the sample calcined at middle temperature (450 °C) is more effective in hydrogen formation than the other two ferrites at least in the range of temperatures that they overlap. Also for this series of experiments acetone was found to be formed in significant quantities starting at 300 °C. Acetone represents a further oxidation of the acetaldehyde and its formation has been proposed to start with the formation of acetates that react among them to form the acetone (Eq.10).

$$2CH_3COO^-_{(a)} \rightarrow CH_3C(O)CH_3 + CO_3^{2-} \hspace{3cm} \text{(Eq. 10)}$$

As regards CO formation it can be pointed out that at lower temperature the sample calcined at 320 °C shows more production of this compound and at higher temperature (350°C) also the sample CF450 produces more CO with respect to the one calcined at 750°C.

(A)

Figure 3.5—28. Main product after ethanol adsorption at different temperatures for The Co-ferrite calcined at 320, 450 and 750 °C (part A)
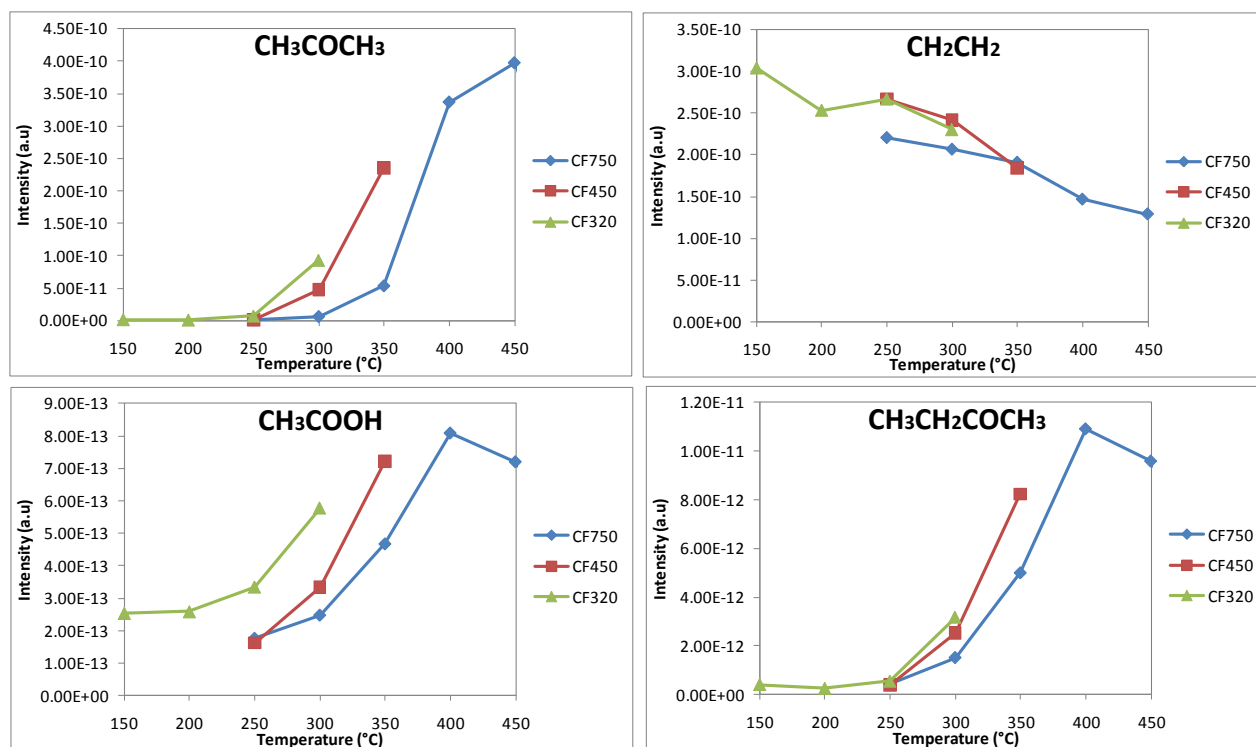
(B)

Figure 3.5—27. Main product after ethanol adsorption at different temperatures for The Co-ferrite calcined at 320, 450 and 750 °C (part B)

Remarks: The adsorption of ethanol on the ferrites is also dependent on some morphological properties which are at the same time product of the synthesis method; In this case for instance when the samples are annealed at low temperature there is no big difference in the spectral features and product distribution according to the composition as it was observed for the samples calcined at 450°C. On the other hand, when the composition is constant and the annealing temperature varies (as presented for the Co-ferrite) the trends remain similar but the sample calcined at 450 °C offers a good balance between morphological characteristics and reactivity since at high temperature (350 °C) it seems to convert more the ethanol and acetaldehyde, producing more hydrogen and oxidation products instead of CO and ethylene.

4. CONCLUSIONS AND PERSPECTIVES

- Diffuse reflectance infrared spectroscopy (DRIFTS) has been an useful tool for the study of the interaction of ethanol with ferrite-like catalysts, since it allowed the detection of species adsorbed on the surface of the materials studied. Combining this information with the analysis of the desorbed products by mass spectrometry, it was possible to propose the pathways for the anaerobic oxidation of ethanol over the samples with similar structure and different composition (for the "clean" surfaces). However, due to the high number of possibilities regarding the experimental setup for this technique, several experiments were done in order to gain more information that could be useful in the understanding of the reactivity of the materials in the steam-iron process.

- When feeding ethanol at different temperatures, the thermal treatment of the catalysts was found to have an impact on the reactivity and product distribution. When the samples are calcined at low temperature (320 °C) the surface area is bigger and this morphological characteristic seems to be more relevant than the composition since not significant differences were found between the samples compared. On the other hand when annealed at higher temperatures, the samples show different behavior depending on the composition of the material. Finally, when the composition is constant and the thermal treatment varies, the material annealed at middle temperature seems to have a better performance especially at higher temperatures.

- The catalyst choice affects the products distribution, a feature that can be used to select the proper composition of the solid in function of the nature of the desired products; for instance, the H_2/CO ratio of the lean gas deriving from the first step of reaction can be greatly affected by the choice of the spinel type. In this case, for instance, the CF450 catalyst could be a good choice but if instead the more oxidant catalyst is required the NF450 fits better. The CuF450 catalyst showed special good properties for hydrogen intermolecular transfer and thus produced a big amount of ethane. This was in part attributed to the segregation of CuO which at the same time affects the reducibility properties.

- Studies of the materials in the lab-scale plant and also a deeper characterization (including Mossbauer spectroscopy, X-ray photoelectron spectroscopy, in-situ X-ray diffraction, etc) are being carried out in the research group in order to have a more general picture of the reaction and finally make a selection of a suitable material and moreover to take advantage of the studies to finally design a new and efficient catalyst for this important process.

Acknowledgments

This research project (and the whole master program) was a wonderful opportunity and a great experience for me, both professional and personal. I would like to thank to all the people that contribute somehow to make it possible. They include, but are not limited to (scientific language):

My supervisor, Professor Fabrizio Cavani. It was an honor to work next to him because he is a great scientist and a great human being, which is a difficult combination these days, now I see why everyone wants to work with him.

My co-supervisor, MSc Cristian Trevisanut, he showed me the way and tried always to help me even in the distance.

To professor Guido Busca for his valuable comments on the DRIFTS experiments.

To the professors and personal from Lille University, especially Professor Sylvain Cristol, Sonja Moreau and Francine Chanier.

To professors and personal from Bologna University, especially Professor Paolo Righi and Dr. Stefano Cocchi.

To my colleagues and now friends who shared this experience with me, Xinxia Ye, Aloïs Mispelon, Marta Anna Brucka, Andy Nave, Felix Bacher, Nguyen Tran.

To my family and Colombian friends because in spite of the huge ocean that separates us, I know I can always count on them. Marta I. Ochoa (my mom!), Andrea and Daniel Velasquez, Jhon J. Velasquez, Jhon A. Pareja, Alejandro Vasquez, Diego Naranjo, Maribel Restrepo, Juliana Salgado, Natalie C. Cortés, etc. (fortunately they are a lot! unfortunately I have no space to write all the names here).

References

1. Edwards, P.P., et al., *Hydrogen and fuel cells: Towards a sustainable energy future.* Energy Policy, 2008. **36**(12): p. 4356-4362.

2. Borthwick, W. and J. Martin-Bermejo, *Hydrogen is on the way*, in *RTD info, magazine on European research*. 2004, Communication Unit of the European Commission's Research DG.: European Community. p. 3.

3. Marshall, A., et al., *Hydrogen production by advanced proton exchange membrane (PEM) water electrolysers—Reduced energy consumption by improved electrocatalysis.* Energy, 2007. **32**(4): p. 431-436.

4. Hurst, S., *Production of hydrogen by the steam-iron method.* Oil & Soap, 1939. **16**(2): p. 29-35.

5. Chen, L., et al., *Carbon monoxide-free hydrogen production via low-temperature steam reforming of ethanol over iron-promoted Rh catalyst.* Journal of Catalysis, 2010. **276**(2): p. 197-200.

6. Hacker, V., et al., *Hydrogen production by steam-iron process.* Journal of Power Sources, 2000. **86**(1): p. 531-535.

7. Cocchi, S., *A chemical loop approach for methanol reforming*, in *Chimica Industriale*. 2012, Alma Mater Studiorum – Università di Bologna: Bologna.

8. Nakamura, T., *Hydrogen production from water utilizing solar heat at high temperatures.* Solar Energy, 1977. **19**(5): p. 467-475.

9. Friák, M., A. Schindlmayr, and M. Scheffler, *Ab initio study of the half-metal to metal transition in strained magnetite.* New Journal of Physics, 2007. **9**(1): p. 1.

10. Verwey, E.J.W. and E.L. Heilmann, *Physical Properties and Cation Arrangement of Oxides with Spinel Structures I. Cation Arrangement in Spinels.* The Journal of Chemical Physics, 1947. **15**(4): p. 174-180.

11. Fresno, F., et al., *Solar hydrogen production by two-step thermochemical cycles: Evaluation of the activity of commercial ferrites.* International Journal of Hydrogen Energy, 2009. **34**(7): p. 2918-2924.

12. Kodama, T., et al., *Thermochemical hydrogen production by a redox system of ZrO2-supported Co(II)-ferrite.* Solar Energy, 2005. **78**(5): p. 623-631.

13. Kodama, T., N. Gokon, and R. Yamamoto, *Thermochemical two-step water splitting by ZrO2-supported NixFe3−xO4 for solar hydrogen production.* Solar Energy, 2008. **82**(1): p. 73-79.

14. Imanishi, H., et al., *Effects of reduction conditions on the cycling performance of hydrogen storage by iron oxides: Storage stage.* Chemical Engineering Science, 2008. **63**(20): p. 4974-4980.

15. Go, K.S., S.R. Son, and S.D. Kim, *Reaction kinetics of reduction and oxidation of metal oxides for hydrogen production.* International Journal of Hydrogen Energy, 2008. **33**(21): p. 5986-5995.

16. Barrett, D., *Partial Oxidation of Methane Using Iron Oxide as Donor.* Industrial & Engineering Chemistry Process Design and Development, 1972. **11**(3): p. 415-420.

17. Bleeker, M.F., *Pure hydrogen from pyrolysis oil by the steam-iron process.* 2009: Enschede, the Netherlands. p. 232.

18. Wiebren de, J., *Sustainable Hydrogen Production by Thermochemical Biomass Processing*, in *Hydrogen Fuel.* 2008, CRC Press. p. 185-225.

19. Hacker, V., et al., *Usage of biomass gas for fuel cells by the SIR process.* Journal of Power Sources, 1998. **71**(1–2): p. 226-230.

20. Ni, M., D.Y.C. Leung, and M.K.H. Leung, *A review on reforming bio-ethanol for hydrogen production.* International Journal of Hydrogen Energy, 2007. **32**(15): p. 3238-3247.

21. Song, H. and U.S. Ozkan, *Economic analysis of hydrogen production through a bio-ethanol steam reforming process: Sensitivity analyses and cost estimations.* International Journal of Hydrogen Energy, 2010. **35**(1): p. 127-134.

22. Buswell, A.M., K. Krebs, and W.H. Rodebush, *Infrared Studies. III. Absorption Bands of Hydrogels between 2.5 and 3.5 μ.* Journal of the American Chemical Society, 1937. **59**(12): p. 2603-2605.

23. Rod Nave, C. *HyperPhysics.* [cited 2012 22/04/2012]; HyperPhysics (©C.R. Nave, 2010) is a continually developing base of instructional material in physics.]. Available from: http://hyperphysics.phy-astr.gsu.edu/hbase/molecule/molec.html.

24. Busca, G., *The use of vibrational spectroscopies in studies of heterogeneous catalysis by metal oxides: an introduction.* Catalysis Today, 1996. **27**(3–4): p. 323-352.

25. Nix, R.M., *An Introduction to Surface Chemistry*. 2012, School of Biological & Chemical Sciences , Queen Mary, Univ. of London

26. Perkin-Elmer, *Technical note - FT-IR Spectroscopy Attenuated Total Reflectance (ATR)*, http://shop.perkinelmer.com/content/technicalinfo/tch_ftiratr.pdf.

27. Ma, Z. and F. Zaera, *Heterogeneous Catalysis by Metals*, in *Encyclopedia of Inorganic Chemistry*. 2006, John Wiley & Sons, Ltd.

28. de Lima, S.M., et al., *Ethanol decomposition and steam reforming of ethanol over CeZrO2 and Pt/CeZrO2 catalyst: Reaction mechanism and deactivation.* Applied Catalysis A: General, 2009. **352**(1–2): p. 95-113.

29. Greenler, R.G., *Infrared Study of the Adsorption of Methanol and Ethanol on Aluminum Oxide.* The Journal of Chemical Physics, 1962. **37**(9): p. 2094-2100.

30. Yee, A., S.J. Morrison, and H. Idriss, *A Study of the Reactions of Ethanol on CeO2 and Pd/CeO2 by Steady State Reactions, Temperature Programmed Desorption, and In Situ FT-IR.* Journal of Catalysis, 1999. **186**(2): p. 279-295.

31. Lin, S.S.Y., D.H. Kim, and S.Y. Ha, *Metallic phases of cobalt-based catalysts in ethanol steam reforming: The effect of cerium oxide.* Applied Catalysis A: General, 2009. **355**(1-2): p. 69-77.

32. Resini, C., et al., *Initial steps in the production of H₂ from ethanol: A FT-IR study of adsorbed species on Ni/MgO catalyst surface.* Reaction Kinetics and Catalysis Letters, 2007. **90**(1): p. 117-126.

33. Nadeem, A.M., G.I.N. Waterhouse, and H. Idriss, *The reactions of ethanol on TiO2 and Au/TiO2 anatase catalysts.* Catalysis Today, 2012. **182**(1): p. 16-24.

34. Petkovic, L.M., S.N. Rashkeev, and D.M. Ginosar, *Ethanol oxidation on metal oxide-supported platinum catalysts.* Catalysis Today, 2009. **147**(2): p. 107-114.

35. Idriss, H., *Ethanol Reactions over the Surfaces of Noble Metal/Cerium Oxide Catalysts.* Platinum Metals Review, 2004. **48**(3): p. 105-115.

36. Busca, G., et al., *Nickel versus cobalt catalysts for hydrogen production by ethanol steam reforming: Ni–Co–Zn–Al catalysts from hydrotalcite-like precursors.* International Journal of Hydrogen Energy, 2010. **35**(11): p. 5356-5366.

37. de Lima, S.M., et al., *H2 production through steam reforming of ethanol over Pt/ZrO2, Pt/CeO2 and Pt/CeZrO2 catalysts.* Catalysis Today, 2008. **138**(3–4): p. 162-168.

38. Choong, C.K.S., et al., *Effect of calcium addition on catalytic ethanol steam reforming of Ni/Al2O3: II. Acidity/basicity, water adsorption and catalytic activity.* Applied Catalysis A: General, 2011. **407**(1-2): p. 155-162.

39. Fuller, M.P. and P.R. Griffiths, *Diffuse reflectance measurements by infrared Fourier transform spectrometry.* Analytical Chemistry, 1978. **50**(13): p. 1906-1910.

40. Busca, G., *Infrared studies of the reactive adsorption of organic molecules over metal oxides and of the mechanisms of their heterogeneously-catalyzed oxidation.* Catalysis Today, 1996. **27**(3–4): p. 457-496.

41. Meunier, F.C., *The design and testing of kinetically-appropriate operando spectroscopic cells for investigating heterogeneous catalytic reactions.* Chemical Society Reviews, 2010. **39**(12): p. 4602-4614.

42. Celeste Morris, B.S.a.H.B. *Introduction to X-ray Diffraction (XRD), Basic Theory: Instrument Design.* Available from: http://www.asdlib.org/onlineArticles/ecourseware/Bullen_XRD/XRDModule_Theory _Instrument%20Design_3.htm.

43. RRUFF™, *http://rruff.info/magnetite/display=default/R061111*, University of Arizona.

44. Shannon, R.D., *Revised Effective Ionic Radii and Systematic Studies of Interatomic Distances in Halides and Chalcogenides.* Acta Crystallographica, 1976. **A32**: p. 16.

45. Khan, A. and P.G. Smirniotis, *Relationship between temperature-programmed reduction profile and activity of modified ferrite-based catalysts for WGS reaction.* Journal of Molecular Catalysis A: Chemical, 2008. **280**(1–2): p. 43-51.

46. Hosterman, B.D., *Raman Spectroscopic Study of Solid Solution Spinel Oxides*, in *Physics.* 2011, University of Nevada, Las Vegas: Las Vegas. p. 156.

47. Waldron, R.D., *Infrared Spectra of Ferrites.* Physical Review, 1955. **99**(6): p. 1727-1735.

48. Yamanaka, T. and M. Ishii, *Raman scattering and lattice vibrations of Ni_2SiO_4 spinel at elevated temperature.* Physics and Chemistry of Minerals, 1986. **13**(3): p. 156-160.

49. Cynn, H., et al., *High-temperature Raman investigation of order-disorder behavior in the $MgAl_2O_4$ spinel.* Physical Review B, 1992. **45**(1): p. 500-502.

50. Verble, J.L., *Temperature-dependent light-scattering studies of the Verwey transition and electronic disorder in magnetite.* Physical Review B, 1974. **9**(12): p. 5236-5248.

51. Chandramohan, P., et al., *Cation distribution and particle size effect on Raman spectrum of CoFe2O4.* Journal of Solid State Chemistry, 2011. **184**(1): p. 89-96.

52. Laguna-Bercero, M.A., M.L. Sanjuán, and R.I. Merino, *Raman spectroscopic study of cation disorder in poly- and single crystals of the nickel aluminate spinel.* Journal of Physics: Condensed Matter, 2007. **19**(18): p. 186217.

53. Jubb, A.M. and H.C. Allen, *Vibrational Spectroscopic Characterization of Hematite, Maghemite, and Magnetite Thin Films Produced by Vapor Deposition.* ACS Applied Materials & Interfaces, 2010. **2**(10): p. 2804-2812.

54. Llorca, J., N. Homs, and P. Ramirez de la Piscina, *In situ DRIFT-mass spectrometry study of the ethanol steam-reforming reaction over carbonyl-derived Co/ZnO catalysts.* Journal of Catalysis, 2004. **227**(2): p. 556-560.

55. de Lima, S.M., et al., *Evaluation of the performance of Ni/La2O3 catalyst prepared from LaNiO3 perovskite-type oxides for the production of hydrogen through steam reforming and oxidative steam reforming of ethanol.* Applied Catalysis A: General, 2010. **377**(1–2): p. 181-190.

56. Rintramee, K., et al., *Ethanol adsorption and oxidation on bimetallic catalysts containing platinum and base metal oxide supported on MCM-41.* Applied Catalysis B: Environmental, 2012. **115–116**(0): p. 225-235.

57. Busca, G., et al., *IR studies on the activation of C–H hydrocarbon bonds on oxidation catalysts.* Catalysis Today, 1999. **49**(4): p. 453-465.

58.   Dömök, M., et al., *Adsorption and reactions of ethanol and ethanol–water mixture on alumina-supported Pt catalysts.* Applied Catalysis B: Environmental, 2007. **69**(3-4): p. 262-272.

59.   de Lima, S.M., et al., *Study of catalyst deactivation and reaction mechanism of steam reforming, partial oxidation, and oxidative steam reforming of ethanol over Co/CeO2 catalyst.* Journal of Catalysis, 2009. **268**(2): p. 268-281.

60.   Mattos, L.V. and F.B. Noronha, *Hydrogen production for fuel cell applications by ethanol partial oxidation on Pt/CeO2 catalysts: the effect of the reaction conditions and reaction mechanism.* Journal of Catalysis, 2005. **233**(2): p. 453-463.

61.   de Lima, S.M., et al., *Hydrogen production from ethanol for PEM fuel cells. An integrated fuel processor comprising ethanol steam reforming and preferential oxidation of CO.* Catalysis Today, 2009. **146**(1–2): p. 110-123.

62.   Mavrikakis, M. and M.A. Barteau, *Oxygenate reaction pathways on transition metal surfaces.* Journal of Molecular Catalysis A: Chemical, 1998. **131**(1–3): p. 135-147.

63.   Padilla, R., et al., *Nickel and cobalt as active phase on supported zirconia catalysts for bio-ethanol reforming: Influence of the reaction mechanism on catalysts performance.* International Journal of Hydrogen Energy, 2010. **35**(17): p. 8921-8928.

64.   Zaki, M.I., et al., *Surface Chemistry of Acetone on Metal Oxides: IR Observation of Acetone Adsorption and Consequent Surface Reactions on Silica−Alumina versus Silica and Alumina.* Langmuir, 1999. **16**(2): p. 430-436.